RICE UNIVERSITY

Magnetism and Fermi Surface in Heavy Fermion Metals

by

Seiji James Yamamoto

A THESIS SUBMITTED
IN PARTIAL FULFILLMENT OF THE
REQUIREMENTS FOR THE DEGREE
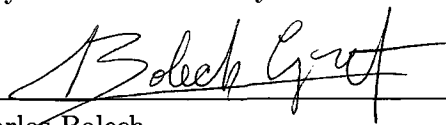
Doctor of Philosophy

APPROVED, THESIS COMMITTEE:

Qimiao Si, Chair
Harry C. and Olga K. Wiess Professor of
Physics and Astronomy

Carlos Bolech
Assistant Professor of Physics and
Astronomy

Junichiro Kono
Associate Professor of Electrical and
Computer Engineering

Houston, Texas

April, 2009

UMI Number: 3362434

INFORMATION TO USERS

The quality of this reproduction is dependent upon the quality of the copy
submitted. Broken or indistinct print, colored or poor quality illustrations
and photographs, print bleed-through, substandard margins, and improper
alignment can adversely affect reproduction.
In the unlikely event that the author did not send a complete manuscript
and there are missing pages, these will be noted. Also, if unauthorized
copyright material had to be removed, a note will indicate the deletion.

UMI®

Abstract

Magnetism and Fermi Surface in Heavy Fermion Metals

by

Seiji James Yamamoto

With a multitude of different phases and quantum critical points, heavy fermion materials should reign supreme as the prototype for competing order, a major contemporary theme in condensed matter physics. One key feature that differentiates the types of magnetic phases and critical points is the presence or absence of Kondo screening. This singlet formation is dramatically manifested in the Fermi surface, which may or may not include atomic f-orbital electron states. To provide a theoretical basis for the different types of magnetism, we have carried out asymptotically exact studies of the Kondo lattice model inside both the antiferromagnetic and ferromagnetic phases. A fundamental aspect of the approach is to map the magnetic Hamiltonian for the f-orbitals onto a quantum nonlinear sigma model (QNLσM). The Kondo interaction results in an effective coupling between the QNLσM fields and the conduction electrons. Renormalization group analyses show that the Fermi surface in the corresponding ordered states is small (not incorporating the f-orbitals) for both the ferromagnetic and antiferromagnetic cases. These results are of relevance

to a number of materials, including $YbRh_2Si_2$ and $CeRu_2Ge_2$, where experimental measurements of magnetotransport and de Haas van Alphen effects have supplied evidence for small Fermi surface phases. The implications of our results for heavy fermion quantum critical points will also be discussed.

Acknowledgments

I would like to thank Qimiao Si for his kind help, guidance, and collaboration during my years at Rice. I am always amazed by the huge scope of his understanding of condensed matter physics. It has been a true privilege to interact so closely with him on a number of scientific projects. I have appreciated the maturity and respect with which he has treated me, for example by granting me access to meet with external visiting physicists on a regular basis. This is a luxury that few graduate students enjoy. I have never had to worry about funding and yet have benefitted from attending numerous workshops/conferences in Europe, South America, and various locations in the United States. Qimiao is the center of the condensed matter theory group at Rice and has been the biggest influence on my career as a physicist.

I thank my committee members, Carlos Bolech and Jun Kono, for their sharp questions during my defense, for their reasonableness, and for their help in improving this thesis. Carlos has also provided good advice on many occasions when I have been stuck on some stubborn puzzle related to my research.

The most useful class I took at Rice was taught by Emilia Morosan who gave me a new understanding of and appreciation for quantum materials and experimental physics in general. This was the first time I got the chance to fit real data and try to extract useful information out of something as simple as a susceptibility curve.

For countless discussions, useful advice, and enjoyable lunches, I thank Paata Kakashvili, Pallab Goswami, Predrag Nikolic, Satyan Bhongale, Leslie Baksmaty,

and, especially, Stefan Kirchner. They have been kind enough to treat me like an equal, despite not yet having earned my PhD. Stefan has always been willing to seriously discuss my ideas and has never turned down anyone on an invitation to get coffee. Early in my time at Rice, I profited from helpful interactions with Kedar Damle, Eugene Pivovarov, Lijun Zhu, and Jun Sun before they all progressed to new levels in their careers.

On the departmental staff, I would especially like to thank Bridgitt Ayers and Barbara Braun who regularly go above and beyond the call of duty. Along with the other members of the staff, they make the Rice Physics Department a pleasant work and study environment.

I thank my family for stressing the importance of education, for always being willing to help financially, emotionally, and otherwise, and for believing in my potential to succeed in life. After graduating from high school, my mother began sending cookies to share with my, visibly jealous, freshman dorm mates. Over a decade later, she continues to send regular shipments of delicious baked goods. For this, my stomach and heart, though not my waistline, offer profound gratitude.

Most of all I must thank my partner in life, Michaela. She is so smart, beautiful, and successful that I'm not sure why she continues to put up with me. She has even managed to remain sweet during my grumpy periods working on this thesis. Although I am proud of the physics achievements summarized in this document, my greatest accomplishment at Rice was finding Michaela.

Contents

List of Figures

List of Tables

Chapter 1

Introduction to Heavy fermions

1.1 Itineracy Versus Locality

The interplay between locality and itineracy is a frequent theme in condensed matter physics. For example, in band theory [1], it is well known that electrons can be understood in either an itinerant Bloch wavefunction basis, or a localized Wannier (tight-binding) representation. In magnetism too, Stoner's description [2] is well suited to, say, Nickel, because it is metallic, while the Heisenberg model seems to work better for insulators. Likewise, for superfluids and superconductors, the BCS picture of Cooper pairs whose partners are widely separated in space works well for a large class of materials [3], while the molecular BEC view of more closely conjoined paired states is better suited to other circumstances, say on the repulsive side of a Feshbach resonance [4]. For heavy fermions, to be defined shortly, we also have itinerant and localized descriptions. The Periodic Anderson Model (PAM) treats f-orbitals as itinerant electrons with strong Coulomb interaction. On the other hand, the Kondo Lattice Model (KLM) views f-orbitals as local moments which are well separated from each other.

The reason for this frequent dual portrayal of the same phenomena perhaps stems from something deep, like Quantum Mechanics. The intention here is not to become involved in philosophical questions, but merely to note that dual descriptions often exist. While the two descriptions are not exactly equivalent, it is not always clear if a sharp distinction can be drawn either. This thesis is concerned with sorting out the sometimes confusing interplay between the localized and itinerant perspectives

in heavy fermion metals where the uncertainty lurks in the nature of the f-orbital. We will show that while many experimental measurements contain some degree of ambiguity, a sharp distinction can in fact be made with regard to the nature of the Fermi surface. The focus of this work will be on magnetically ordered phases, but to put this in perspective with the field more broadly, the first few chapters will discuss more general aspects of heavy fermions and quantum criticality.

1.2 Heavy Fermions

Heavy fermions are a class of materials that almost always contain an element with f-orbitals, such as Ce, U, and Yb [5]. This includes elements from the Lanthanoid ($4f$) and Actinoid ($5f$) series.* Some examples include UPt_3, UGe_2, $PuCoGa_5$, UPd_2Al_3, $CeCu_2Si_2$, $YbRh_2Si_2$, and $CeRu_2Ge_2$. The Lanthanides are usually tri- or tetra-valent. For example, Ce^{3+} has a valence shell configuration of $4f^1$, which is $S = 1/2$, $L = 3$ and $J = 5/2$. Due to the strong spin-orbit coupling, J is the good quantum number. In a crystalline environment, the $(2J + 1)$-fold degenerate multiplet gets split. For an odd number of electrons, and in the absence of time reversal symmetry breaking terms, a doublet ground state is guaranteed by Kramers' Theorem. It is this Kramers doublet that is modeled as the effective SU(2) system and is usually implicated as the relevant local degree of freedom involved in Kondo physics.

The reason these materials are called "heavy" fermions is because they experimentally exhibit paramagnetic Fermi liquid properties, but with an extremely large

---

*IUPAC has been recommending since 1985 that Actinoid and Lanthanoid be used rather than Actinide and Lanthanide, even though the latter are in widespread use. This is because "-ide" implies ionic charge, whereas "-oid" simply means "similar to." No attempt will be made in this thesis to adhere strictly to one convention or another.

effective mass. In practice, this means that, at least within part of the phase diagram, they have a quadratic temperature dependence of the resistivity ($\rho = \rho_0 + AT^2$), a temperature independent Pauli paramagnetic static magnetic susceptibility ($\chi \sim$ const.), and an unusually large linear in temperature specific heat coefficient ($\gamma \equiv C/T > 10$ mJ/mol.K^2). The specific heat coefficient is a measure of the effective mass; for CeAl$_3$, $\gamma \sim 1.5$ J/mol.K^2, which is over 1000 times the bare mass of the electron, hence the modifier "heavy" [6]. Incidentally, CeAl$_3$ was the first heavy fermion to be discovered by Andres, Graebner, and Ott [7].

Having introduced what they are, we may now describe why people find them interesting. First, they exhibit many unusual phases such as unconventional superconductivity, a variety of magnetic orders, and even coexistence between the two. CeCu$_2$Si$_2$ is one of the most famous examples of a heavy fermion since the discovery of its superconductivity by Steglich *et al.* sparked the widespread interest in these materials [8]. Previously, it had been thought that magnetism is so toxic to superconductivity that the two can never coexist.

A second motivation to study heavy fermions comes from the ability we have to tune them between the phases described above. As a result, they provide a convenient test-bed for theories of quantum criticality (more on that in the next chapter) that are relevant to other classes of materials [9]. Ease of tunability is never guaranteed, but it is the happy circumstance heavy fermions provide due to the small energy scales involved. Relatively modest amounts of pressure, doping, or external field strengths are needed to take them all the way across one, or even several, phase transitions [10]. Of course, the preponderance of phases means that these materials are often studied outside the heavy Fermi liquid phase, *i.e.* where they are no longer heavy. Since "rare earth intermetallic" or some similar designation is rather clumsy,

we will instead continue to call the material a heavy fermion if it is somehow easily tunable to a phase in which it can become heavy, even if this means changing its chemical composition by doping.

1.3 Microscopic Hamiltonians

Two microscopic models are most commonly encountered in theoretical investigations of heavy fermions: the Periodic Anderson Model (PAM) and the Kondo Lattice Model (KLM). The latter can be derived from the former in a particular parameter regime via a generalized Schrieffer-Wolff transformation [11, 12]. The Periodic Anderson Model (sometimes also referred to as the Anderson Lattice) can be written:

$$
\begin{aligned}
H_{\text{PAM}} &= \sum_{k\sigma} c_{k\sigma}^\dagger c_{k\sigma} (\epsilon_k^c - \mu) + \sum_{k\sigma} f_{k\sigma}^\dagger f_{k\sigma} (\epsilon_k^f - \mu) + U \sum_i f_{i\uparrow}^\dagger f_{i\uparrow} f_{i\downarrow}^\dagger f_{i\downarrow} \\
&\quad + \sum_{k\sigma} (V_k f_{k\sigma}^\dagger c_{k\sigma} + h.c.)
\end{aligned}
\tag{1.1}
$$

In this model, the difference between conduction electrons and f-orbital electrons is simply that the latter have some correlation, modeled by a Hubbard U, while conduction electrons are treated as free-electron like. The two species hybridize with each other through V_k which is in general momentum dependent, though this is often approximated by a simple constant.

The "Kondo regime" of the Anderson model corresponds to the limit where the correlation is strong and the f-level sits far below the Fermi level, that is:

$$
\epsilon_f \ll \mu \ll \epsilon_f + U
\tag{1.2}
$$

where we have assumed that the width of the band described by ϵ_k^f is so much narrower than the band described by ϵ_k^c that we can treat the former as a constant with characteristic energy $\epsilon_f \equiv \epsilon_{k=0}^f$. To be in the Kondo regime, in addition to the

condition above, the width of the band ϵ_k^f must be much smaller than the intervals $|\mu - \epsilon_f|$ and $|\epsilon_f + U - \mu|$. In this parameter regime a "local moment" exists at every lattice site because it would be energetically costly to populate the f-orbital with either 0 or 2 electrons. Of course, this is somewhat of a caricature of a real material where the "local moment" consists of the lowest doublet of the crystal field split J-multiplet. Nonetheless, this has been a useful model for the past three decades.

When we know that a material sits in the Kondo regime, it is convenient to map the PAM to the KLM, where the local moments are represented by spins attached to the lattice rather than itinerant, though strongly correlated, f-orbitals. This model can be expressed by the following Hamiltonian:

$$H_{\text{KLM}} = \sum_{k\sigma} c_{k\sigma}^\dagger c_{k\sigma} (\epsilon_k - \mu) + J_K \sum_{i\alpha\beta} c_{i\alpha}^\dagger \frac{\vec{\sigma}_{\alpha\beta}}{2} c_{i\beta} \cdot \vec{S}_i \qquad (1.3)$$

where $\vec{\sigma}$ is the vector of Pauli matrices and J_K is the Kondo coupling. Within weak-coupling perturbation theory, the Kondo interation can be shown to generate an effective coupling between the local moments via the so-called RKKY interaction [13, 14, 15] which can be pictured as the spin analog of Friedel oscillations [16]. It is therefore often convenient to introduce the Kondo Heisenberg Lattice, which is sometimes also referred to as the Kondo Lattice Model:

$$H_{\text{KLM}} = \sum_{k\sigma} c_{k\sigma}^\dagger c_{k\sigma} (\epsilon_k - \mu) + J_K \sum_{i\alpha\beta} c_{i\alpha}^\dagger \frac{\vec{\sigma}_{\alpha\beta}}{2} c_{i\beta} \cdot \vec{S}_i + \sum_{ij} I_{ij} \vec{S}_i \cdot \vec{S}_j \qquad (1.4)$$

The spin-spin coupling I_{ij} is proportional to the density of states times J_K^2 if it is of purely RKKY origin, though other exchange interactions may exist in the material; we lump them all together in I_{ij}. This model will serve as the starting point for the studies of this thesis and will be discussed at great length later. The Kondo-Heisenberg Model has been used by a number of authors in the context of heavy fermions; see for example [17, 18, 19, 20]. On the issue of double counting, see [21].

On intuitive grounds we would expect the PAM to be useful for studying heavy fermions when it is known that the f-orbital needs to be in some sense itinerant. For example, the mixed-valent problem [16] corresponds to situations in which the f-orbital occupancy tends to fluctuate because the f^n and $f^{n\pm1}$ states are nearly degenerate in energy. Since this is outside the Kondo regime where the mapping PAM $\rightarrow$ KLM breaks down, we expect the PAM to be more suitable than the KLM at least for the mixed-valent problem. Indeed, in the limit $U \rightarrow \infty$, several authors have devised a large-N (where N is the number of fermion flavors) slave-boson technique that appears to work well in this situation, as well as within the Kondo regime for the paramagnetic heavy Fermi liquid phase [22, 23, 24].

In fact, for the paramagnetic heavy Fermi liquid phase, strong theoretical arguments exist suggesting that the f-orbitals are always itinerant in character for both the PAM [25] and, surprisingly, the KLM [26]. This is rather unexpected since it suggests that within the local moment parameter regime, the f-orbitals can actually acquire itinerant character. How this is possible will be discussed in the next section, but here we briefly point out that, in principle, there may also be situations in which the f-orbital states behave as if they are localized. Such a situation would of course be sensible in the local moment parameter regime, suggesting that the KLM should be the appropriate starting point. This thesis will be dedicated to understanding one such circumstance where the f-orbitals assume a localized nature even at $T = 0$, namely when there is magnetic ordering. What is meant by itinerant will be described as we go, and it will turn out to be closely related to the nature of the Fermi surface.

1.4 Why is it heavy?

A standard lore exists which describes how the electrons become so heavy within the paramagnetic phase [5]. A brief account of the story goes like this. At high temperatures, an f-orbital local moment can be found at every site of a well defined lattice. These should be thought of as angular momentum degrees of freedom which do not contribute to conduction. The material is metallic, but the conducting electrons are completely distinct from the f-orbitals. As we lower the temperature, some sort of many-body entanglement occurs whereby the local angular momentum degrees of freedom become screened by the conduction electrons to form an overall singlet state. When this happens, the local moments are said to be "quenched" and the susceptibility crosses over from a Curie to Pauli form. In this low temperature phase, the Fermi surface becomes anomalously large. In fact, the Luttinger sum rule [27], which relates the density of electrons to the Fermi volume, indicates that the f-orbitals must now be considered itinerant in any bandstructure calculation in order to obtain the correct Fermi surface. The local moments have thus "dissolved" into the Fermi sea and are in a sense no longer local even though the lattice structure may be such that the pure f-orbital wavefunctions cannot directly overlap.

This is a rather remarkable story, especially if viewed from the perspective of the KLM. In this model, the f-orbitals are not electrons at all, but merely spin degrees of freedom. Indeed, the original work by RKKY [13, 14, 15] was concerned with nuclear spins, and the story above would suggest that the heavy Fermi liquid paramagnet can develop even if the local moments are of nuclear origin [5]. Would it really make sense in that case to say that the local moments have dissolved into the Fermi sea, or is something else going on? This is the fundamental issue in heavy fermions: are f-orbitals localized, or itinerant?

Perhaps a better way to understand the situation is by labeling phases according to clear-cut experimental criteria. We will show in the next section that for many measurements related to itineracy, the answer is not completely clear. However, what seems unambiguous is the size of the Fermi surface, and we propose to use this as a criterion for categorizing phases.
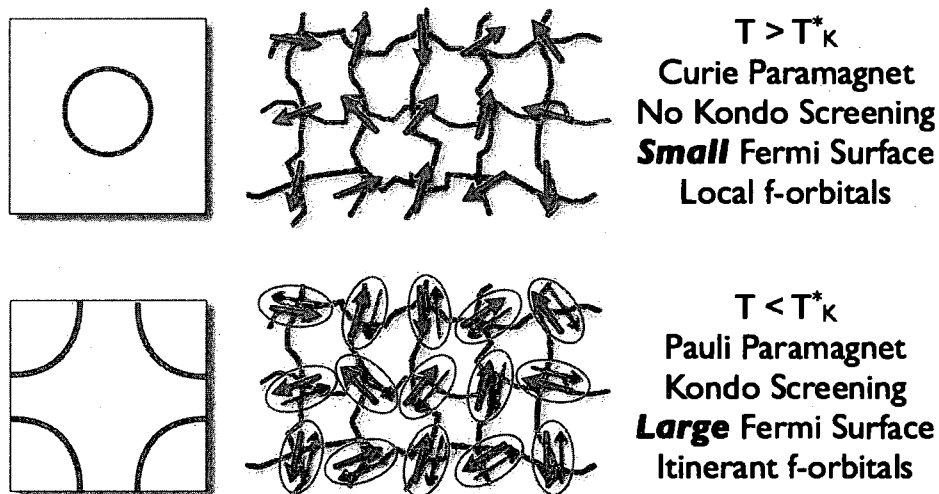
Figure 1.1 : Large and small Fermi surfaces of the paramagnetic phase. The large Fermi surface corresponds to Kondo screening, while the small Fermi surface has no Kondo singlet. Here, the distinction is slightly less useful because, technically, the Fermi surface is only sharply defined at $T = 0$ and the transformation of states is only a crossover rather than a sharp phase transition. For magnetic phases at $T = 0$, the distinction becomes sharp, as described in the text.

1.5 f-Orbital Itineracy and the Fermi Surface

In this section we review some of the ways to adjudicate the itineracy of f-orbitals as usually presented in the literature. Given any heavy fermion metal, the first thing to do is measure the temperature dependence of the susceptibility. When local moments are unquenched (localized) we expect this to track a Curie-Weiss form:

$$\chi_{\mathrm{CW}}(T) \;=\; \frac{C}{T - \theta_W} \tag{1.5}$$

where θ_W is the Weiss temperature and C is the Curie constant. In an unfrustrated system, the Weiss temperature can give us a handle on the relevant coupling strength, whereas the Curie constant gives a measurement of the size of the effective local moment. In particular $\mu_{eff} = \mu_B\sqrt{8C}$, where μ_B is the Bohr magneton. Experimentally, the susceptibility is usually found by measuring the magnetization of the sample using a SQUID in response to some small applied magnetic field, and simply taking the ratio $\chi \approx M/H$. The Curie-Weiss form is derived from a mean-field treatment of the Heisenberg Model, so it is expected to work well when the spin degrees of freedom responding to the applied magnetic field are of localized nature. Since the treatment is only mean field, the true ordering temperature found experimentally (usually called the Curie or Neel temperature, depending on the type of order) almost always differs from the Weiss temperature. The latter is defined by fitting the high temperature inverse susceptibility and extrapolating to zero. Another way to say this is that the experimental plot of $1/\chi(T)$ is rarely a perfectly straight line.

In contrast, when the spins are of itinerant nature, we expect quite different behavior. Here, the susceptibility takes a Pauli form which is temperature independent:

$$\chi_{\mathrm{P}}(T) = \rho(E_F) \tag{1.6}$$

In the zero temperature, zero frequency, zero momentum limit, χ_P gives a measure of the density of states at the Fermi level, assuming no ordering intervenes to lowest temperatures. This is useful information in itself, but for our discussion the important point is that χ_P is independent of temperature.

When the susceptibility crosses over from an inverse temperature dependence to a constant, this is interpreted as experimental evidence for the quenching of local moments. However, as seen in figure 1.2, susceptibility data alone does not make it obvious when or if f-orbitals are itinerant. Features in the resistivity data have a
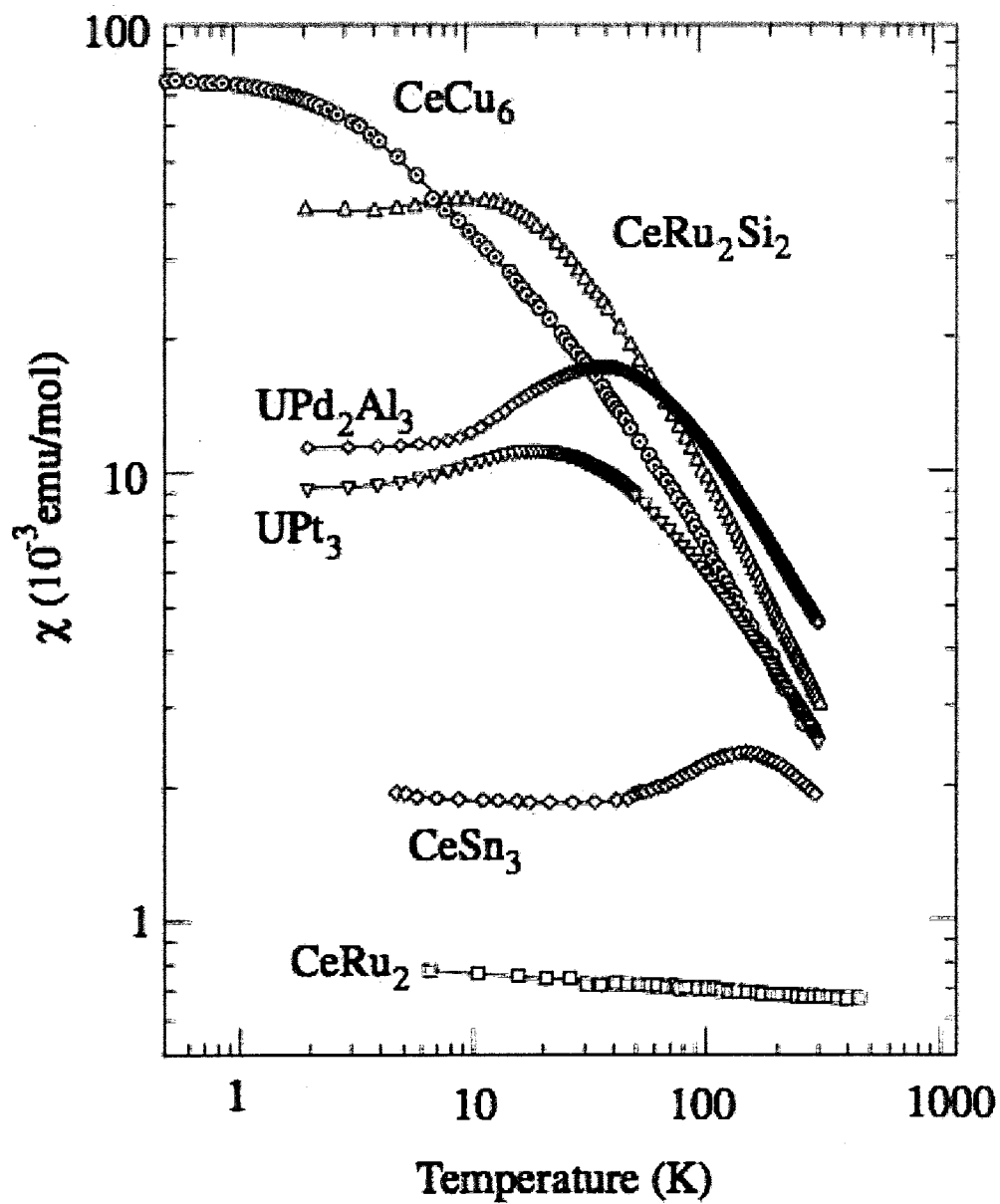
Figure 1.2 : Temperature dependence of the susceptibility for several different heavy fermion compounds, from [28]. Notice the Curie form at high temperature, and the Pauli form at low temperatures.

similar problem of indirectness. More problematic is that magnetic or superconducting order might take over at lower temperatures leading to a different temperature dependence and making it difficult to assess the itineracy or locality of f-orbitals over a sharply defined range of temperatures.

Inside a magnetically ordered phase, the temperature dependence of the susceptibility does not tell us anything about the locality or itineracy of f-orbitals. In such a case, the size of the moment is often used as a criteria for categorizing the magnet as itinerant or local. The moment size can be determined from neutron scattering, directly from a magnetometer, or by integrating the specific heat to determine the entropy, and thus the degeneracy, of the angular momentum degree of freedom.

In figure 1.3 is the so-called Rhodes-Wohlfarth plot [29, 30]. On the vertical axis is the rato μ_{eff}/μ_{sat}, while the horizontal axis is the Curie temperature (this is only relevant to ferromagnetic materials). Known local ferromagnets tend to lie on a flat line, whereas itinerant ferromagnets tend to fall on the curve. For large T_c, the difference is rather difficult to ascertain, but at least for small values of T_c this appears to provide a useful empirical trend.

Now, the reason for f-orbital itineracy could be something simple like direct wavefunction overlap. In the case of actinides, Hill's limit has been established which separates overlapping from non-overlapping compounds, see table 1.1 and reference [31]. For U-based compounds, Hill's limit is about 0.34 nm. When the distance between f-orbitals is less than Hill's limit, the wavefunctions overlap. Comparing table 1.1 to the Rhodes-Wohlfarth plot in figure 1.3, it is easy to identify several materials which are beyond Hill's limit (meaning f-orbital wavefunctions do not overlap), yet nonetheless appear to fall on the curve identifying them as itinerant. Therefore, for some materials, something other than direct wavefunction overlap is causing them to
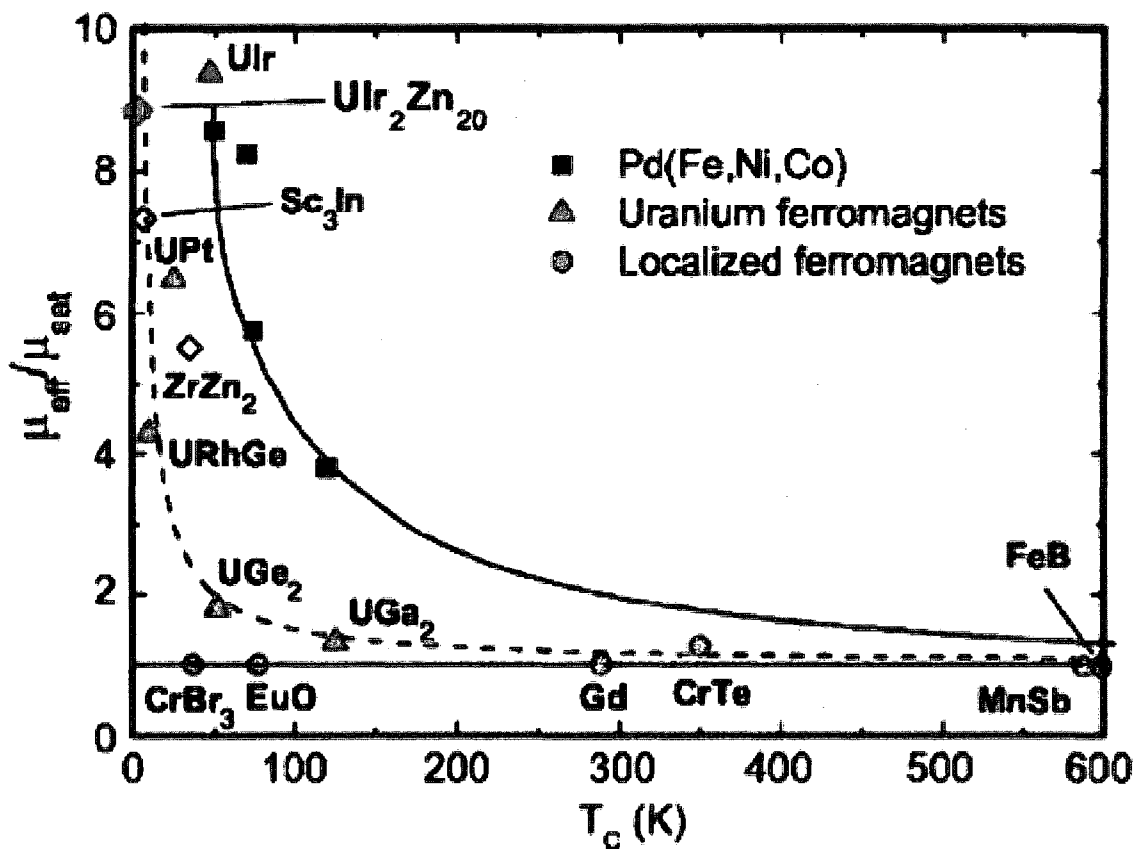
Figure 1.3 : The Rhodes-Wohlfarth plot, from [30]. Local moment ferromagnets tend to lie on the horizontal line, whereas itinerant ferromagnets fall on the curve. The vertical axis is the ratio of the effective to saturation moment.

Table 1.1 : Hill's limit is the distance between atomic sites containing f-orbitals below which wavefunctions begin to overlap. For uranium, Hill's limit corresponds to $d_c = 0.34$ nm. The data for this table can be found in [31].

material	d (nm)
α-U	0.31
β-U	0.31
γ-U	0.29
UCo	0.31
U_6Ni	0.32
UPt_3	0.41
UBe_{13}	0.51
URu_2Si_2	0.41
UGe_2	0.38
UPd_2Al_3	0.40
URhGe	0.35
$PuCoGa_5$	0.42
$PuRhGa_5$	0.43
Am	0.30

behave as if the f-orbitals are itinerant. This is usually ascribed to the lattice analog of Kondo screening, as discussed above.

All of the experimental methods discussed so far that are commonly used to determine the itineracy or locality of f-orbitals are in some way indirect, or potentially ambiguous. However, a clear-cut measure does exist which is simply the size of the Fermi surface. The Fermi surface can be directly measured by Angle Resolved Photoemission Spectroscopy (ARPES) and the de Haas van Alphen (dHvA) effect. Since these techniques are confined to surface studies and relatively high magnetic fields, respectively, magnetotransport (such as the Hall coefficient) can yield information about the Fermi surface as well. If the Fermi surface is only consistent with bandstructure calculations that treat the f-orbital as itinerant, which we call a Large Fermi surface, then we know that it contributes to the single-electron excitation spectrum. On the other hand, if Fermi surface measurements yield something which only matches calculations which do not include the f-orbital, then we expect the material to be a local moment metal and this tells us that, at least statically, Kondo singlets cannot exist. Measurements of the Fermi surface therefore provide a sharp test for the itineracy or locality of f-orbitals. We differentiate magnetic metal phases by the size of their Fermi surfaces. When the Fermi surface is large, we use the subscript "L." When the Fermi surface is small, we label it with "S." See table 1.2.

Table 1.2 : Notation for different types of magnetic metal phases.

Magnetic order	f-orbital type	Fermi surface	Notation
Ferromagnetic	Itinerant	Large	F_L
Ferromagnetic	Local	Small	F_S
Antiferromagnetic	Itinerant	Large	AF_L
Antiferromagnetic	Local	Small	AF_S

Chapter 2

Quantum Criticality in Heavy Fermions

The goal of this chapter is to introduce the idea of unconventional Kondo break-down quantum criticality in heavy fermions, as well as experimental evidence for its relevance to $YbRh_2Si_2$ and $CeCu_{6-x}Au_x$. An understanding of criticality in these materials will set the stage for the main research question of this thesis which will focus on magnetically ordered phases rather than criticality itself.

2.1   Strongly Correlated Electrons

The field of strongly correlated electrons is generally concerned with situations in which a description based on a weakly interacting gas of fermions no longer works well. One way this comes about is when interactions between electrons are so strong that perturbation theory is no longer justifiable. This view leads to the exclusion of a number of theoretical methods, but it does not clearly describe the physical systems at the focus of our attention. One theme of the field that is easier to understand is the notion that electrons should cease to be the main protagonists of the story.

No longer the most convenient entities at the heart of our descriptions, electrons must give way to fundamentally different types of excitations. An old motif from the early days of condensed matter physics was the concept of collective excitations of many-body systems [32]. At about the same time, high energy physicists were developing ideas about symmetry breaking, massless excitations, and non-trivial vacua (*i.e.* ground states) [33]. These concepts naturally converged in the fields of phase transitions and renormalization which allowed us to understand how changes of phase

can lead to a dramatic reconstruction of the excitation spectrum. In one phase, electrons might constitute an excellent approximation to the low lying spectrum, but such a description is not guaranteed to hold after the system experiences a phase transition.

Despite the strong interplay between quantum field theory, statistical mechanics, and phase transitions, it was not until the late 1970's that the word quantum began to be emphasized in the context of phase transitions [34]. The main idea here is that situations exist in which the phase transition can be induced by tuning a control parameter other than temperature. In fact, a quantum phase transition can be operationally defined as a phase transition that occurs at strictly zero temperature.

It is easy enough to appreciate the conceptual profundity of the idea of a quantum phase transition, but it is not as easy a task to identify experimentally accessible systems in which the phase transition can be traced to quantum rather than thermal effects. Today, it might seem relatively simple to recognize a large number of systems where quantum criticality is at play, but this was not so obvious 30 years ago. In fact, as mentioned previously, the experimental scarcity of quantum critical systems was one of the early motivations behind the high levels of interest in heavy fermion materials: their rich phase diagrams make them a veritable cornucopia of phase transitions.

This chapter will review some notions about classical and quantum phase transitions, then discuss several specific issues particular to heavy fermion criticality. We will then finally be ready to make contact with the new contributions this thesis offers, namely the development of models appropriate to the small Fermi surface phases of heavy fermion magnets.

2.2 Classical Phase Transitions

Although this thesis is concerned with electrons in solid state environments, the concept of a phase is obviously much more general. Solids, liquids, and gases comprise the entirety of all matter familiar to the vast majority of non-scientists. These form the intuitive basis upon which our modern understanding of more exotic electronic phases is founded. We even name them as such: Fermi gas, spin liquid, Wigner crystal, etc. Quantum mechanics happens to feature conspicuously in each of these examples, as it will in most problems in the field of strongly correlated electrons. However, a large body of knowledge has grown over the years on the topic of classical phase transitions, or classical critical phenomena. The elements of critical phenomena we wish to mention are the order parameter, Landau theory, the correlation length, and universality.

The order parameter is something we can define that takes a non-zero value in the ordered phase, and a value of zero in the non-ordered (or disordered) phase. Usually, it is the average value of a quantity that can be defined locally. For example, in the Ising model, when the average value of the spin, $\langle S_i \rangle \equiv m$, takes a non-zero value we label it with the letter m and call it the magnetization. When $m = 0$ we say the system is disordered (paramagnetic), whereas when $m \neq 0$ the system is ordered. For a more mundane material like water, which exhibits solid, liquid, and gaseous phases, the order parameter is related to the density.

The most influential phenomenological theory that encodes this idea of an order parameter is due to Landau and coworkers [35]. At the crudest level, Landau theory is simply a quartic polynomial:

$$L[m] \quad = \quad am^2 + bm^4 \tag{2.1}$$

where m is the order parameter, $b > 0$, and a controls the phase transition. If $a < 0$ the system is ordered, if $a > 0$ it is not. A slightly more sophisticated view would call this "ϕ^4-theory" and allow the order parameter to become a function of space. The action is given by

$$\mathcal{S} = \int d^3x \left[(\nabla \phi(\vec{x}))^2 + r\phi^2(\vec{x}) + u\phi^4(\vec{x}) \right] \tag{2.2}$$

Once again, the sign of r controls the phase transition, so it is usually defined by $r = r_0(T - T_c)$ where r_0 is some constant and T_c is the transition temperature. When $u = 0$, the theory is called Gaussian because the partition function takes the form of a Gaussian integral: $Z \sim \int \mathcal{D}\phi e^{-\int \phi^2}$.

The critical point is captured at $T = T_c$ where it can be shown that the correlation length of this statistical field theory diverges as $T \to T_c$. In fact, this defines the critical exponent ν via:

$$\xi \sim (T - T_c)^{-\nu} \tag{2.3}$$

The divergence of this length scale is the driving force behind universality. At the heart of universality is nothing but dimensional analysis. Near the critical point, the biggest scale in the problem is always the correlation length ξ, which dwarfs every other scale in the problem thus making many details irrelevant. Quite a lot of information can therefore be had at criticality simply by dimensional analysis with ξ as the only length scale.

2.3 Quantum Phase Transitions

In quantum statistical mechanics a correspondence can be drawn between a quantum problem in d dimension and a classical problem in $d + 1$. This is not always the case,

but often works because the path integral formalism of statistical mechanics formally treats temperature effects by integrating over an additional dimension. One way to think about this is by allowing the Landau functional (action) to become dependent on an imaginary time dimension:

$$\mathcal{S} \;=\; \int d^3x \int_0^\beta d\tau \left[(\nabla\phi(\vec{x},\tau))^2 + r\phi^2(\vec{x},\tau) + u\phi^4(\vec{x},\tau) \right] \tag{2.4}$$

where $\beta = 1/T$. This is seemingly innocuous, but only because we are doing phenomenology. The main conceptual difference is that the quadratic coefficient can now be understood to represent a non-thermal tuning parameter: $r = a(\delta - \delta_c)$, where δ can represent pressure, doping, magnetic field, etc. Another conceptual difference is that the fluctuations that cause the phase transition are due to quantum zero-point motion rather than classical thermal vibrations. That is why the theory is fundamentally related to quantum mechanics.

In this thesis we are interested in metals, so we need a theory for phase transitions of metals. One of the early models of quantum criticality [34] was in fact concerned with metallic antiferromagnets, sometimes interchangeably referred to as spin-density wave antiferromagnets [36]. The idea is to begin with an electronic model, decouple the four-fermion interaction using an auxiliary Hubbard-Stratonovich field, then completely integrate out the fermions to arrive at an effective field theory involving only the bosonic auxiliary fields. This methodology will be utilized in chapter 3, but here we merely want to note that this new theory turns out to take the form of a quantum ϕ^4 theory as described above. Nowadays, this is often called Hertz-Millis-Moriya theory [34, 37, 38] and has served for many years as the prevailing paradigm for the magnetic quantum phase transition of metals. This theory turns out to fail under certain circumstances, which is the narrative we turn to next.

2.4   QCPs in Heavy Fermions

Although heavy fermion materials exhibit a diverse set of phases, we will primarily be focused on magnetism. Whenever the phrase Quantum Critical Point is used it should always be understood, at least within this thesis, to be a *magnetic* QCP. In most cases, the magnetic QCP in question is metallic on both sides of the transition, so for many years it was thought that the Hertz-Millis-Moriya theory of the SDW QCP was sufficient to describe the transition.

However, that picture began to be challenged in the late 1990's when neutron scattering studies of $CeCu_{6-x}Au_x$ revealed [39, 40] ω/T scaling in the imaginary part of the dynamical susceptibility:

$$\chi''(\omega, T) = T^{-\alpha} g(\omega/T) \tag{2.5}$$

with $g(y) \equiv c\sin[\alpha\arctan(y)]/(y^2+1)^{\alpha/2}$ and $\alpha \approx 0.74$. Though a seemingly obscure result, what it means is that the QCP must be non-Gaussian. This important observation rules out the SDW theory of the QCP because, for $d > 2$, the Hertz-Millis-Moriya theory sits above its upper critical dimension, $d_c^+ \equiv 4 - z = 2$. Here, all the couplings beyond quadratic order are irrelevant in the RG sense (to be discussed later) and the theory is controlled by a Gaussian fixed point. Such a Gaussian theory will have a susceptibility (propagator) with the following quantum critical form [41]:

$$\chi(\vec{q}, \omega) = \frac{1}{f(\vec{q}) + \kappa(\vec{q}, T) - ia\omega} \tag{2.6}$$

where a is a constant, $f(\vec{q}) \propto (\vec{q} - \vec{Q})^2$ with $\vec{Q}$ the ordering wavevector, and the function $\kappa(\vec{q}, T)$ has the property $\lim_{T \to 0} \kappa(\vec{q}, T) = 0$. Clearly, this form does not exhibit ω/T scaling as indicated by the experimental fit of the neutron data in equation (2.5). Therefore, the Hertz-Millis-Moriya theory of a simple SDW cannot explain the QCP

observed in $CeCu_{6-x}Au_x$. One example of a theory that fits the data better is local quantum criticality [17, 42]. The word "local" applies because the theory predicts the fractional frequency (and temperature) exponent in the susceptibility, α above, to be independent of wavevector.

The theory of local criticality is one example of the more general idea that at certain QCP's in heavy fermions the Kondo effect may be a crucial part of the quantum critical fluctuation spectrum. Intuitively, this is clear since the Kondo effect occurs locally at every lattice site where an f-orbital exists. This is the main physical difference between the SDW picture and what we will now label as the Kondo breakdown scenario. If we begin in the paramagnetic heavy Fermi liquid, there are two doorways to magnetism. We can either achieve magnetic order through the conventional SDW QCP gateway, or we might pass through a totally different kind of QCP where the Kondo effect breaks down simultaneously with the development of magnetic order. For this reason, we call this somewhat unconventional route a Kondo breakdown QCP. See figures 2.1 and 2.2.

Besides the form of the dynamical susceptibility, these two different types of QCPs can be experimentally distinguished by other means. One of the early tests was the temperature dependence of the Grueneisen ratio at criticality [44, 45], defined as the thermal expansion coefficient divided by the specific heat: $\Gamma = \alpha/C_P$. For the SDW scenario we expect $\Gamma \sim T^{-1}$, while for the LQCP we expect $\Gamma \sim T^{-0.66}$. For $CeNi_2Ge_2$ the exponent was found to be very close to -1, while for $YbRh_2(Si_{0.95}Ge_{0.05})_2$ the exponent was about -0.7. Notably, the Bose-Fermi Kondo Model within an ϵ-expansion predicts -0.62 at first order and -0.66 at second order [45]. This suggest that $YbRh_2Si_2$ may provide an example of Kondo breakdown criticality.

More recent work indicates that other experimentally measurable quantities (mag-
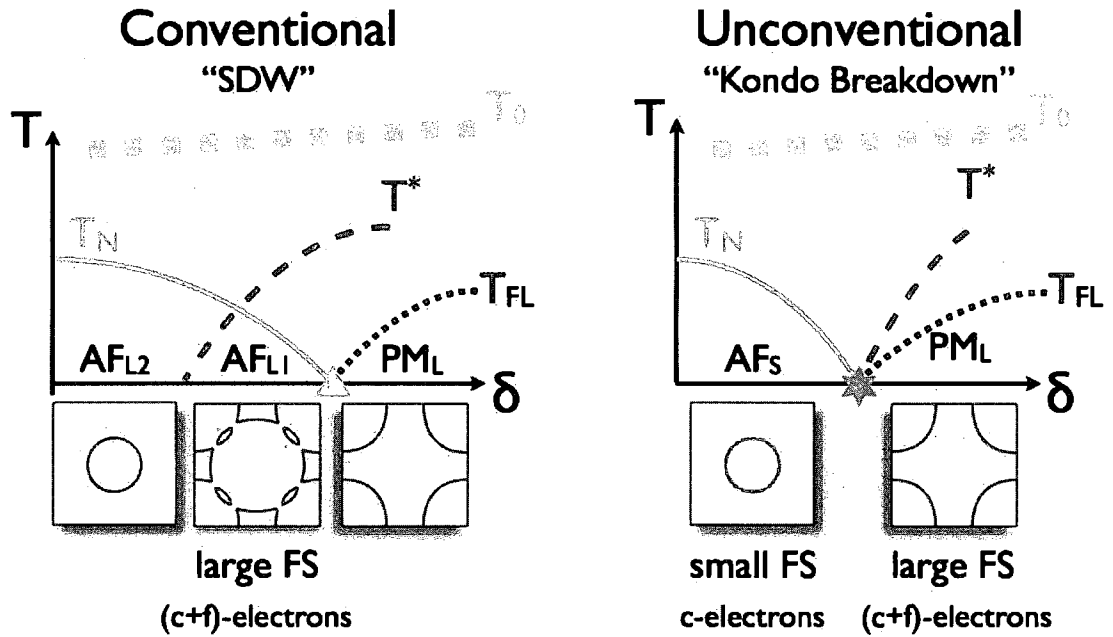
Figure 2.1 : Two different types of quantum critical point scenarios for heavy fermion metals. In the Kondo breakdown scenario, a direct transition from the paramagnetic large Fermi surface (PM_L) to the antiferromagnetic small Fermi surface (AF_S) phase is possible. In the SDW scenario, Kondo screening persists on both sides of the critical point, so both phases are labelled large: $PM_L \rightarrow AF_{L1}$. As the order parameter grows, the system can undergo a Lifshitz electronic topological transition, thus reach another antiferromagnetic phase which we label AF_{L2}.
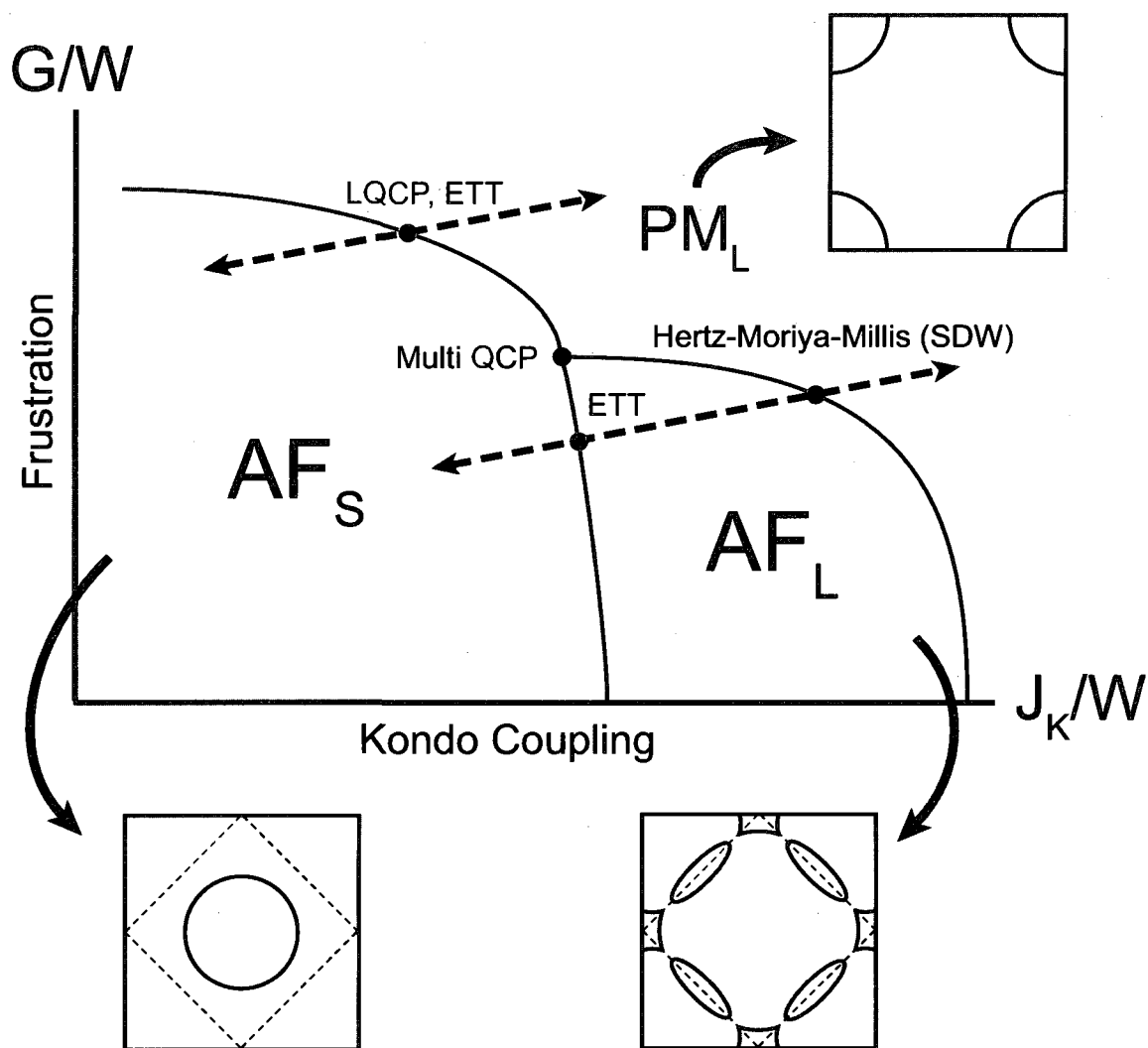
Figure 2.2 : Global phase diagram at $T = 0$. The horizontal axis is the strength of the Kondo coupling. The vertical axis represents some control of frustration in the local moment component, labelled by G. For example, if we have both nearest-neighbor (I_{nn}) and next-nearest-neighbor (I_{nnn}) RKKY coupling, the frustration parameter could be measured by $G = I_{nnn}/I_{nn}$. All units are normalized by the conduction electron bandwidth, W. Notice the presence of several different types of QCPs. ETT stands for the Lifshitz electronic topological transition [43], while LQCP and SDW are discussed in the text.

netostriction, magnetization, Hall resistivity) all demonstrate that multiple energy scales converge to zero precisely at the magnetic QCP [10]. The reader is referred to [46] for further details. We describe next the Hall coefficient experiment because it is more closely connected with the main topic of this thesis.

2.5 Fermi Surface and Criticality

Looking at figure 2.2, we see that the existence of two different QCPs implies that two different types of antiferromagnetic phases must exist. The distinction between the two, as also seen in figure 2.1, is that Kondo screening can be found on both sides of the SDW QCP, whereas no Kondo screening is expected in the magnetic phase proximate to the Kondo breakdown QCP. As discussed in the previous chapter, if there is no Kondo screening, we expect the Fermi surface to be small in the sense that local moment f-orbitals do not constitute itinerant states. Such an assumption makes a big difference in bandstructure calculations and provides a sharp, experimentally testable distinction between the two types of phases. Thus, the size of the Fermi surface is crucial and, as described in Table 1.2, we denote the Kondo screened antiferromagnet by AF_L because it will have a large Fermi surface, and the non-Kondo screened antiferromagnet by AF_S because the conduction electrons will be completely decoupled from the local moments, thus comprising a small Fermi surface. Experimentally, how do we tell the difference between AF_S and AF_L?

There are three common ways to measure the Fermi surface: Angle Resolved Photoemission Spectroscopy (ARPES), the de Haas van Alphen (dHvA) effect, and magnetotransport measurements such as the Hall coefficient. The latter has been carefully scrutinized for the material $YbRh_2Si_2$, confirming the Kondo breakdown scenario [47]. The way this is determined is via the way the Hall coefficient changes

across the transition. In the conventional SDW scenario, magnetic ordering is expected to slowly gap out portions of Fermi surface close to hot spots defined by the ordering wavevector $\vec{Q}$, with the gapped-out regions slowly increasing in expanse as the size of the magnetic order parameter increases. In contrast, for the Kondo breakdown QCP, a dramatic reconstruction of the Fermi surface is expected as f-orbitals are immediately ejected from the Fermi sea. The difference in the evolution of the Hall coefficient is schematically depicted in figure 2.3.
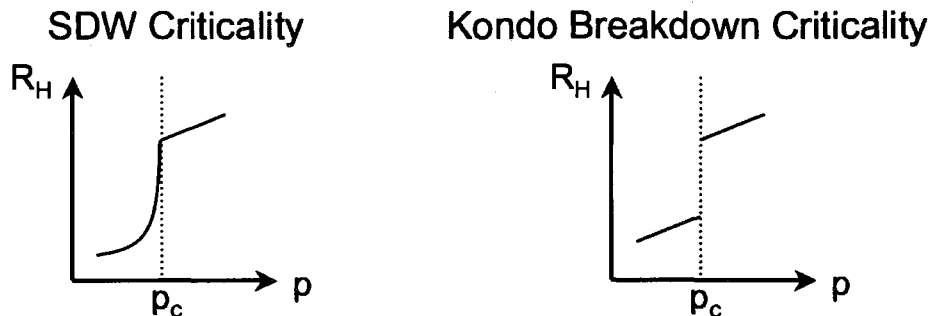
Figure 2.3 : Evolution of the Hall coefficient for the two different types of QCP. The left figure shows a smooth evolution of the Hall coefficient for the SDW scenario, while the right figure shows a jump in the Hall coefficient for the Kondo breakdown QCP [48].

While the dichotomy of QCPs and, correspondingly, ordered phases, has been well established for antiferromagnetic heavy fermions, in principle the same classification could exist for ferromagnetic heavy fermions. Can both large (F_L) and small (F_S) ferromagnetic phases exist? Are there different types of ferromagnetic QCPs? Very little theoretical work has hitherto been devoted to the ferromagnetic problem, but we will devote the latter half of this thesis to this issue. First, however, we begin our attack on the antiferromagnetic problem.

Chapter 3

Antiferromagnetism in the Kondo Lattice

Chapter 1 provided an introduction to heavy fermion materials and explained how they fit into the larger framework of the study of strongly correlated systems. Chapter 2 narrowed the scope by reviewing the on-going debate in the community regarding the types of quantum critical points in these materials, while at the same time providing a brief reminder of the salient features of phase transition theory relevant to our discussion. We now begin to present new contributions to the field. The goal of this chapter is to derive a representation of the Kondo Lattice Hamiltonian in terms of a Quantum Nonlinear Sigma Model (QNLσM). The next chapter will develop the methodological tools necessary to analyze this model, and the chapter after that will apply those techniques to the model developed here. There, we will finally be able to answer the question raised in the previous two chapters concerning the stability of the antiferromagnetic phase with a small Fermi surface.

The results of the next three chapters have already appeared in two brief publications [49, 50], but the detailed explanations are presented here for the first time. Some of the exposition and figures, however, will have significant overlap with these publications.

3.1 Summary of the Mapping

Since an explicit demonstration of the mapping will take a fair amount of space, in this section we summarize the essential points of the story. Subsequent subsections will provide the details.

We consider the Kondo lattice model:

$$\mathcal{H} = \mathcal{H}_f + \mathcal{H}_c + \mathcal{H}_K \tag{3.1}$$

Here, $\mathcal{H}_c = \sum_{\vec{k}\sigma} \epsilon_{\vec{k}} \psi_{\vec{k}\sigma}^\dagger \psi_{\vec{k}\sigma}$ describes a band of free conduction c−electrons, with a bandwidth W. For now, we will consider the electron concentration, x per site, to be such that the Fermi surface of $\mathcal{H}_c$ alone does not touch the antiferromagnetic zone boundary. Later, we will discuss the modifications necessary for the more general case. $\mathcal{H}_K = \sum_i J_K \vec{S}_i \cdot \vec{s}_{c,i}$ specifies the Kondo interaction of strength J_K; here the conduction electron spin $\vec{s}_{c,i} = \frac{1}{2} \sum_{\sigma\sigma'} \psi_{\sigma,i}^\dagger \vec{\tau}_{\sigma\sigma'} \psi_{\sigma',i}$, where $\vec{\tau}$ is the vector of Pauli matrices. Finally, $\mathcal{H}_f = \frac{1}{2} \sum_{ij} I_{ij} \vec{S}_i \cdot \vec{S}_j$ is the magnetic Hamiltonian for the spin-$\frac{1}{2}$ f−moments, $\vec{S}_i$, for which there is 1 per site. The strength of the exchange interactions, I_{ij}, is characterized by, say, the nearest neighbor value, I.

We focus on the parameter region with $J_K \ll I \ll W$. Here, it is appropriate to expand around the limit $J_K = 0$, where the local-moment and conduction-electron components are decoupled. We will consider, for simplicity, square or cubic lattices, although our results will be generally valid provided the ground state is a collinear antiferromagnet. $\mathcal{H}_f$ can be mapped to a quantum non-linear sigma model (QNLσM) by standard means [51, 52]. Details of this mapping are given in subsequent sections. The low-lying excitations are concentrated in momentum space near $\vec{q} = \vec{Q}$ (the staggered magnetization) and near $\vec{q} = \vec{0}$ (the total magnetization being conserved):

$$2\vec{S}_i \rightarrow \eta_{\vec{x}} \vec{n}(\vec{x}, \tau) \sqrt{1 - \left(2a^d \vec{L}(\vec{x}, \tau)\right)^2} + 2a^d \vec{L}(\vec{x}, \tau) \tag{3.2}$$

where $\vec{x}$ labels the position, $\eta_{\vec{x}} = \pm 1$ on even and odd sites, a is the lattice constant, and we have used $S = 1/2$. The linear coupling $\vec{n} \cdot \vec{s}_c$ cannot connect two points on the Fermi surface and is hence unimportant for low energy physics (such a kinematic constraint has appeared in other contexts, *e.g.* Ref. [53]); see Fig. 3.1b. The Kondo

coupling is then replaced by an effective one, $\vec{S} \cdot \vec{s}_c \rightarrow a^d \vec{L} \cdot \vec{s}_c$, corresponding to forward scattering for the conduction electrons; see Fig. 3.1a.

$$(a) \qquad\qquad (b)$$
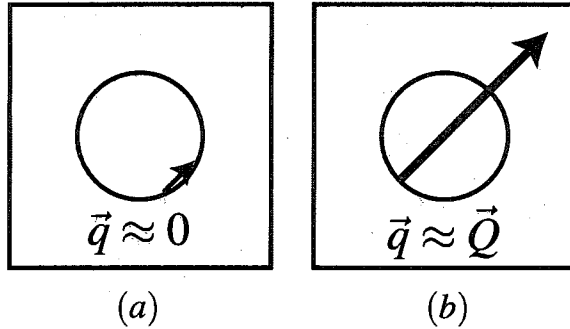
Figure 3.1 : When the Fermi surface (FS) of the conduction-electron component does not touch the antiferromagnetic zone boundary, only the uniform component ($\vec{q} \approx 0$) of the local moments can interact with states near the FS, as shown in (a). The linear coupling involving the staggered component, $\vec{n} \cdot \vec{s}_c$, is not kinematically favorable, as shown in (b).

The mapping to the QNLσM can now be implemented by integrating out the $\vec{L}$ field. The effective action is

$$
\begin{aligned}
\mathcal{S} &= \mathcal{S}_{\text{QNL}\sigma\text{M}} + \mathcal{S}_{\text{Berry}} + \mathcal{S}_K + \mathcal{S}_c \\
\mathcal{S}_{\text{QNL}\sigma\text{M}} &\equiv \frac{c}{2g} \int d^d x d\tau \left[(\nabla \vec{n}(\vec{x},\tau))^2 + \left(\frac{\partial \vec{n}(\vec{x},\tau)}{c\, \partial \tau} \right)^2 \right] \\
\mathcal{S}_K &\equiv \lambda \int d^d x d\tau \left[\vec{s}_c(\vec{x},\tau) \cdot \vec{\varphi}(\vec{x},\tau) \right] \\
\mathcal{S}_c &\equiv \int d^d K d\varepsilon \sum_\sigma \psi_\sigma^\dagger(\vec{K}, i\varepsilon) \left(i\varepsilon - \xi_K \right) \psi_\sigma(\vec{K}, i\varepsilon) + \lambda^2 \int \psi^4
\end{aligned}
\tag{3.3}
$$

where $\xi_K \equiv v_F(K - K_F)$. The Berry phase term for the $\vec{n}$ field, $\mathcal{S}_{\text{Berry}}$, is not important inside the Néel phase, which is very different from the ferromagnetic case to be discussed in a later chapter. What is meant by "the Berry phase" requires some clarification. Certainly some aspects of the geometric term do indeed contribute to the physics, but this will be spelled-out in the next section. We have introduced a vector boson field $\vec{\varphi}$ which is shorthand for $\vec{n} \times \frac{\partial \vec{n}}{\partial \tau}$. The $\vec{n}$ field satisfies the constraint

$\vec{n}^2 = 1$, which is solved by $\vec{n} = (\vec{\pi}, \sigma)$, where $\vec{\pi}$ labels the Goldstone magnons and $\sigma \equiv \sqrt{1 - \vec{\pi}^2}$ is the massive field. We will consider the case of a spherical Fermi surface; since only forward scattering is important, our results will apply for more complicated Fermi-surface geometries. The parameters for the QNLσM will be considered as phenomenological [52], though they can be explicitly written in terms of the microscopic parameters. The effective Kondo coupling is $\lambda = iJ_K/(4dIa^d)$, which will be explicitly demonstrated below.

This summarizes the structure and setup of the effective field theory for the antiferromagnetic phase of the Kondo Lattice Model. We now describe the details of how this is done.
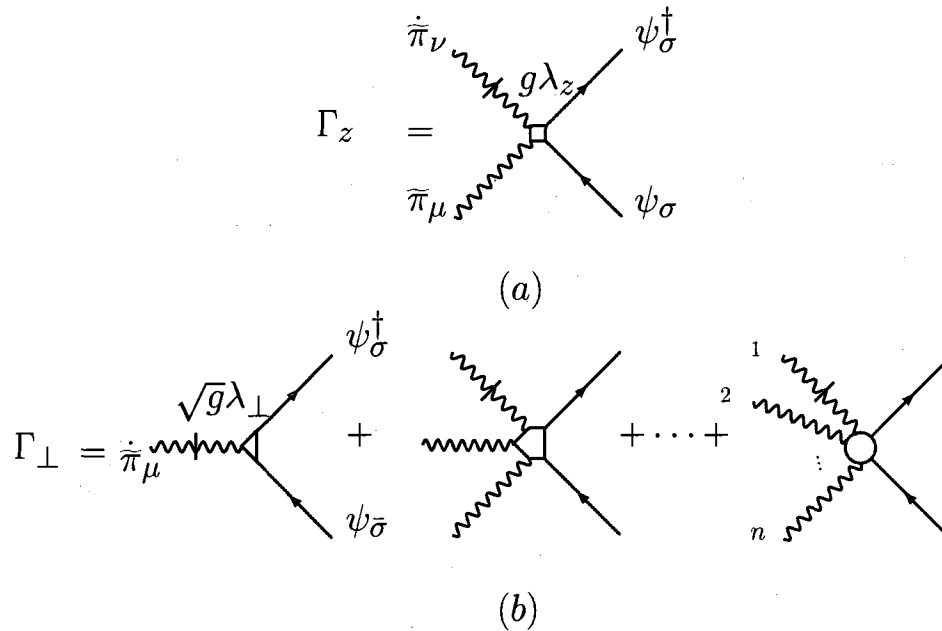
Figure 3.2 : The Feynman rules associate wavy lines with magnons ($\widetilde{\pi}$ fields), and solid straight lines with itinerant electrons (ψ fields). A slash through a boson line indicates a time derivative (i.e. $\dot{\widetilde{\pi}}$). (a) represents the four diagrams in Γ_z. (b) describes the infinite number of spin-flip vertices, $\Gamma_\perp$, involving an odd number of magnons.

3.2 Coherent State Representation of the Partition Function

In this and the next sections, we set up our notations by considering in some detail the standard case of the Heisenberg model. This will help us perform the analgous mapping for the Kondo lattice model, which is essentially the same but includes conduction electron coupling. We will focus on a square lattice with nearest-neighbor (nn) and next-nearest-neighbor (nnn) spin-exchange interactions, I_1 and I_2 respectively.

$$
\begin{aligned}
H &= \sum_{i,j} I_{ij} \mathbf{S}_i \cdot \mathbf{S}_j \\
&= I_1 \sum_{\langle ij \rangle}^{nn} \mathbf{S}_i \cdot \mathbf{S}_j + I_2 \sum_{\langle\langle ij \rangle\rangle}^{nnn} \mathbf{S}_i \cdot \mathbf{S}_j \\
&= I_1 \sum_{x,\alpha} \mathbf{S}_x \cdot \mathbf{S}_{x+\alpha} + I_2 \sum_{x,\beta} \mathbf{S}_x \cdot \mathbf{S}_{x+\beta}
\end{aligned}
\tag{3.4}
$$

where x runs over all lattice sites, α runs over the nn sites for each lattice site x, and β runs over nnn sites for each site x. After the mapping is completed, it will be clear that the coupling constant g of the quantum non-linear sigma model (QNLσM) can be tuned by changing I_1 and I_2.

The coherent state spin path integral representation of the partition function for quantum spin systems is now a standard formalism that can be found in textbooks (e.g. [54, 55]). We will briefly sketch the main idea. The partition function can be written

$$
Z = \mathrm{Tr}\, e^{-\beta H} = \lim_{M \to \infty} \int \mathcal{D}\Lambda(\tau) \prod_{k=1}^{M-1} \langle \Lambda(\tau_{k+1}) | 1 - \epsilon H | \Lambda(\tau_k) \rangle
\tag{3.5}
$$

where the many-particle basis is a direct product of single-site spin coherent states: $|\Lambda(\tau)\rangle \equiv \prod_x |\Omega_x(\tau)\rangle$. Here M is the number of discrete time slices in the Trotter decomposition, and $\epsilon = \beta/M$. Recall that at each lattice site, $\langle \Omega | \mathbf{S} | \Omega \rangle = S\Omega$, where the

unit spin vector is represented by $\boldsymbol{\Omega} = \frac{1}{\sqrt{S(S+1)}}\mathbf{S} \approx \mathbf{S}/S = (\cos\phi\sin\theta, \sin\phi\sin\theta, \cos\theta)$. Using this (overcomplete) basis, the matrix elements of the Heisenberg Hamiltonian can thus be written, to leading order in ϵ,

$$
\begin{aligned}
\langle\boldsymbol{\Lambda}(\tau_{k+1})|H|\boldsymbol{\Lambda}(\tau_k)\rangle &= S^2\langle\boldsymbol{\Lambda}(\tau_{k+1})|\boldsymbol{\Lambda}(\tau_k)\rangle \\
&\times \left(I_1\sum_{x,\alpha}\boldsymbol{\Omega}_x(\tau_k)\cdot\boldsymbol{\Omega}_{x+\alpha}(\tau_k) + I_2\sum_{x,\beta}\boldsymbol{\Omega}_x(\tau_k)\cdot\boldsymbol{\Omega}_{x+\beta}(\tau_k) \right)
\end{aligned}
\tag{3.6}
$$

This allows us to write the Hamiltonian in terms of classical variables $\boldsymbol{\Omega}_x$. To linear order in ϵ,

$$
\langle\boldsymbol{\Lambda}(\tau_{k+1})|(1-\epsilon H)|\boldsymbol{\Lambda}(\tau_k)\rangle = \langle\boldsymbol{\Lambda}(\tau_{k+1})|\boldsymbol{\Lambda}(\tau_k)\rangle e^{-\epsilon H_{cl}(\tau_k)}
\tag{3.7}
$$

where

$$
H_{cl}(\tau) \equiv S^2 I_1\sum_{x,\alpha}\boldsymbol{\Omega}_x(\tau)\cdot\boldsymbol{\Omega}_{x+\alpha}(\tau) + S^2 I_2\sum_{x,\beta}\boldsymbol{\Omega}_x(\tau)\cdot\boldsymbol{\Omega}_{x+\beta}(\tau)
\tag{3.8}
$$

The penalty for the classical representation is the additional overlap $\langle\boldsymbol{\Lambda}(\tau_{k+1})|\boldsymbol{\Lambda}(\tau_k)\rangle$ which is the Berry phase accumulated from the adiabatic evolution from the time-slice τ_k to τ_{k+1}. Including the Berry phase accounts for quantum corrections, and is crucial to obtain the proper mapping to the QNLσM. We can write it more clearly as follows:

$$
\begin{aligned}
\langle\boldsymbol{\Lambda}(\tau_{k+1})|\boldsymbol{\Lambda}(\tau_k)\rangle &= \prod_{x,x'}\langle\boldsymbol{\Omega}_x(\tau_{k+1})|\boldsymbol{\Omega}_{x'}(\tau_k)\rangle
\end{aligned}
\tag{3.9}
$$

$$
= \prod_{x}\langle\boldsymbol{\Omega}_x(\tau_{k+1})|\boldsymbol{\Omega}_x(\tau_k)\rangle
\tag{3.10}
$$

$$
= \prod_{x}e^{-iS[1-\cos\theta_x(\tau_k)][\phi_x(\tau_{k+1})-\phi_x(\tau_k)]}
\tag{3.11}
$$

In the partition function we need an infinite product of such overlaps, which leads to

a continuum representation in imaginary time

$$\lim_{M\to\infty} \prod_{k=1}^{M-1} \langle \Lambda(\tau_{k+1}) | \Lambda(\tau_k) \rangle \;=\; \lim_{M\to\infty} \prod_{x,k} e^{-iS[1-\cos\theta_x(\tau_k)][\phi_x(\tau_{k+1})-\phi_x(\tau_k)]}$$

$$=\; \lim_{M\to\infty} e^{-iS\sum_{x,k}[1-\cos\theta_x(\tau_k)][\phi_x(\tau_{k+1})-\phi_x(\tau_k)]}$$

$$=\; e^{-iS\sum_x \int_0^\beta d\tau[1-\cos\theta_x(\tau)]\frac{d\phi_x}{d\tau}}$$

$$=\; e^{-iS\sum_x \omega(\Omega_x)} \tag{3.12}$$

where $\omega(\Omega_x) = \int_0^\beta d\tau[1 - \cos\theta_x(\tau)]\frac{d\phi_x}{d\tau}$ is the Berry phase for a single spin at site x. We have represented it with a set of parameters θ_x and ϕ_x for familiarity, but this need not be specified. The important thing to note is that the total Berry phase contribution to the action in the path integral is given by the sum of the Berry phases of all the lattice site spins: $\mathcal{S}_B = iS\sum_x \omega(\Omega_x)$. A convenient representation for the Berry phase of a single spin is given by

$$\omega(\Omega) \;=\; \int_0^\beta d\tau \int_0^1 du \left[\Omega(\tau,u) \cdot \frac{\partial\Omega(\tau,u)}{\partial u} \times \frac{\partial\Omega(\tau,u)}{\partial\tau} \right] \tag{3.13}$$

where by convention $\Omega(\tau, u = 1) = \Omega(\tau)$ and $\Omega(\tau, u = 0) = (0,0,1) = |0\rangle = |S, m = S\rangle$ (see [9] p. 244). [In technical jargon, $\Omega(\tau, u)$ is a homotopy of $\Omega(\tau)$.]

Now, in a similar way to what was done above for the Berry phase, we can take the continuum limit to express the Hamiltonian term, H_{cl}, as an integration over imaginary time. The partition function then becomes

$$Z \;=\; \int \mathcal{D}\Lambda(\tau) e^{-\mathcal{S}} \tag{3.14}$$

$$\mathcal{S} \;=\; \mathcal{S}_B + \int_0^\beta d\tau H_{cl}(\tau) \tag{3.15}$$

$$\mathcal{S}_B \;=\; iS\sum_x \int_0^\beta d\tau \int_0^1 du \left[\Omega_x(\tau,u) \cdot \frac{\partial\Omega_x(\tau,u)}{\partial u} \times \frac{\partial\Omega_x(\tau,u)}{\partial\tau} \right] \tag{3.16}$$

$$H_{cl}(\tau) \;=\; S^2 I_1 \sum_{x,\alpha}^{nn} \Omega_x(\tau) \cdot \Omega_{x+\alpha}(\tau) + S^2 I_2 \sum_{x,\beta}^{nnn} \Omega_x(\tau) \cdot \Omega_{x+\beta}(\tau) \tag{3.17}$$

3.3 QNLσM Mapping for the Heisenberg Model

We assume an antiferromagnetic order in which case we can represent each spin as the sum of a staggered component $\mathbf{n}_x$ representing the local Neel field, and uniform ($q \approx 0$) fluctuations $\mathbf{L}_x$,

$$\boldsymbol{\Omega}_x(\tau) \equiv \eta_x \mathbf{n}_x(\tau) \sqrt{1 - \left(\frac{a^d}{S}\mathbf{L}_x(\tau)\right)^2} + \frac{a^d}{S}\mathbf{L}_x(\tau) \tag{3.18}$$

The factor $\eta_x \in \pm 1$ is either positive or negative, depending on which sublattice x falls in, while the factor a^d/S in front of the uniform fluctuation field $\mathbf{L}$ ensures that integrating around any small volume will yield the total magnetization contained in that volume. Here a is the lattice constant. Recall that the spin variable is constrained by the condition $\boldsymbol{\Omega}_x \cdot \boldsymbol{\Omega}_x = 1$ at each site. With the above choice, this constraint now becomes $\mathbf{n}_x \cdot \mathbf{n}_x = 1$ and $\mathbf{n}_x \cdot \mathbf{L}_x = 0$. Note that the total number of degrees of freedom in the system remains the same because in the $\mathbf{n}$, $\mathbf{L}$ representation we must restrict ourselves to the magnetic Brillouin zone; there are twice as many degrees of freedom on half as many sites.

We now wish to write the action in terms of $\mathbf{n}$ and $\mathbf{L}$ rather than $\boldsymbol{\Omega}$. We will consider the Berry phase first, then the H_{cl} term.

3.3.1 Berry phase

Let us first consider what happens when we substitute this expression for the spin into the Berry phase part of the action. We need the expressions for the τ and u derivatives:

$$\frac{\partial \boldsymbol{\Omega}_x}{\partial u} \equiv \boldsymbol{\Omega}_u = \eta\gamma\mathbf{n}_u - \frac{\eta}{\gamma}\frac{a^d}{S}(\mathbf{L}\cdot\mathbf{L}_u)\mathbf{n} + \frac{a^d}{S}\mathbf{L}_u \tag{3.19}$$

$$\frac{\partial \boldsymbol{\Omega}_x}{\partial \tau} \equiv \boldsymbol{\Omega}_\tau = \eta\gamma\mathbf{n}_\tau - \frac{\eta}{\gamma}\frac{a^d}{S}(\mathbf{L}\cdot\mathbf{L}_\tau)\mathbf{n} + \frac{a^d}{S}\mathbf{L}_\tau \tag{3.20}$$

where we temporarily dropped the site index, x, and instead use subscripts to denote differentiation. We have also defined $\gamma \equiv \sqrt{1 - \left(\frac{a^d}{S}\mathbf{L}\right)^2}$. Plugging this into equation (3.16):

$$
\begin{aligned}
\mathcal{S}_B &= iS\sum_x \int_0^\beta d\tau \int_0^1 du \left[\left(\eta\gamma\mathbf{n} + \frac{a^d}{S}\mathbf{L}\right) \cdot \left(\eta^2\gamma^2\mathbf{n}_u \times \mathbf{n}_\tau - \eta^2\frac{a^d}{S}(\mathbf{L}\cdot\mathbf{L}_u)\mathbf{n}_u \times \mathbf{n}\right.\right. \\
&\quad \left. +\eta\gamma\frac{a^d}{S}\mathbf{n}_u \times \mathbf{L}_\tau \right. \\
&\quad \left. -\eta^2\frac{a^d}{S}(\mathbf{L}\cdot\mathbf{L}_u)\mathbf{n} \times \mathbf{n}_\tau + \frac{\eta^2 a^{2d}}{\gamma^2 S^2}(\mathbf{L}\cdot\mathbf{L}_u)(\mathbf{L}\cdot\mathbf{L}_\tau)\mathbf{n} \times \mathbf{n} - \frac{\eta}{\gamma}\frac{a^{2d}}{S^2}(\mathbf{L}\cdot\mathbf{L}_u)\mathbf{n} \times \mathbf{L}_\tau \right. \\
&\quad \left.\left. +\eta\gamma\frac{a^d}{S}\mathbf{L}_u \times \mathbf{n}_\tau - \frac{\eta}{\gamma}\frac{a^{2d}}{S^2}(\mathbf{L}\cdot\mathbf{L}_\tau)\mathbf{L}_u \times \mathbf{n} + \frac{a^{2d}}{S^2}\mathbf{L}_u \times \mathbf{L}_\tau\right)\right] \quad (3.21)
\end{aligned}
$$

To simplify this equation requires knowing that $\mathbf{n}_u$, $\mathbf{n}_\tau$ and $\mathbf{L}$ are all perpendicular to $\mathbf{n}$. This means their triple product must vanish: $\mathbf{L}\cdot\mathbf{n}_u \times \mathbf{n}_\tau = 0$. We also neglect terms higher than linear order in $\mathbf{L}$ [terms quadratic in $\mathbf{L}$ are small compared to those kept in Eq. (3.32)], leading to

$$
\mathcal{S}_B \approx iS\sum_x \int_0^\beta d\tau \int_0^1 du \left[\eta^3\gamma^3\mathbf{n}\cdot\mathbf{n}_u \times \mathbf{n}_\tau + \eta^2\gamma^2\frac{a^d}{S}\mathbf{n}\cdot(\mathbf{n}_u \times \mathbf{L}_\tau + \mathbf{L}_u \times \mathbf{n}_\tau)\right] \quad (3.22)
$$

Note also that $\eta_x^2 = 1$ and $\eta_x^3 = \eta_x$. We then obtain

$$
\begin{aligned}
\mathcal{S}_B &\approx iS\sum_x \int_0^\beta d\tau \int_0^1 du \left[\eta\mathbf{n}\cdot\mathbf{n}_u \times \mathbf{n}_\tau + \frac{a^d}{S}\mathbf{n}\cdot(\mathbf{n}_u \times \mathbf{L}_\tau + \mathbf{L}_u \times \mathbf{n}_\tau)\right] \\
&= iS\sum_x \int_0^\beta d\tau \int_0^1 du \left[\eta_x\mathbf{n}_x\cdot\frac{\partial\mathbf{n}_x}{\partial u} \times \frac{\partial\mathbf{n}_x}{\partial\tau} + \frac{a^d}{S}\mathbf{n}_x\cdot\left(\frac{\partial\mathbf{n}_x}{\partial u} \times \frac{\partial\mathbf{L}_x}{\partial\tau}\right.\right. \\
&\quad \left.\left. +\frac{\partial\mathbf{L}_x}{\partial u} \times \frac{\partial\mathbf{n}_x}{\partial\tau}\right)\right] \\
&= iS\sum_x \int_0^\beta d\tau \int_0^1 du \left[\eta_x\mathbf{n}_x\cdot\frac{\partial\mathbf{n}_x}{\partial u} \times \frac{\partial\mathbf{n}_x}{\partial\tau} + \frac{a^d}{S}\frac{\partial}{\partial\tau}\left(\mathbf{n}_x\cdot\frac{\partial\mathbf{n}_x}{\partial u} \times \mathbf{L}_x\right)\right. \\
&\quad \left. +\frac{a^d}{S}\frac{\partial}{\partial u}\left(\mathbf{n}_x\cdot\mathbf{L}_x \times \frac{\partial\mathbf{n}_x}{\partial\tau}\right)\right] \quad (3.23)
\end{aligned}
$$

In the second line we have restored the full notation, while the third line can be written with total derivatives since the terms proportional to $\frac{\partial^2 \mathbf{n}}{\partial \tau \partial u}$ cancel thanks to the triple product identity $\zeta \cdot \mathbf{b} \times \mathbf{c} = -\mathbf{b} \cdot \zeta \times \mathbf{c}$. The second term in the third line vanishes after integrating the total τ derivative and using the periodicity of the fields. The third term in the third line can be integrated over u, and the value at $u = 0$ is zero due to the orthogonality at the north pole. We finally find,

$$
\mathcal{S}_B = iS \sum_x \eta_x \int_0^\beta d\tau \int_0^1 du \left(\mathbf{n}_x \cdot \frac{\partial \mathbf{n}_x}{\partial u} \times \frac{\partial \mathbf{n}_x}{\partial \tau} \right) - i \sum_x a^d \int_0^\beta d\tau \left(\mathbf{L}_x \cdot \mathbf{n}_x \times \frac{\partial \mathbf{n}_x}{\partial \tau} \right)
$$

$$(3.24)$$

The first term is precisely the Berry phase for the Neel component $\mathbf{n}$, while the second term is something additional that must be added to the total action. Although both terms came from the expression for the Berry phase of $\boldsymbol{\Omega}$, it is only the first term that is often referred to as the Berry phase for the antiferromagnet.

3.3.2 Hamiltonian

Next we compute the contribution to the action from the Hamiltonian $H_{cl}(\tau)$ expressed in terms of $\mathbf{n}$ and $\mathbf{L}$ fields. Plugging (3.18) into (3.17),

$$
\begin{aligned}
H_{cl}(\tau) &= S^2 I_1 \sum_{x,\alpha}^{nn} \left[\eta_x \mathbf{n}_x(\tau) \sqrt{1 - \left(\frac{a^d}{S}\mathbf{L}_x(\tau)\right)^2} + \frac{a^d}{S}\mathbf{L}_x(\tau) \right] \\
&\quad \cdot \left[\eta_{x+\alpha}\mathbf{n}_{x+\alpha}(\tau)\sqrt{1 - \left(\frac{a^d}{S}\mathbf{L}_{x+\alpha}(\tau)\right)^2} + \frac{a^d}{S}\mathbf{L}_{x+\alpha}(\tau) \right] \\
&\quad + S^2 I_2 \sum_{x,\beta}^{nnn} \left[\eta_x \mathbf{n}_x(\tau)\sqrt{1 - \left(\frac{a^d}{S}\mathbf{L}_x(\tau)\right)^2} + \frac{a^d}{S}\mathbf{L}_x(\tau) \right] \\
&\quad \cdot \left[\eta_{x+\beta}\mathbf{n}_{x+\beta}(\tau)\sqrt{1 - \left(\frac{a^d}{S}\mathbf{L}_{x+\beta}(\tau)\right)^2} + \frac{a^d}{S}\mathbf{L}_{x+\beta}(\tau) \right] \\
&\approx S^2 I_1 \sum_{x,\alpha}^{nn} \left[\eta_x \mathbf{n}_x(\tau)\left(1 - \frac{1}{2}\left(\frac{a^d}{S}\mathbf{L}_x(\tau)\right)^2\right) + \frac{a^d}{S}\mathbf{L}_x(\tau) \right] \\
&\quad \cdot \left[\eta_{x+\alpha}\mathbf{n}_{x+\alpha}(\tau)\left(1 - \frac{1}{2}\left(\frac{a^d}{S}\mathbf{L}_{x+\alpha}(\tau)\right)^2\right) + \frac{a^d}{S}\mathbf{L}_{x+\alpha}(\tau) \right] \\
&\quad + S^2 I_2 \sum_{x,\beta}^{nnn} \left[\eta_x \mathbf{n}_x(\tau)\left(1 - \frac{1}{2}\left(\frac{a^d}{S}\mathbf{L}_x(\tau)\right)^2\right) + \frac{a^d}{S}\mathbf{L}_x(\tau) \right] \\
&\quad \cdot \left[\eta_{x+\beta}\mathbf{n}_{x+\beta}(\tau)\left(1 - \frac{1}{2}\left(\frac{a^d}{S}\mathbf{L}_{x+\beta}(\tau)\right)^2\right) + \frac{a^d}{S}\mathbf{L}_{x+\beta}(\tau) \right]
\end{aligned}
$$

$$(3.25)$$

Since $\mathbf{n}$ is a unit vector, we have the identity $\mathbf{n}_x \cdot \mathbf{n}_y = 1 - \frac{1}{2}(\mathbf{n}_x - \mathbf{n}_y) \cdot (\mathbf{n}_x - \mathbf{n}_y)$. We also know that at every site $\mathbf{n}_x \cdot \mathbf{L}_x = 0$. Using these two identities and dropping the

τ label for brevity, the Hamiltonian can be expressed as follows:

$$
\begin{aligned}
H_{cl} =\ & S^2 I_1 \sum_{x,\alpha} \Bigg\{ \eta_x \eta_{x+\alpha} \left[1 - \frac{1}{2}(\mathbf{n}_x - \mathbf{n}_y) \cdot (\mathbf{n}_x - \mathbf{n}_y) \right] \left[1 - \frac{a^{2d}}{2S^2}(\mathbf{L}_x^2 + \mathbf{L}_{x+\alpha}^2) \right] \\
& + \frac{a^d}{2S^2} \eta_x \mathbf{n}_x \cdot (\mathbf{L}_{x+\alpha} - \mathbf{L}_x) + \frac{a^d}{2S^2} \eta_{x+\alpha} \mathbf{n}_{x+\alpha} \cdot (\mathbf{L}_x - \mathbf{L}_{x+\alpha}) \\
& + \frac{a^{2d}}{2S^2} \left[\mathbf{L}_x^2 + \mathbf{L}_{x+\alpha}^2 - (\mathbf{L}_x - \mathbf{L}_{x+\alpha})^2 \right] \Bigg\} \\
& + S^2 I_2 \sum_{x,\beta} \Bigg\{ \eta_x \eta_{x+\beta} \left[1 - \frac{1}{2}(\mathbf{n}_x - \mathbf{n}_y) \cdot (\mathbf{n}_x - \mathbf{n}_y) \right] \left[1 - \frac{a^{2d}}{2S^2}(\mathbf{L}_x^2 + \mathbf{L}_{x+\beta}^2) \right] \\
& + \frac{a^d}{2S^2} \eta_x \mathbf{n}_x \cdot (\mathbf{L}_{x+\beta} - \mathbf{L}_x) + \frac{a^d}{2S^2} \eta_{x+\beta} \mathbf{n}_{x+\beta} \cdot (\mathbf{L}_x - \mathbf{L}_{x+\beta}) \\
& + \frac{a^{2d}}{2S^2} \left[\mathbf{L}_x^2 + \mathbf{L}_{x+\beta}^2 - (\mathbf{L}_x - \mathbf{L}_{x+\beta})^2 \right] \Bigg\}
\end{aligned} \tag{3.26}
$$

where we used $2\mathbf{L}_x \cdot \mathbf{L}_{x+\alpha} = \mathbf{L}_x^2 + \mathbf{L}_{x+\alpha}^2 - (\mathbf{L}_x - \mathbf{L}_{x+\alpha})^2$ and similarly for β. We have written the expression in this way in order to take advantage of a Taylor series between different lattice sites:

$$
n_{x+\alpha}^b - n_x^b \approx a(\vec{\alpha} \cdot \nabla) n_x^b + \cdots \tag{3.27}
$$

$$
n_{x+\beta}^b - n_x^b \approx a\sqrt{2}(\vec{\beta} \cdot \nabla) n_x^b + \cdots \tag{3.28}
$$

where b runs over the components of the vector field. Note that nearest neighbor (nn) sites x and $x + \alpha$ are separated by a distance a, while next nearest neighbor (nnn) sites x and $x + \beta$ are separated by a distance $a\sqrt{2}$. Expressing all lattice differences

in this way leads to:

$$
\begin{aligned}
H_{cl} = {} & S^2 I_1 \sum_{x,\alpha} \Bigg\{ \eta_x \eta_{x+\alpha} \left[1 - \frac{a^2}{2} [(\vec{\alpha} \cdot \nabla) n_x^b]^2 \right] \\
& + \frac{a^{2d}}{2S^2} \left[(1 - \eta_x \eta_{x+\alpha})(\mathbf{L}_x^2 + \mathbf{L}_{x+\alpha}^2) - a^2 [(\vec{\alpha} \cdot \nabla) L_x^b]^2 \right] \\
& + \frac{a^{d+1}}{S^2} \left[\eta_x n_x^b \nabla L_x^b - \eta_{x+\alpha} n_{x+\alpha}^b \nabla L_{x+\alpha}^b \right] \Bigg\} \\
& + S^2 I_2 \sum_{x,\beta} \Bigg\{ \eta_x \eta_{x+\beta} \left[1 - \frac{2a^2}{2} [(\vec{\beta} \cdot \nabla) n_x^b]^2 \right] \\
& + \frac{a^{2d}}{2S^2} \left[(1 - \eta_x \eta_{x+\beta})(\mathbf{L}_x^2 + \mathbf{L}_{x+\beta}^2) - 2a^2 [(\vec{\beta} \cdot \nabla) L_x^b]^2 \right] \\
& + \frac{a^{d+1}\sqrt{2}}{S^2} \left[\eta_x n_x^b \nabla L_x^b - \eta_{x+\beta} n_{x+\beta}^b \nabla L_{x+\beta}^b \right] \Bigg\}
\end{aligned}
\tag{3.29}
$$

After summing over lattices sites and neighbors, each term proportional to a^{d+1} sums to zero, so,

$$
\begin{aligned}
H_{cl} = {} & S^2 I_1 \sum_{x,\alpha} \Bigg\{ \eta_x \eta_{x+\alpha} \left[1 - \frac{a^2}{2} [(\vec{\alpha} \cdot \nabla) n_x^b]^2 \right] \\
& + \frac{a^{2d}}{2S^2} \left[(1 - \eta_x \eta_{x+\alpha})(\mathbf{L}_x^2 + \mathbf{L}_{x+\alpha}^2) - a^2 [(\vec{\alpha} \cdot \nabla) L_x^b]^2 \right] \Bigg\} \\
& + S^2 I_2 \sum_{x,\beta} \Bigg\{ \eta_x \eta_{x+\beta} \left[1 - a^2 [(\vec{\beta} \cdot \nabla) n_x^b]^2 \right] \\
& + \frac{a^{2d}}{2S^2} \left[(1 - \eta_x \eta_{x+\beta})(\mathbf{L}_x^2 + \mathbf{L}_{x+\beta}^2) - 2a^2 [(\vec{\beta} \cdot \nabla) L_x^b]^2 \right] \Bigg\}
\end{aligned}
\tag{3.30}
$$

Now, to our order of approximation, $\mathbf{L}_{x+\alpha}^2 \approx \mathbf{L}_x^2$. Also, since α runs over nearest-neighbors, while β runs over next-nearest-neighbors, we have $\eta_x \eta_{x+\alpha} = -1$ and $\eta_x \eta_{x+\beta} = +1$. On the square lattice, the number of nn and nnn sites is $2d$, and

to avoid double counting we divide by 2.

$$
\begin{aligned}
H_{cl} &= S^2 I_1 d \sum_x \left\{ -1 + \frac{a^2}{2d} (\nabla \mathbf{n}_x)^2 + \frac{a^{2d}}{2S^2} \left[4 \mathbf{L}_x^2 - \frac{a^2}{d} (\nabla \mathbf{L}_x)^2 \right] \right\} \\
&\quad + S^2 I_2 d \sum_x \left\{ 1 - \frac{a^2}{d} (\nabla \mathbf{n}_x)^2 + \frac{a^{2d}}{2S^2} \left[-\frac{2a^2}{d} (\nabla \mathbf{L}_x)^2 \right] \right\}
\end{aligned}
$$

$$(3.31)$$

Note that $(\nabla \mathbf{n}_x)^2$ should be interpreted as $\sum_{\mu=1}^{d} \sum_{b=1}^{N} \left(\frac{\partial n_x^b}{\partial x^\mu} \right)^2$. We also used $\sum_{x,\alpha} [(\vec{\alpha} \cdot \nabla) n_x^b]^2 = \sum_x [(\frac{\partial}{\partial x} + \frac{\partial}{\partial y} + \frac{\partial}{\partial z}) n_x^b]^2 = \sum_x (\nabla \mathbf{n}_x)^2$, and similarly for β and $\mathbf{L}$ terms.

To be consistent with our expansion in small powers of a and $1/S$ we should also ignore gradient terms like $(\nabla \mathbf{L})^2$. The expression simplifies to

$$
\begin{aligned}
H_{cl} &= S^2 d \sum_x \left\{ I_2 - I_1 + \frac{a^2}{2d} (I_1 - 2I_2)(\nabla \mathbf{n}_x)^2 + \frac{2 I_1 a^{2d}}{S^2} \mathbf{L}_x^2 \right\} \\
&= S^2 d \mathcal{N}_{site} (I_2 - I_1) + S^2 \frac{a^2}{2} (I_1 - 2I_2) \sum_x (\nabla \mathbf{n}_x)^2 + 2 d I_1 a^{2d} \sum_x \mathbf{L}_x^2 \quad (3.32)
\end{aligned}
$$

Finally, we take the continuum limit with the correspondence $\sum_x \to a^{-d} \int d^d x$,

$$
H_{cl}(\tau) = const_1 + S^2 a^{2-d} (I_1/2 - I_2) \int d^d x \, (\nabla \mathbf{n}(\vec{x}, \tau))^2 + 2 d I_1 a^d \int d^d x \mathbf{L}^2(\vec{x}, \tau)
$$

$$(3.33)$$

We have introduced the constant factor $const_1 \equiv \mathcal{N}_{site} d S^2 (I_2 - I_1)$ which is unimportant for our purposes.

3.3.3 Completing the square and the QNLσM mapping

At this point the total action is given by

$$Z \;\; = \;\; \int \mathcal{D}\mathbf{n}\mathcal{D}\mathbf{L}\; \delta(\mathbf{n}^2 - 1)\delta(\mathbf{n} \cdot \mathbf{L})e^{-\mathcal{S}[\mathbf{n},\mathbf{L}]} \tag{3.34}$$

$$\mathcal{S}[\mathbf{n}, \mathbf{L}] \;\; = \;\; const_1 + \mathcal{S}'_B[\mathbf{n}] + S^2 a^{2-d}(I_1/2 - I_2)\int_0^\beta d\tau \int d^d x\, (\nabla \mathbf{n}(\vec{x},\tau))^2$$

$$+2dI_1 a^d \int_0^\beta d\tau \int d^d x \mathbf{L}^2(\vec{x},\tau)$$

$$-i\int_0^\beta d\tau \int d^d x \left(\mathbf{L}(\vec{x},\tau) \cdot \mathbf{n}(\vec{x},\tau) \times \frac{\partial \mathbf{n}(\vec{x},\tau)}{\partial \tau} \right) \tag{3.35}$$

$$\mathcal{S}'_B[\mathbf{n}] \;\; \equiv \;\; iS\sum_x \eta_x \int_0^\beta d\tau \int_0^1 du \left(\mathbf{n}_x \cdot \frac{\partial \mathbf{n}_x}{\partial u} \times \frac{\partial \mathbf{n}_x}{\partial \tau} \right) \tag{3.36}$$

where the Berry phase $\mathcal{S}'_B[\mathbf{n}]$ now only depends on the $\mathbf{n}$ field. The delta functionals enforce the local constraints. To deal with them, we use the integral representation of the delta functional and introduce a scalar Lagrange multiplier field $\alpha(\vec{x},\tau)$:

$$\delta(\mathbf{n} \cdot \mathbf{L}) \;\; = \;\; \int \mathcal{D}\alpha\; e^{-\int_0^\beta d\tau \int d^d x\; i\alpha(\vec{x},\tau)\mathbf{n}(\vec{x},\tau)\cdot \mathbf{L}(\vec{x},\tau)} \tag{3.37}$$

It is now clear that the functional integral is Gaussian with respect to $\mathbf{L}$, so we may "complete the square" and integrate it out completely. If we use the identity $\int \mathcal{D}\mathbf{L}e^{\int -\zeta \mathbf{L}^2 + \mathbf{b}\cdot \mathbf{L}} = \pi^{M/2}(\det \zeta)^{-1/2}e^{\mathbf{b}^2/4\zeta}$, the correspondence is $\zeta = 2dI_1 a^d$ and $\mathbf{b} = i\mathbf{n} \times \dot{\mathbf{n}} - i\alpha\,\mathbf{n}$. We also need the quadruple vector product identity $(\mathbf{n} \times \dot{\mathbf{n}})^2 = \dot{\mathbf{n}}^2\mathbf{n}^2 - (\dot{\mathbf{n}} \cdot \mathbf{n})^2$, and the relations $\dot{\mathbf{n}} \cdot \mathbf{n} = 0$ and $\mathbf{n}^2 = 1$ and $\mathbf{n} \cdot \mathbf{n} \times \dot{\mathbf{n}} = 0$. This leads

to $\frac{b^2}{4\zeta} = -\frac{1}{8dI_1a^d}(\dot{n}^2 + \alpha^2)$, and hence

$$Z = \int \mathcal{D}n\mathcal{D}\alpha\, \delta(n^2 - 1)e^{-\mathcal{S}[n,\alpha]} \tag{3.38}$$

$$\mathcal{S}[n,\alpha] = \beta\,const_1 - \frac{1}{2}\log\frac{\pi^M}{2dI_1a^d} + S^2a^{2-d}(I_1/2 - I_2)\int_0^\beta d\tau \int d^dx\,(\nabla n(\vec{x},\tau))^2$$

$$+\frac{1}{8dI_1a^d}\int_0^\beta d\tau \int d^dx\left[\left(\frac{\partial n(\vec{x},\tau)}{\partial\tau}\right)^2 + \alpha^2(\vec{x},\tau)\right] + \mathcal{S}'_B[n]$$

$$\equiv const_2 + \mathcal{S}'_B[n] + \frac{c}{2g}\int_0^\beta d\tau \int d^dx\left[(\nabla n(\vec{x},\tau))^2 + \frac{1}{c^2}\left(\frac{\partial n(\vec{x},\tau)}{\partial\tau}\right)^2\right]$$

$$+\frac{1}{2gc}\int_0^\beta d\tau \int d^dx\, \alpha^2(\vec{x},\tau) \tag{3.39}$$

where we have defined

$$c \equiv 2aSI_1\sqrt{d}\sqrt{\frac{I_1 - 2I_2}{I_1}} \tag{3.40}$$

$$g \equiv \frac{2a^{d-1}\sqrt{d}}{S}\sqrt{\frac{I_1}{I_1 - 2I_2}} \tag{3.41}$$

$$const_2 \equiv \beta\,const_1 - \frac{1}{2}\log\frac{\pi^M}{2dI_1a^d} \tag{3.42}$$

Recall that M is the number of time slices and may be considered to be of order $\mathcal{N}_{site}$.

All that remains is to perform the gaussian integral over α: $\int \mathcal{D}\alpha\, e^{-\frac{1}{2gc}\int \alpha^2} = \sqrt{2gc\pi^M} = e^{(1/2)\log(2gc\pi^M)}$. Our final answer becomes:

$$Z = \int \mathcal{D}n\, \delta(n^2 - 1)e^{-\mathcal{S}[n]} \tag{3.43}$$

$$\mathcal{S}[n] = const_3 + \mathcal{S}'_B[n] + \frac{c}{2g}\int_0^\beta d\tau \int d^dx\left[(\nabla n(\vec{x},\tau))^2 + \frac{1}{c^2}\left(\frac{\partial n(\vec{x},\tau)}{\partial\tau}\right)^2\right] \tag{3.44}$$

where $const_3 \equiv const_2 - \frac{1}{2}\log(2gc\pi^M) = \beta\mathcal{N}_{site}S^2d(I_2 - I_1) - \log(2\pi^M)$. These results for the constants c and g agree with [56] who considered first, second and third neighbor couplings. Clearly, by adjusting I_1 and I_2 we can tune g. This model

can also be expressed in terms of the spin-wave stiffness and transverse magnetic susceptibility. They are given by

$$\rho_s = \frac{c}{g} = S^2 a^{2-d}(I_1 - 2I_2) \tag{3.45}$$

$$\chi_\perp = \frac{1}{cg} = \frac{1}{4a^d I_1 d} \tag{3.46}$$

Notice that $\chi_\perp$ is independent of I_2, which means that nnn interactions do not renormalize the transverse magnetic susceptibility.

3.4 QNLσM Mapping for the Kondo Lattice Model

We have now shown how to map the quantum Heisenberg AF to the QNLσM. Next, we want to incorporate the Kondo interaction which couples the local moment spin, $\mathbf{S}$, to the conduction election spin, $\mathbf{s}_c$. This adds the following term:

$$
\begin{aligned}
J_K S \sum_x \mathbf{\Omega}_x(\tau) \cdot \mathbf{s}_{c,x}(\tau) &= J_K S a^{-d} \int d^d x \, d\tau \, \mathbf{s}_c(\vec{x}, \tau) \cdot \mathbf{\Omega}(\vec{x}, \tau) \\
&= J_K S a^{-d} \int d^d x \, d\tau \left[\eta_x \big(\mathbf{n}(\vec{x}, \tau) \cdot \mathbf{s}_c(\vec{x}, \tau) \big) \right. \\
&\quad \times \sqrt{1 - \left(\frac{a^d}{S} \mathbf{L}(\vec{x}, \tau) \right)^2} \\
&\quad \left. + \frac{a^d}{S} \mathbf{L}(\vec{x}, \tau) \cdot \mathbf{s}_c(\vec{x}, \tau) \right] \\
&\approx J_K \int d^d x \, d\tau \, \mathbf{L}(\vec{x}, \tau) \cdot \mathbf{s}_c(\vec{x}, \tau) \tag{3.47}
\end{aligned}
$$

The last line follows due to $\mathbf{n} \cdot \mathbf{s}_c \approx 0$. The latter is because we have, as discussed earlier, chosen to work with a Fermi surface that does not intersect the magnetic zone boundary (see Fig. 3.1); what remains of the Kondo interaction is the (nearly) forward scattering channel for the conduction electrons. The assumption we make is not necessarily that the density of conduction electrons is infinitesimally small, but

only that it does not intersect the AFBZ boundary. Specifically, we requires $Q > 2K_F$. In section 5.7 (Appendix 5C) we will discuss the modifications to the theory when the Fermi surface does indeed intersect the magnetic zone boundary [50], *i.e.* when $Q < 2K_F$.

Let us return to the action for the quantum AF before completing the square (equation 3.35), and add to that the above Kondo coupling. The total action for the Kondo Lattice Model, $\mathcal{S}_{KLM}$, now has something extra coupled to the **L** field:

$$
Z = \int \mathcal{D}\mathbf{n}\mathcal{D}\mathbf{L}\mathcal{D}\alpha\mathcal{D}\psi^\dagger\mathcal{D}\psi\ \delta(\mathbf{n}^2 - 1)
$$
$$
\times e^{-\mathcal{S}_{KLM}[\mathbf{n},\mathbf{L},\alpha,\mathbf{s}_c]-\mathcal{S}_c[\psi^\dagger,\psi]-\mathcal{S}'_B[\mathbf{n}]} \tag{3.48}
$$

$$
\mathcal{S}_{KLM}[\mathbf{n},\mathbf{L},\alpha,\mathbf{s}_c] = const_1 + S^2 a^{2-d}(I_1/2 - I_2)\int_0^\beta d\tau \int d^d x\, (\nabla\mathbf{n}(\vec{x},\tau))^2
$$
$$
+ 2dI_1 a^d \int_0^\beta d\tau \int d^d x \mathbf{L}^2(\vec{x},\tau)
$$
$$
- \int_0^\beta d\tau \int d^d x \mathbf{L}(\vec{x},\tau)\cdot\left(i\mathbf{n}(\vec{x},\tau)\times\frac{\partial\mathbf{n}(\vec{x},\tau)}{\partial\tau} - J_K\mathbf{s}_c(\vec{x},\tau)\right.
$$
$$
\left. -i\alpha(\vec{x},\tau)\mathbf{n}(\vec{x},\tau)\right) \tag{3.49}
$$

where $const_1$ and $\mathcal{S}'_B[\mathbf{n}]$ are as defined previously, and $\mathcal{S}_c[\psi^\dagger,\psi]$ is the conduction electron component of the action. Just like before, the functional integral is Gaussian with respect to the **L** field. With the identity $\int \mathcal{D}\mathbf{L} e^{\int -\zeta\mathbf{L}^2+\mathbf{b}\cdot\mathbf{L}} = \sqrt{\pi^M/\det\zeta}\, e^{\mathbf{b}^2/4\zeta}$, the correspondence is now $\zeta = 2dI_1 a^d$ and $\mathbf{b} = i\mathbf{n}\times\dot{\mathbf{n}} - J_K\mathbf{s}_c - i\alpha\mathbf{n}$. The important quantity is:

$$
\frac{\mathbf{b}^2}{4\zeta} = \frac{1}{8dI_1 a^d}\Big[-(\mathbf{n}\times\dot{\mathbf{n}})^2 - iJ_K\mathbf{s}_c\cdot\mathbf{n}\times\dot{\mathbf{n}} + \alpha\mathbf{n}\cdot\mathbf{n}\times\dot{\mathbf{n}} - iJ_K\mathbf{s}_c\cdot\mathbf{n}\times\dot{\mathbf{n}} + J_K^2\mathbf{s}_c^2
$$
$$
+ iJ_K\alpha\mathbf{s}_c\cdot\mathbf{n} + \alpha\mathbf{n}\cdot\mathbf{n}\times\dot{\mathbf{n}} + iJ_K\mathbf{s}_c\cdot\mathbf{n} - \alpha^2\mathbf{n}^2\Big] \tag{3.50}
$$

To simplify this expression, we need the following identities

$$\mathbf{n}^2 = 1 \tag{3.51}$$

$$\dot{\mathbf{n}} \cdot \mathbf{n} = 0 \tag{3.52}$$

$$(\mathbf{n} \times \dot{\mathbf{n}})^2 = \dot{\mathbf{n}}^2\mathbf{n}^2 - (\dot{\mathbf{n}} \cdot \mathbf{n})^2 = -\dot{\mathbf{n}}^2 \tag{3.53}$$

$$\mathbf{n} \cdot \mathbf{n} \times \dot{\mathbf{n}} = 0 \tag{3.54}$$

$$\mathbf{s}_c \cdot \mathbf{n} \approx 0 \tag{3.55}$$

$$\mathbf{s}_c^2 = \sum_{a,\alpha,\beta,\gamma,\delta} \psi_\alpha^\dagger \frac{\tau^a}{2} \psi_\beta \psi_\gamma^\dagger \frac{\tau^a}{2} \psi_\delta = \frac{3}{4}\left(\sum_\sigma \psi_\sigma^\dagger \psi_\sigma - 2\psi_\uparrow^\dagger \psi_\uparrow \psi_\downarrow^\dagger \psi_\downarrow \right) \tag{3.56}$$

This leads to:

$$\frac{\mathbf{b}^2}{4\zeta} = \frac{1}{8dI_1 a^d}\Bigg[-\dot{\mathbf{n}}^2 - 2iJ_K \mathbf{s}_c \cdot \mathbf{n} \times \dot{\mathbf{n}} + \frac{3J_K^2}{4}\left(\sum_\sigma \psi_\sigma^\dagger \psi_\sigma - 2\psi_\uparrow^\dagger \psi_\uparrow \psi_\downarrow^\dagger \psi_\downarrow \right)$$
$$-\alpha^2\mathbf{n}^2\Bigg] \tag{3.57}$$

Note that the terms that came from $\mathbf{s}_c^2$ serve only to renormalize the direct quadratic and quartic fermion couplings, which can be incorporated into $\mathcal{S}_c[\psi^\dagger, \psi]$. So after integrating out the $\mathbf{L}$ field we find:

$$Z = \int \mathcal{D}\mathbf{n}\mathcal{D}\alpha\mathcal{D}\psi^\dagger\mathcal{D}\psi \,\, \delta(\mathbf{n}^2 - 1)e^{-\mathcal{S}_{KLM}[\mathbf{n},\alpha,\mathbf{s}_c]-\mathcal{S}_c[\psi^\dagger,\psi]-\mathcal{S}'_B[\mathbf{n}]} \tag{3.58}$$

$$\mathcal{S}_{KLM}[\mathbf{n},\alpha,\mathbf{s}_c] = const_2 + \frac{c}{2g}\int_0^\beta d\tau \int d^dx \left[(\nabla\mathbf{n}(\vec{x},\tau))^2 + \frac{1}{c^2}\left(\frac{\partial\mathbf{n}(\vec{x},\tau)}{\partial\tau} \right)^2 \right]$$
$$+\lambda \int d^dx d\tau \left(\mathbf{s}_c(\vec{x},\tau) \cdot \mathbf{n}(\vec{x},\tau) \times \frac{\partial\mathbf{n}(\vec{x},\tau)}{\partial\tau} \right)$$
$$+\frac{1}{2gc}\int_0^\beta d\tau \int d^dx \,\alpha^2(\vec{x},\tau) \tag{3.59}$$

The constants g, c, and $const_2$ are defined exactly as before, and the new Kondo coupling constant is:

$$\lambda \equiv \frac{iJ_K}{4dI_1 a^d} \tag{3.60}$$

Finally, we integrate out the α field which only contributes the same constant as before. The final result is:

$$Z = \int \mathcal{D}\mathbf{n}\mathcal{D}\psi^\dagger\mathcal{D}\psi \,\, \delta(\mathbf{n}^2 - 1)e^{-\mathcal{S}_{QNL\sigma M}-\mathcal{S}_K[\mathbf{n},\mathbf{s}_c]-\mathcal{S}_c[\psi^\dagger,\psi]-\mathcal{S}'_B[\mathbf{n}]} \quad (3.61)$$

$$\mathcal{S}_{\text{QNL}\sigma\text{ M}}[\mathbf{n}] = const_3 + \frac{c}{2g}\int_0^\beta d\tau \int d^dx \left[(\nabla\mathbf{n}(\vec{x},\tau))^2 \right.$$
$$\left. + \frac{1}{c^2}\left(\frac{\partial\mathbf{n}(\vec{x},\tau)}{\partial\tau}\right)^2 \right] \quad (3.62)$$

$$\mathcal{S}_K[\mathbf{n},\mathbf{s}_c] = \lambda \int d^dx d\tau \left(\mathbf{s}_c(\vec{x},\tau)\cdot\mathbf{n}(\vec{x},\tau)\times\frac{\partial\mathbf{n}(\vec{x},\tau)}{\partial\tau} \right) \quad (3.63)$$

$$\mathcal{S}_c[\psi^\dagger,\psi] = \int d^dK d\varepsilon \sum_\sigma \psi_\sigma^\dagger(\vec{K},i\varepsilon)(i\varepsilon-\xi_K)\psi_\sigma(\vec{K},i\varepsilon) + u\int \psi^4 \quad (3.64)$$

Note that terms from $\mathbf{s}_c^2$ have been absorbed in u and ξ_K. This completes the mapping from the microscopic Kondo Lattice Hamiltonian to the effective field theory, as claimed earlier.

Now that we have demonstrated this mapping in detail, we are confronted with doing the renormalization group analysis. The next chapter is devoted to this theoretical development.

Chapter 4

Scaling and Renormalization with a Fermi Surface

Although the theory of renormalization has profoundly affected our conceptual understanding of many-body systems, its calculational framework is imperfect and continually evolving. In the end, we are interested in how couplings flow under changes of scale, but a variety of distinct procedures exist, each with its own advantages and drawbacks. An incomplete list of the assortment of programs includes the multiplicative RG, real space decimation, functional RG, exact RG, flow equations, and various flavors of ϵ-expansion, such as the classic minimal subtraction which expands around $d = 4$, or expansions around some other parameter, such as the deviation of the range of the interaction from a suitable reference value [57, 58]. Each method has its own limits of practicality, ease of use, and range of problems to which it may be usefully employed. One of the most popular engines for condensed matter problems has been Wilson's momentum-shell approach [59, 34]. However, in the early 1990's a few people recognized [60, 61, 62] that the standard momentum-shell procedure must be modified for problems involving a Fermi surface. A campaign soon followed attempting to understand Fermi Liquid Theory from an RG perspective. An excellent and influential summary of the pure fermion RG can be found in [63].

Another indication that the RG for fermions required more scrutiny came from the study of quantum critical points in itinerant electron magnets. The usual Hertzian picture [34] uses an auxiliary (Hubbard-Stratonovich) field to decouple the fermion interaction for the purpose of completely integrating out the fermions. The resulting effective theory is then expressed in terms of the remaining bosonic auxiliary field,

to which standard bosonic RG techniques can be employed. This turned out to be inappropriate for both the ferromagnet [64] and the antiferromagnet [65]. The process of integrating out the fermions robs us of important information required for an accurate understanding of the critical properties of itinerant electron magnets. It therefore becomes necessary to devise an RG scheme capable of simultaneously handling both bosons and fermions with a Fermi surface.

Of course, besides the critical itinerant magnets, a mixed fermionic-bosonic RG formalism would be quite useful for a huge assortment of problems. For example, in the context of the gauge-fermion problem several authors [66, 67, 68, 69] have developed their own schemes for counting dimensions in mixed theories. All have in common the subdivision of the Fermi surface into a large number of patches, but results vary and despite the intervening 15 years since the pioneering work on the RG for the gauge-fermion problem, little progress has been made. The importance of the gauge-fermion problem is historically linked to an interesting path to non-Fermi liquid behavior [70, 71]. More recently, effective gauge theories have become rather fashionable in condensed matter physics [72], thus providing new incentives for a resuscitation of the RG program for the gauge-fermion problem.

We should mention in passing a growing body of work on the functional RG which may be amenable to mixed theories [73, 74]. Our aim here is rather more modest, which is to develop a scaling scheme for mixed theories with a high score in the "ease of use" category. This was the chief virtue of the original Wilsonian RG which could quickly identify the relevant and irrelevant operators with a minimum of fuss. The emphasis of this chapter is to carefully explain how to extend Shankar's scheme to include bosons while maintaining the easy-to-use spirit of the Wilsonian approach.

In section 4.1 we introduce the main actors by writing down the action we wish

to subject to a scaling analysis. Briefly, in section 4.2 we remind the reader of the essential points of the bosonic Wilson-Hertz scaling. Section 4.3 quickly moves on to discuss scaling in fermionic systems, largely paraphrasing what has already been done, but emphasizing a slightly different perspective on the matter. The next section, 4.4, explains the way to properly scale in mixed theories which contains the central result of this chapter. The appendix to this chapter discusses some pitfalls.

4.1 The Action

The most general problem we are concerned with can be decomposed into bosonic, fermionic, and interaction terms:

$$\mathcal{S} = \mathcal{S}^f + \mathcal{S}^b + \mathcal{S}^{bf} \tag{4.1}$$

The fermionic and bosonic pieces can be further divided into quadratic and quartic pieces.

$$\mathcal{S}^b = \mathcal{S}_2^b + \mathcal{S}_4^b \tag{4.2}$$

$$\mathcal{S}^f = \mathcal{S}_2^f + \mathcal{S}_4^f \tag{4.3}$$

Theories based upon $\mathcal{S}^b$ or $\mathcal{S}^f$ alone have already been subjected to momentum-shell renormalization group analyses; see, for example, [34] and [63].

For the bosonic case, the quartic part of the action can be schematically written $\mathcal{S}_4^b = u_b \int \phi^4$, while the quadratic part can take several different forms depending on

the value of z. For example,

$$\mathcal{S}_2^b(z=1) = \int d^d q d\omega \; \phi^*(aq^2 + b\omega^2)\phi \tag{4.4}$$

$$\mathcal{S}_2^b(z=2) = \int d^d q d\omega \; \phi^*(aq^2 + b\omega)\phi \tag{4.5}$$

$$\mathcal{S}_2^b(z=3) = \int d^d q d\omega \; \phi^* \left(aq^2 + b\frac{\omega}{q} \right) \phi \tag{4.6}$$

$$\mathcal{S}_2^b(z=4) = \int d^d q d\omega \; \phi^* \left(aq^2 + b\frac{\omega}{q^2} \right) \phi \tag{4.7}$$

The bosons might represent phonons, magnons, photons, or some collective mode of an underlying fermionic theory. At this point, we need not be specific. The important point is that the form of $\mathcal{S}_2^b$ establishes a precise relationship between the scaling dimensions of bosonic energies and momenta, namely

$$[q] = [\omega]/z \tag{4.8}$$

If we make the choice $[\omega] = 1$, the scale invariance of $\mathcal{S}_2^b$, which is necessary to define a fixed point, dictates that $[q] = 1/z$ and $[\phi] = -\frac{1}{2}([d^d q] + 1 + 2/z)$. Thus we require knowledge of the way the measure transforms under scaling, which will be determined in the next section. In addition, there is a further subtlety regarding the argument of the field. In defining the fixed point, we fix the way the field transforms under a specific operation on its arugment, _e.g._ $\phi(sq) \to s^{-[\phi]}\phi(q)$. If, however, the argument of the field is not q, but something more complicated, we will not know how the field scales. More on this later.

For fermions, the quartic part can be represented by $\mathcal{S}_4^f = u_f \int \psi^4$, while the quadratic part is written

$$\mathcal{S}_2^f = \int d^d K d\epsilon \bar{\psi} \left(i\epsilon - v_F k \right) \psi \tag{4.9}$$

The explanation of this form of $\mathcal{S}_2^f$ will be given later. For now, simply note that it

implies the important relation

$$[\epsilon] \quad = \quad [k] \tag{4.10}$$

which furthermore necessitates $[\psi] = -\frac{1}{2}([d^d K] + 2[\epsilon])$ if $\mathcal{S}_2^f$ is to be scale invariant. Once again, we need to know how the measure transform, and this will turn out to be different from the bosonic case.

Now that we have introduced the objects of analysis, let us briefly review how the scaling is done for bosons, then indulge in a slightly more detailed exposition of the procedure for fermions.

4.2   Boson Scaling

The Wilsonian RG for bosons is well-known [59] so we only review those elements crucial to the comparisons we wish to make later with the fermionic RG. Consider a d-dimensional integral in momentum space with a cutoff, Λ, to high-energy and therefore large-q modes.

$$
\begin{aligned}
\int^{\Lambda} d^d q &\equiv \int d^{d-1}\Omega_{\vec{q}} \int_0^{\Lambda} q^{d-1} dq \\
&= \int d^{d-1}\Omega_{\vec{q}} \left[\int_0^{\Lambda/s} q^{d-1} dq + \int_{\Lambda/s}^{\Lambda} q^{d-1} dq \right]
\end{aligned}
$$

Here, $d^{d-1}\Omega_{\vec{q}}$ represents the measure for integration over all angular coordinates in $\vec{q}$-space, $q \equiv |\vec{q}|$ is the radial coordinate, and $s \gtrsim 1$. We have ignored factors of 2π. At the tree level we simply throw away the shell integral. To regain the original form of the action we rescale the radial coordinate in a trivial way: $q' = sq$. This leads to

$$\int d^{d-1}\Omega_{\vec{q}} \int_0^{\Lambda} s^{-(d-1)} q'^{d-1} s^{-1} \, dq' \quad = \quad s^{-d} \int^{\Lambda} (d^d q)'$$

We conclude that the scaling dimension of the measure is given by $[d^d q] = d[q]$. Note that rescaling the radial variable, q, is the same as rescaling all the components of $\vec{q}$

since $q = \sqrt{\sum_\alpha^d q_\alpha^2}$. For this to be consistent with $q' = sq$, we must have $q'_\alpha = sq_\alpha$ for all components $\alpha \in \{x, y, z, ...\}$. This is an important difference from the fermionic case to be discussed next.

If we apply this to the quadratic part of the boson action we may now make the statement.

$$[\phi] = -\frac{1}{2z}(d + z + 2) \tag{4.11}$$

where we used $[q] = [\omega]/z$ and defined $[\omega] = 1$. However, we must be careful what is meant by this. More specifically, we have only determined:

$$\phi'(q', i\omega') \equiv s^{-(d+z+2)/(2z)} \phi(s^{1/z}q, si\omega) \tag{4.12}$$

If we were to scale the argument of the field in some other way, this statement would no longer be true. This excludes a particular scaling choice that we will be confronted with later. See appendix 4A.

4.3 Fermion Scaling: Shankar's RG

Now we review Shankar's formulation of the fermionic RG [63]. We shall use Shankar's notation and label momenta measured with respect to the Brillouin zone center with a capital letter $\vec{K} = (K_x, K_y, ...)$. In contrast to the bosonic case, low energy modes live near an extended surface (the Fermi Surface) rather than a single point (the Brillouin Zone center). For a spherical Fermi surface, a high energy cutoff can be implemented on $\vec{K}$-integrals as follows:

$$\int^\Lambda d^d K \equiv \int d^{d-1}\Omega_{\vec{K}} \int_{K_F-\Lambda}^{K_F+\Lambda} K^{d-1} dK$$

Here, $d^{d-1}\Omega_{\vec{K}}$ represents the measure for integration over all angular coordinates in $\vec{K}$-space, while $K \equiv |\vec{K}|$ is the radial coordinate. Usually, we work at fixed fermion

density which, by Luttinger's Theorem, dictates that we design our scaling scheme in such a way that the Fermi volume remains invariant. To preserve the Fermi surface* under rescaling we cannot simply scale the radial coordinate as we did in the bosonic case. To see this, observe that after mode elimination the expression we wish to rescale is given by

$$\int^{\Lambda/s} d^d K \;\equiv\; \int d^{d-1}\Omega_{\vec{K}} \int_{K_F-\Lambda/s}^{K_F+\Lambda/s} K^{d-1} dK \tag{4.13}$$

Clearly, no simple rescaling of K will return the integral to its original form. This is the principle disparity between the fermionic and bosonic RG. To make progress we define the lower case letter $k \equiv |\vec{K}| - K_F$. Note that $k = 0$ corresponds to $\xi_{\vec{K}} = \epsilon_{\vec{K}} - \mu = 0$ since $\xi_{\vec{K}} = \frac{K^2 - K_F^2}{2m} \approx v_F(K - K_F) = v_F k$. Small k corresponds to low energy whereas small K does not. Such a change of variables greatly facilitates rescaling.

$$\int d^{d-1}\Omega_{\vec{K}} \int_{-\Lambda/s}^{\Lambda/s} (K_F + k)^{d-1} dk$$
$$= K_F^{d-1} \int d^{d-1}\Omega_{\vec{K}} \int_{-\Lambda/s}^{\Lambda/s} \left(1 + \frac{k}{K_F}\right)^{d-1} dk$$
$$\approx K_F^{d-1} \int d^{d-1}\Omega_{\vec{K}} \int_{-\Lambda/s}^{\Lambda/s} dk \tag{4.14}$$

We have neglected certain terms above for two reasons: they are of order Λ/K_F relative to what has been kept, and they are less relevant in the RG sense. To see the latter, note that the integral can be restored to its original form with the simple rescaling $k' = sk$. This determines the scaling dimension $[k] = 1$. However, note well that the variable k is not a vector, nor is it a radial coordinate since it can take negative values. Later, we will discuss another scheme, which we call patching, that

---

*We shall not consider constant-volume Fermi surface shape changes. In principle, such a scheme could be devised by, for example, incorporating the real part of the self energy.

decomposes the momenta into components parallel ($\vec{k}_{\parallel}$) and perpendicular ($k_{\perp}$) to the Fermi surface. This method will be applied to the ferromagnetic problem, which involves $z > 1$. For now, we specialize to $z = 1$.

To further emphasize the dissimilarity between the fermionic and bosonic cases, observe that after rescaling

$$
\begin{aligned}
\int^{\Lambda} d^d K &\approx K_F^{d-1} \int d^{d-1}\Omega_{\vec{K}} \int_{-\Lambda}^{\Lambda} s^{-1} dk' \\
&= s^{-1} \int^{\Lambda} (d^d K)'
\end{aligned}
\tag{4.15}
$$

which implies $[d^d K] = 1$. Here, the angular variables are truly untouched after rescaling in contrast to the bosonic case; this is necessary to maintain the Fermi surface. Unfortunately, the straightforward transformation $k' = sk$ does not translate into a simple transformation on the components of $\vec{K}$. Care must therefore be exercised to write all expressions in terms of k before the scaling procedure can begin. For example, after mode elimination and rescaling of energy and momentum, the quadratic part of the fermionic action is given by:

$$
\mathcal{S}_2^f \propto s^{-3} \int dk' d\epsilon' \bar{\psi}(K_F + s^{-1}k', s^{-1}i\epsilon')\left(i\epsilon' - v_F k'\right)\psi(K_F + s^{-1}k', s^{-1}i\epsilon')
$$

In order to make $\mathcal{S}_2^f$ invariant to the RG transformation we must demand that the fermion field obeys:

$$
s^{-3/2}\psi(K_F + s^{-1}k', s^{-1}i\epsilon') = \psi'(K_F + k', i\epsilon')
\tag{4.16}
$$

where we have not explicitly written the dependence of ψ on angular variables since these do not scale. Equation (4.16) tells us two important things. First, the dimension of the fermion field is simply:

$$
[\psi] = -3/2
\tag{4.17}
$$

Second, the RG transformation of the fermion field does *not* take the form of a generalized homogeneous function as was the case for the bosonic field; see equation (4.12). Thus, the momentum argument of the fermion field $\vec{K}$ has a magnitude equal to the Fermi wavevector plus a small deviation: $K = K_F + k$. Only the deviation k scales, while K_F remains constant. This important difference from the bosonic case will be discussed further in appendix 4A.

The story so far seems relatively elementary, but the true subtleties materialize when we try to determine the dimension of the ψ^4 coupling function u_f based on the dimension assignments required to make $\mathcal{S}_2^f$ scale invariant. The quartic part of the action can be written

$$
\mathcal{S}_4^f = \prod_{i=1}^{4} \int^{\Lambda} d^d K_i \int d\epsilon_i \bar{\delta}^{(d)}(\vec{K}_1 + \vec{K}_2 - \vec{K}_3 - \vec{K}_4)\delta(\epsilon_1 + \epsilon_2 - \epsilon_3 - \epsilon_4)
$$
$$
\bar{\psi}(4)\bar{\psi}(3)\psi(2)\psi(1)\, u_f(4,3,2,1) \tag{4.18}
$$

The δ-functions explicitly enforce the conservation of energy and momentum (up to a reciprocal lattice vector). Of course, this results from the local nature of the interaction in position space: $\psi^4(x)$. We might integrate one of the momenta, say $\vec{K}_4$, against the delta function to yield an integral over three independent momenta $\vec{K}_1$, $\vec{K}_2$, and $\vec{K}_3$.

$$
\mathcal{S}_4^f = \prod_{i=1}^{3} \int^{\Lambda} d^d K_i \int d\epsilon_i \bar{\psi}(1+2-3)\bar{\psi}(3)\psi(2)\psi(1)
$$
$$
\times u_f(1+2-3,3,2,1) \quad \text{(wrong)} \tag{4.19}
$$

But this expression is not quite right. The problem is that not all momentum-conserving processes should be included in the low-energy effective field theory. We must respect the cutoff imposed on the quadratic part of the action, which only allows excursion into states within a distance $\pm\Lambda$ of the Fermi surface. Imposing a cutoff

amounts to constraining the momentum integrals. Until now, we have implemented the constraints by writing them explicitly in the limits of integration, but let us re-express them as

$$\int^\Lambda d^d K_i = \int d^d K_i \Theta(\Lambda - |k_i|) \tag{4.20}$$

where, as usual, $k_i \equiv |\vec{K}_i| - K_F$. With all momentum integrals written in this way, we can safely use the δ-functions to eliminate one variable, say $\vec{K}_4$ and ϵ_4.

$$
\begin{aligned}
\mathcal{S}_4^f &= \prod_{i=1}^3 \int d^d K_i \int d\epsilon_i \bar{\psi}(1+2-3)\bar{\psi}(3)\psi(2)\psi(1)u_f(1+2-3,3,2,1) \\
&\quad \times \Theta(\Lambda - |k_1|)\Theta(\Lambda - |k_2|)\Theta(\Lambda - |k_3|)\Theta(\Lambda - |\mathcal{K}_4|) \\
&= \prod_{i=1}^3 \int^\Lambda d^d K_i \int d\epsilon_i \bar{\psi}(1+2-3)\bar{\psi}(3)\psi(2)\psi(1)u_f(1+2-3,3,2,1) \\
&\quad \Theta(\Lambda - |\mathcal{K}_4|)
\end{aligned}
\tag{4.21}
$$

The constraints on $\vec{K}_1$, $\vec{K}_2$, and $\vec{K}_3$ have been put back in the limits of integration, but we have the additional constraint $|\mathcal{K}_4| < \Lambda$ where

$$\mathcal{K}_4 \equiv |\vec{K}_3 - \vec{K}_2 - \vec{K}_1| - K_F \tag{4.22}$$

We can implement this constraint in a number of ways. One way is to allow $\vec{K}_1$ and $\vec{K}_2$ to range anywhere inside the annuli defined by $-\Lambda < k_1, k_2 < \Lambda$, but restrict $\vec{K}_3$ as appropriate to satisfy $|\mathcal{K}_4| < \Lambda$. The outcome of a proper phase space analysis shows that once $\vec{K}_1$ and $\vec{K}_2$ have been chosen, the angle for $\vec{K}_3$ is highly constrained [63].

To see this in more detail, observe that to leading order in Λ/K_F,

$$\mathcal{K}_4 \approx K_F(|\vec{\Delta}| - 1) \tag{4.23}$$

where $\vec{\Delta} \equiv \hat{K}_1 + \hat{K}_2 - \hat{K}_3$, and where the $\hat{K}_i$ are unit vectors, each pointing in the

direction of $\vec{K}_i$. After mode elimination, the momentum integrals become:

$$\prod_{i=1}^{3} \int^{\Lambda/s} d^d K_i \Theta \left(\Lambda/s - K_F \left| |\vec{\Delta}| - 1 \right| \right)$$

$$= \prod_{i=1}^{3} \int^{\Lambda/s} d^d K_i \Theta \left(\Lambda - s K_F \left| |\vec{\Delta}| - 1 \right| \right) \qquad (4.24)$$

Simply rescaling $k_i' = s k_i$ is not sufficient to regain the original form of the action for generic values of k_i. The obvious snag is the annoying way the Θ-function transforms under rescaling. There are, however, certain special values of the k_i where the situation is transparent. Indeed, when $|\vec{\Delta}| = 1$ (i.e. $\mathcal{K}_4 = 0$) the Θ-function is always satisfied. Since $\vec{\Delta}$ is composed of unit vectors, its modulus will be unity in the following three cases: i) $\vec{K}_3 = \vec{K}_1$ and $\vec{K}_2 = \vec{K}_4$; ii) $\vec{K}_3 = \vec{K}_2$ and $\vec{K}_1 = \vec{K}_4$; iii) $\vec{K}_1 = -\vec{K}_2$ and $\vec{K}_3 = -\vec{K}_4$. For these values of the momenta, the rescaling $k_i' = s k_i$ works flawlessly and it is easy to show that u is marginal at the tree level. In Shankar's notation, cases (i) and (ii) correspond to $u = F$ and case (iii) $u = V$.

The condition $\mathcal{K}_4 = 0$ is a special limit where the constraint function is exactly satisfied, but it is conceptually different from the $\Lambda/K_F \to 0$ limit. To see this, let us rewrite the condition $\mathcal{K}_4 = 0$ as follows:

$$|\vec{K}_3 - \vec{K}_2 - \vec{K}_1| = K_F \qquad (4.25)$$

To understand the geometric implication of this constraint, define $\vec{P} \equiv \vec{K}_1 + \vec{K}_2$ which obviously gives

$$|\vec{K}_3 - \vec{P}| = K_F \qquad (4.26)$$

This says that the the vector joining the tip of $\vec{K}_3$ to the tip of $\vec{P}$ must have magnitude precisely equal to K_F. Figure 4.1 depicts the situation. Geometrically, the choices available to $\vec{K}_3$ once $\vec{K}_2$ and $\vec{K}_1$ have been selected are given by the thick gray lines

$\vec{K}_3$ must stay within the annulus

$\vec{K}_3 - \vec{P}$ must be a point on this circle
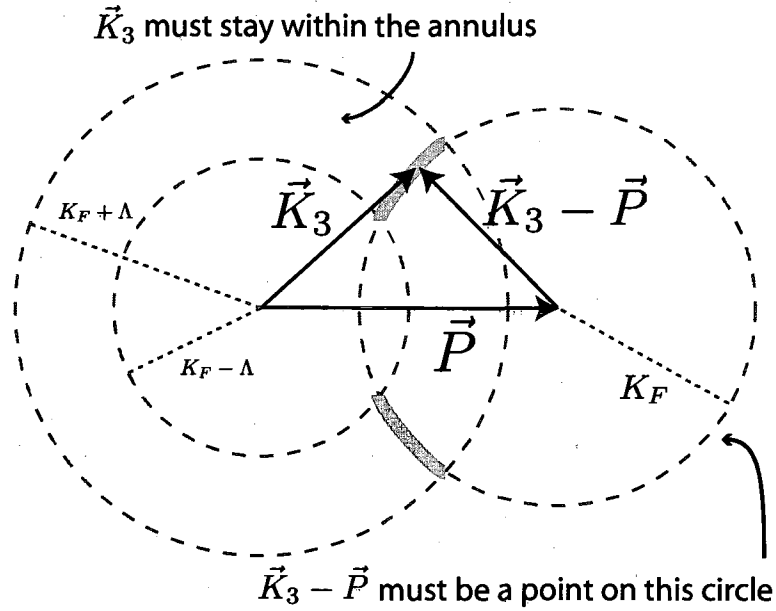
Figure 4.1 : Once $\vec{K}_1$ and $\vec{K}_2$ have been chosen the conservation of momentum and the requirement that $\vec{K}_3$ respect the cutoffs of the field theory strongly constrain the phase space available to $\vec{K}_3$, as depicted by the thick gray lines.

in the figure. Notice that while k_3 can still take any values $-\Lambda < k_3 < \Lambda$ within the annulus, the angle of $\vec{K}_3$ has become highly constrained. However, it is clear that even when $\mathcal{K}_4 = 0$ the value of Λ/K_F can still be nonzero.

The three cases corresponding to $\mathcal{K}_4 = 0$ constitute only a small portion of $(\vec{K}_1, \vec{K}_2, \vec{K}_3)$-space. To see what happens to the coupling function $u(3, 2, 1)$ for other values of momenta, Shankar had the insight to employ a soft cutoff: $\Theta(\Lambda - |k_i|) \approx e^{-|k_i|/\Lambda}$. Using this device, the rescaled constraint for arbitrary k_i values becomes

$$\Theta \left(\Lambda - sK_F \left| |\vec{\Delta}| - 1 \right| \right) \approx e^{-sN_\Lambda \left| |\vec{\Delta}| - 1 \right|}$$

$$= e^{-N_\Lambda \left| |\vec{\Delta}| - 1 \right|} e^{-(s-1)N_\Lambda \left| |\vec{\Delta}| - 1 \right|}$$

where we have defined the large parameter $N_\Lambda \equiv K_F/\Lambda$ (generally, we have the hierarchy $k < \Lambda \ll K_F$, which means $N_\Lambda \gg 1$). We choose to write the constraint in this second way because then clearly when $|\vec{\Delta}| = 1$, corresponding to the three cases

listed above, this becomes a factor of unity. For any $|\vec{\Delta}| \neq 1$, which means all other values of the k_i, the constraint $\to 0$ in the limit $N_\Lambda \to \infty$ provided $s > 1$. While we do not know how the coupling function $u(3, 2, 1)$ scales for values of the momenta where $|\vec{\Delta}| \neq 1$, it does not matter because these couplings will be exponentially suppressed in the limit $1/N_\Lambda = \Lambda/K_F \to 0$.

Note that the condition $|\vec{\Delta}| = 1$ is simply the statement that $\mathcal{K}_4$ should not scale. Indeed, it means $\mathcal{K}_4 = 0$, but in particular $\mathcal{K}_4' \neq s\mathcal{K}_4$. This is perfectly reasonable since $\mathcal{K}_4$ is not a free variable, but rather that special combination of the other momenta which should be scale invariant if we are to simultaneously satisfy the conservation of momentum and the condition that all processes remain inside the prescribed cutoff for the low-energy field theory. This useful interpretation will be used again later when we extend the formalism to include bosons.

4.4   Boson+Fermion Scaling

We are finally ready to incorporate bosons. Consider the following interaction term involving two fermions and one boson:

$$
\begin{aligned}
\mathcal{S}^{bf} &= \int d^d K_1 d^d K_2 d^d q \; g(\vec{K}_1, \vec{K}_2, \vec{q}) \; \bar{\psi}_{\vec{K}_2} \psi_{\vec{K}_1} \phi_{\vec{q}} \\
&\quad \times \delta^{(d)}(\vec{K}_2 - \vec{K}_1 - \vec{q})\Theta(\Lambda - |k_1|)\Theta(\Lambda - |k_2|)\Theta(\Lambda - |\vec{q}|) \quad (4.27)
\end{aligned}
$$

g is the coupling function which plays the same role as u_f in the 4-fermion problem. For simplicity we have suppressed frequency integrals and assumed $\Lambda_b \sim \Lambda_f \sim \Lambda$. Note that more boson legs can be included as a composite field provided the interaction vertex is local. Now, to conserve momentum we have two choices: use the δ-function to eliminate a fermionic momentum $\vec{K}_i$, or the bosonic momentum $\vec{q}$. This

gives either

$$\int^{\Lambda} d^d K d^d q \left[\bar{\psi}_{\vec{K}+\vec{q}} \psi_{\vec{K}} \phi_{\vec{q}} g(\vec{K}, \vec{q}) \Theta(\Lambda - |\mathcal{K}_2|) \right] \tag{4.28}$$

or

$$\int^{\Lambda} d^d K_1 d^d K_2 \left[\bar{\psi}_{\vec{K}_2} \psi_{\vec{K}_1} \phi_{K_2 - K_1} g(\vec{K}_2, \vec{K}_1) \Theta(\Lambda - |\vec{\mathcal{Q}}|) \right] \tag{4.29}$$

with the definitions $\mathcal{K}_2 \equiv |\vec{K} + \vec{q}| - K_F$ and $\vec{\mathcal{Q}} \equiv \vec{K}_1 - \vec{K}_2$.

The first scheme turns out to be the proper choice because a self-consistent scaling procedure can be constructed, which is not the case for the second choice. The reason is because, for the second choice, the argument of the boson will have magnitude $|\vec{K}_1 - \vec{K}_2| \approx K_F \sqrt{2(1 - \cos\theta_{12})}[1 + (k_1 + k_2)/(2K_F)]$. Under the rescaling $k_i' = sk_i$, the argument of the boson scales in a rather unusual way whose form is more closely akin to that of a fermion. However, in order to ensure scale invariance of $\mathcal{S}_2^b$, the boson field needs to scale homogeneously. We have no idea what dimension to assign to the boson in the non-homogenous case, so we cannot use this scaling choice. More details on such issues are provided in Appendix 4A. For the rest of this chapter, we will commit to the first choice which expresses the integration with one fermionic and one bosonic momentum, rather than two fermion momenta.

Since we integrated against the delta functions, momentum and energy are explicitly conserved. However, just like the pure fermion case, not all momentum conserving processes are allowed because some might fall outside the high-energy cutoff. We must further restrict the coupling function g with the constraint $\Theta(\Lambda - |\mathcal{K}_2|)$. Unfortunately, this quantity does not scale in a simple way in the most general circumstances.

Recall from the form of $\mathcal{S}_2^f$ that we have the relation $[k] = [\epsilon]$, while $\mathcal{S}_2^b$ demands

$[q] = [\omega]/z$. We have the freedom to make the choice $[\omega] = 1$, which then determines:

$$[\epsilon] = [k] = [q] = 1/z \tag{4.30}$$

$$[\omega] = 1 \tag{4.31}$$

$$[\psi] = -\frac{3}{2z} \tag{4.32}$$

$$[\phi] = -\frac{d+z+2}{2z} \tag{4.33}$$

Mode elimination and rescaling according to this scheme leads to the following interaction term (we reinstate the energy integrals):

$$
\mathcal{S}^{bf} = s^{\frac{4-z-d}{2z}} g \int^{\Lambda} d^d q' dk' d^{d-1}\Omega_{\vec{K}} d\epsilon' d\omega' \bar{\psi}' \psi' \phi'
$$
$$
\times \Theta\left(\Lambda - s^{1/z}\left|\sqrt{(s^{-1/z}k' + K_F)^2 + s^{-2/z}q'^2 + 2(s^{-1/z}k' + K_F)s^{-1/z}q'\cos\theta_{Kq}}\right.\right.
$$
$$
\left.\left. - K_F\right|\right) \tag{4.34}
$$

where

$$
\cos\theta_{Kq} \equiv \begin{cases} \cos(\theta_K - \theta_q) & , \quad d = 2 \\ \cos\theta_K \cos\theta_q + \sin\theta_K \sin\theta_q \cos(\varphi_K - \varphi_q) & , \quad d = 3 \end{cases} \tag{4.35}
$$

Clearly, the constraint does not return to itself after rescaling. To make progress, we take the same strategy used in the pure-fermion problem by focusing our consideration on the phase space where the constraint does scale perfectly, namely when $\mathcal{K}_2 = 0$. This is analogous to $\mathcal{K}_4 = 0$ (or $|\vec{\Delta}| = 1$) in $\mathcal{S}_4^f$. This new condition can also be written

$$|\vec{K} + \vec{q}| = K_F \tag{4.36}$$

Thus, besides staying within their respective cutoffs, the choices available to $\vec{K}$ and $\vec{q}$ in this particular limit are restricted in such a way that their sum vector must sit

precisely on the Fermi surface. Once $\vec{K}$ is chosen, $\vec{q}$ is obligated to connect $\vec{K} + \vec{q}$ to the Fermi surface which limits its permissible magnitudes and angles. This is depicted in figure 4.2.
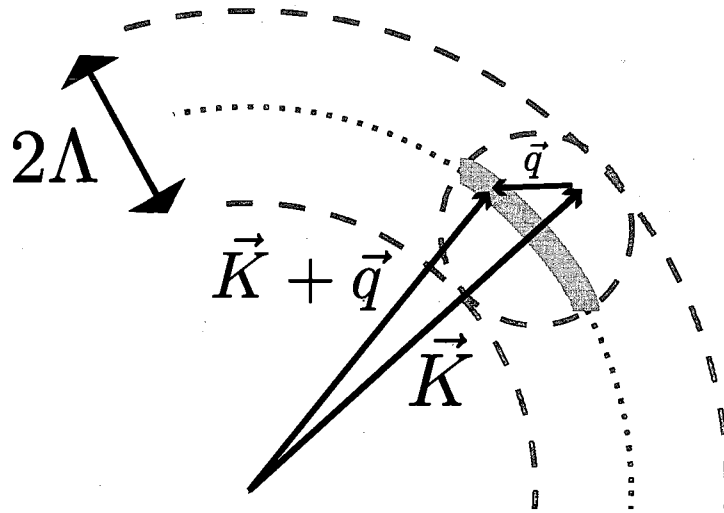
Figure 4.2 : $\vec{K}$ must stay within the annulus while $\vec{q}$ must stay inside the little circle of radius Λ. In the limit where $\mathcal{K}_2 = 0$, the sum $\vec{K} + \vec{q}$ must sit precisely on the Fermi surface. Clearly, the limit $\mathcal{K}_2 = 0$ is not the same as $\Lambda/K_F = 0$. The only phase space that satisfies all three constraints is the thick gray line which represents a small patch of the Fermi surface of size $O(\Lambda^{d-1})$.

Thus, for those portions of phase space where $\mathcal{K}_2 = 0$ the dimension of the coupling function can be readily found. What about other values of momenta? It turns out that for the special case $z = 1$, it is possible to find a self-consistent scheme with only a minor modification to the situation where $\mathcal{K}_2$ is strictly zero. We now specialize to this case, which is central to the analysis of the antiferromagnetic phase of the Kondo lattice. Later, after discussing the ferromagnetic phase, we will introduce a scheme that can be used when $z \neq 1$ using a very different approach.

Let us rewrite the expression involved in the constraint:

$$
\begin{aligned}
|\mathcal{K}_2| &= \left| |\vec{K} + \vec{q}| - K_F \right| \\
&= \left| \left[(K_F + k)^2 + q^2 - 2(K_F + k)q\cos\theta_{Kq} \right]^{1/2} - K_F \right| \\
&\approx K_F \left| \left[1 + \frac{2}{K_F}(k + q\cos\theta_{Kq}) \right]^{1/2} - 1 \right| \\
&\approx K_F \left| 1 + \frac{1}{K_F}(k + q\cos\theta_{Kq}) - 1 \right| \\
&= |k + q\cos\theta_{Kq}|
\end{aligned}
\tag{4.37}
$$

which is valid to leading order in Λ/K_F. This is an important observation because it shows that using this representation, the constraint function transforms in the following way:

$$
\begin{aligned}
\Theta(\Lambda/s - |\vec{\mathcal{K}}_2|) &\approx \Theta(\Lambda/s - |k + q\cos\theta_{Kq}|) \\
&= \Theta(\Lambda - s|k + q\cos\theta_{Kq}|)
\end{aligned}
\tag{4.38}
$$

which returns to its original form by simply rescaling $k' = sk$ and $q' = sq$. Clearly, this is only valid for $z = 1$, but that is an important case as we will show in the next chapter. This representation is quite convenient because it does not even require the soft cutoff needed for the pure-fermion problem.

The boson-fermion coupling can now be written:

$$
\mathcal{S}^{bf} = s^{\frac{3-d}{2}} g \int^\Lambda d^d q'\, dk'\, d^{d-1}\Omega_{\vec{K}}\, d\epsilon'\, d\omega'\, \bar{\psi}'\psi'\phi'\, \Theta\left(\Lambda - |k' + q'\cos\theta_{Kq}| \right)
\tag{4.39}
$$

where we used $z = 1$. This is equivalent to

$$
[g] = (3 - d)/2
\tag{4.40}
$$

For this choice of the boson field, the coupling is marginal in $d = 3$ and relevant in $d = 2$. In the next chapter we will describe how to do the scaling for the antiferromagnetic

phase with a small Fermi surface where the bosonic field has a different dimension, and therefore the dimension of the Kondo coupling will be different than the result described here.

At this point, a few issues are worth emphasizing.

- Since we integrated against the delta functions, energy and momentum are explicitly conserved.

- The quantity $\mathcal{K}_2$ is not a free variable and it does not need to scale in the same way as bosonic or fermionic momenta. This is consistent with the non-scaling of $\mathcal{K}_4$ in the pure-fermion problem.

- In this scheme, all components of $\vec{q}$ scale the same way. In particular, $[d^d q] = d/z$. At the same time, only fermionic momenta in the direction perpendicular to the Fermi surface scale.

- Importantly, k is not a vector. It does not have parallel or perpendicular components as discussed in certain patch schemes. For more on the patch scheme, see Chapter 7.

4.5   Appendix 4A: Choice of Boson-Fermion Integration

In this appendix we show why the alternative decomposition of the interaction term:

$$\int^{\Lambda} d^d K_1 d^d K_2 \left[\bar{\psi}_{\vec{K}_2} \psi_{\vec{K}_1} \phi_{K_2 - K_1} \, g(\vec{K}_2, \vec{K}_1) \Theta(\Lambda - |\vec{\mathcal{Q}}|) \right]$$

is not an appropriate starting point to determine the scaling dimension of the boson-fermion coupling. The problem is that the argument of the boson field, $\mathcal{Q} = \vec{K}_1 - \vec{K}_2$, does not transform homogeneously, so we do not know what dimension to assign to

the boson itself. To see this, write:

$$
\begin{aligned}
|\vec{\mathcal{Q}}| &= \left[K_1^2 + K_2^2 - 2K_1 K_2 \cos\theta_{12}\right]^{1/2} \\
&= \left[(K_F + k_1)^2 + (K_F + k_2)^2 - 2(K_F + k_1)(K_F + k_2)\cos\theta_{12}\right]^{1/2} \\
&\approx K_F \sqrt{2}\left[(1 - \cos\theta_{12})\left(1 + \frac{k_1 + k_2}{K_F}\right)\right]^{1/2} \\
&\approx K_F \sqrt{2(1 - \cos\theta_{12})}\left(1 + \frac{k_1 + k_2}{2K_F}\right)
\end{aligned}
\tag{4.41}
$$

which is true to leading order in $1/N_\Lambda$, and where

$$
\cos\theta_{12} \equiv
\begin{cases}
\cos(\theta_1 - \theta_2) & , \quad d = 2 \\
\cos\theta_1 \cos\theta_2 + \sin\theta_1 \sin\theta_1 \cos(\varphi_1 - \varphi_2) & , \quad d = 3
\end{cases}
\tag{4.42}
$$

Since we have chosen to make $\mathcal{S}_2^f$ scale invariant by not scaling any angular components of fermion momenta, mode elimination and rescaling will result in the following form

$$
\begin{aligned}
\mathcal{S}_3^{bf} &= \int^\Lambda s^{-1}dk_1' s^{-1}dk_2' s^{-1}d\epsilon_1' s^{-1}d\epsilon_2' \left[\bar{\psi}'(K_F + k_2', i\epsilon_2')\psi'(K_F + k_1', i\epsilon_1')\right. \\
&\quad \times \phi\left(K_F \sqrt{2(1 - \cos\theta_{12})}\left[1 + \frac{k_1' + k_2'}{2sK_F}\right], i\epsilon_2' - i\epsilon_1'\right) \\
&\quad \left. \times g(2,1)\Theta(\Lambda/s - |\vec{\mathcal{Q}}|)\right]
\end{aligned}
$$

where

$$
\Theta(\Lambda/s - |\vec{\mathcal{Q}}|) \equiv \Theta\left(\Lambda - K_F\sqrt{2(1 - \cos\theta_{12})}\left[s + \frac{k_1' + k_2'}{2K_F}\right]\right)
\tag{4.43}
$$

There are two problems. First, the constraint function does not return to its original form, making it impossible to compare the flow of the coupling function before and after the RG transformation. Second, we do not know how the ϕ field transforms under this change of argument. All we know is that

$$
\phi'(q', i\omega') \equiv s^{-(d+z+2)/(2z)}\phi(s^{1/z}q, si\omega)
\tag{4.44}
$$

which states that the boson scales in a homogeneous fashion. If we transform the boson arguments in a non-homogeneous way, we are not guaranteed that the transformation will induce a simple multiplicative prefactor. Note that the mathematical requirement that the boson field transform homogeneously means that the relative angle between the incoming and outgoing fermions must be allowed to scale, which is not allowed in this scheme. We therefore cannot adopt this scaling procedure. Also note that selecting a scheme where the angular variables of, say, $\vec{K}_2$ scale in addition to the deviations k_i will seemingly yield a dimension for the boson-fermion coupling that appears consistent with the scheme adopted in the main text, however such a procedure cannot be justified because the quadratic part of the action which defined the fixed point explicitly does *not* scale the angular parts of the fermionic momentum measure.

One might wonder why we are being so strict on the homogeneity requirement when it seems like the other scheme

$$\int^{\Lambda} d^d K d^d q \left[\bar{\psi}_{\vec{K}+\vec{q}} \psi_{\vec{K}} \phi_{\vec{q}} g(\vec{K}, \vec{q}) \Theta(\Lambda - |\mathcal{K}_2|) \right] \tag{4.45}$$

also violates this principle. In fact, the fermion is not required to be a homogeneous function of momentum anyway. All that we need is:

$$\psi(K_F + s^{-1}k') = s^{3/2} \psi'(K_F + k') \tag{4.46}$$

The incoming fermion is clearly of this form, whereas the outgoing fermion can be written:

$$\bar{\psi}(|\vec{K} + \vec{q}|) \approx \bar{\psi}(K_F + s^{-1}k' + s^{-1}q' \cos\theta_{Kq}) \tag{4.47}$$

In this form, we know this expression is equivalent to:

$$\bar{\psi}(K_F + s^{-1}k' + s^{-1}q' \cos\theta_{Kq}) = s^{3/2} \bar{\psi}'(K_F + k' + q' \cos\theta_{Kq}) \tag{4.48}$$

In equation (4.45) we know how all fields transform under the same energy and momentum scalings used in the quadratic parts of the action, therefore this is a good scaling scheme.

With this new understanding, we should also check that in the pure fermion problem the field $\psi(\mathcal{K}_4)$ transforms in a consistent manner. To see this, we need to keep a few more higher order terms than what we showed earlier.

$$
\begin{aligned}
|\vec{K}_4|^2 &= K_1^2 + K_2^2 + K_3^2 + 2\vec{K}_1 \cdot \vec{K}_2 - 2\vec{K}_1 \cdot \vec{K}_2 - 2\vec{K}_3 \cdot \vec{K}_2 && (4.49) \\
&\approx 2K_F(k_1 + k_2 + k_3 + 3/2) + 2K_F\hat{K}_1 \cdot \hat{K}_2(k_1 + k_2 + K_F) \\
&\quad -2K_F\hat{K}_1 \cdot \hat{K}_3(k_1 + k_3 + K_F) - 2K_F\hat{K}_3 \cdot \hat{K}_2(k_3 + k_2 + K_F) && (4.50) \\
&= 2K_F\Big\{ K_F(\hat{K}_1 \cdot \hat{K}_2 - \hat{K}_1 \cdot \hat{K}_3 - \hat{K}_3 \cdot \hat{K}_2 + 3/2) \\
&\quad + k_1[1 + \hat{K}_1 \cdot (\hat{K}_2 - \hat{K}_3)] + k_2[1 + \hat{K}_2 \cdot (\hat{K}_1 - \hat{K}_3)] \\
&\quad + k_3[1 + \hat{K}_3 \cdot (\hat{K}_1 + \hat{K}_2)]\Big\} && (4.51)
\end{aligned}
$$

In the special case where $\vec{K}_1 = \vec{K}_3$, corresponding to forward scattering, we have

$$
|\vec{K}_4| \approx K_F + k_2 + (k_1 - k_3)\hat{K}_1 \cdot \hat{K}_2 \tag{4.52}
$$

This shows

$$
\psi(\mathcal{K}_4') = \psi(K_F + sk_2 + s(k_1 - k_3)\hat{K}_1 \cdot \hat{K}_2) \tag{4.53}
$$

which is precisely the scaling form appropriate for a fermion. In the same way, it is easy to show that the fermion scales appropriately for the cases $\hat{K}_2 = \hat{K}_3$ and $\hat{K}_1 = -\hat{K}_2$.

To summarize, $\psi(\mathcal{K}_4)$ scales like a fermion, $\psi(\mathcal{K}_2)$ scales like a fermion, but $\phi(\mathcal{Q})$ does *not* scale like a boson.

Chapter 5

Fermi Surface and Antiferromagnetism in the Kondo lattice

In chapter 3 we showed how to map the microscopic Kondo Lattice Hamiltonian onto an effective field theory involving a QNLσM coupled to itinerant electrons with a Fermi surface. In chapter 4 we developed a new renormalization group framework that can be used to study problems involving bosons and fermions with a Fermi surface. In this chapter, we will apply this RG framework to analyze the antiferromagnetic phase of the Kondo lattice. First we find the scaling dimension at the tree level, then we examine the one-loop vertex correction. We then explain why, in this scheme, we are allowed to neglect vertex corrections on general grounds. The conclusion is that the Kondo coupling is exactly marginal to all orders. Since there is no flow to strong coupling, Kondo resonances can never develop and the Fermi surface of the antiferromagnetic phase is small. The contents of this chapter are heavily based upon a recent publication [49]. Appendices 5A and 5B give unpublished details of the vertex correction and large-N_Λ calculations. The results of Appendix 5C appeared in [50], but further details are provided there to explain the scaling analysis when the Fermi surface intersects the antiferromagnetic Brillouin zone boundary.

5.1 Scaling at the tree Level

We will describe the $d = 2$ case for the most part, but our conclusions remain valid for any other $d > 1$ dimensions. Our analysis involves a combination of the bosonic RG for the QNLσM [52, 75, 76] and the fermionic RG [63], as developed in Chapter 3. (We

note in passing that a combined bosonic/fermionic RG has been used in the context of several other problems [77, 74].) Without loss of generality, we take the ultraviolet energy cutoffs for the fermions (Λ_f) and bosons (Λ_b) to be $\Lambda \sim \Lambda_f \sim \Lambda_b$. Unless otherwise specified, the variables ($\vec{q}, \omega$) belong to bosonic fields, while ($\vec{K}, \varepsilon$) belong to fermionic fields, with $\vec{K}$ measured from the Brillouin zone center and $k \equiv K - K_F$ is measured relative to the Fermi surface. Under scaling, $\omega \to s\omega$, $\varepsilon \to s\varepsilon$, $\vec{q} \to s\vec{q}$, and $k \to sk$. The fermionic kinetic term specifies [63] that $[\psi(\vec{K}, \varepsilon)] = -3/2$.

For the QNLσM, we write $\vec{n}(\vec{x}, \tau) = \left[\pi_+(\vec{x}, \tau), \pi_-(\vec{x}, \tau), \sqrt{1 - \pi_+^2 - \pi_-^2}\right]$, and define the composite vector boson field $\vec{\varphi}$ by

$$
\vec{n}(\vec{x}, \tau) = \begin{pmatrix} \pi_+(\vec{x}, \tau) \\ \pi_-(\vec{x}, \tau) \\ \sqrt{1 - \pi_+^2 - \pi_-^2} \end{pmatrix}
$$

$$
\dot{\vec{n}}(\vec{x}, \tau) \equiv \frac{\partial \vec{n}(\vec{x}, \tau)}{\partial \tau} = \begin{pmatrix} \dot{\pi}_+(\vec{x}, \tau) \\ \dot{\pi}_-(\vec{x}, \tau) \\ \frac{-\dot{\pi}_+ \pi_+ - \dot{\pi}_- \pi_-}{\sqrt{1 - \pi_+^2 - \pi_-^2}} \end{pmatrix}
$$

$$
\vec{\varphi}(\vec{x}, \tau) \equiv \vec{n}(\vec{x}, \tau) \times \dot{\vec{n}}(\vec{x}, \tau)
$$

$$
= \begin{pmatrix} \frac{1}{\sigma}\left(-\dot{\pi}_- - \dot{\pi}_+ \pi_+ \pi_- + \pi_+ \pi_+ \dot{\pi}_-\right) \\ \frac{1}{\sigma}\left(\dot{\pi}_+ + \dot{\pi}_- \pi_- \pi_+ - \pi_- \pi_- \dot{\pi}_+\right) \\ \dot{\pi}_- \pi_+ - \pi_- \dot{\pi}_+ \end{pmatrix} \tag{5.1}
$$

The square-root factors can be expanded, for example $\frac{1}{\sigma} = \frac{1}{\sqrt{1 - \pi_+^2 - \pi_-^2}} \approx 1 + (1/2)(\pi_+^2 + \pi_-^2) + (3/8)(\pi_+^2 + \pi_-^2)^2 + \cdots$. The scaling dimensions are

$$
[\vec{\varphi}(\vec{x}, \tau)] = [\dot{\pi}(\vec{x}, \tau)] = \left[\frac{\partial}{\partial \tau}\right] = 1 \tag{5.2}
$$

from which it follows that

$$
\begin{aligned}
[\vec{\varphi}(\vec{q},\omega)] &= \left[d^d x \, d\tau \, \vec{\varphi}(\vec{x},\tau) \right] \\
&= -d \quad\quad\quad\quad\quad\quad\quad\quad (5.3)
\end{aligned}
$$

while the coupling constant g has the scaling dimension $[g] = 1 - d$, as is well known for the QNLσM [52]. The dimension of the boson field is a result of the nonlinear constraint and differs markedly from the boson field dimension we found in Chapter 4. As a result, the boson-fermion coupling will have a correspondingly different dimension. Note that in order for the boson-fermion coupling term to satisfy homogeneity, the relative angle (which does not appear in the measure) between $\vec{K}$ and $\vec{K} + \vec{q}$ also needs to scale [77]. As explained in the previous chapter, this is why we choose to write the integral as involving one fermionic momentum and one bosonic momentum, rather than two fermionic momenta. The scaling dimension of the Kondo interaction term is given by

$$
\begin{aligned}
[\mathcal{S}_K] &= \left[dk \, d\varepsilon \, d^d q \, d\omega \, \psi_\alpha^\dagger(\vec{k}+\vec{q},\epsilon+\omega)\psi_\beta(\vec{k},\omega)\, \vec{\sigma}_{\alpha\beta} \cdot \vec{\varphi}(\vec{q},\omega) \right] \\
&= 1 + 1 + d + 1 + 2(-3/2) + (-d) \\
&= 0 \quad\quad\quad\quad\quad\quad\quad\quad\quad\quad\quad\quad\quad (5.4)
\end{aligned}
$$

We reach the important conclusion that $[\lambda] = 0$: at the tree level, the Kondo coupling is marginal in arbitrary spatial dimensions. But this is only the tree-level result. In order to determine if the Kondo coupling is marginally relevant or marginally irrelevant we need consider higher order terms. This is the subject of the next section.

5.2 One-Loop

The Kondo interaction can be written as the sum of longitudinal and spin-flip terms: $\mathcal{S}_K \equiv \Gamma_z + \Gamma_\perp$. It will be convenient to rescale the Goldstone field, $\pi = \sqrt{g}\,\widetilde{\pi}$, and
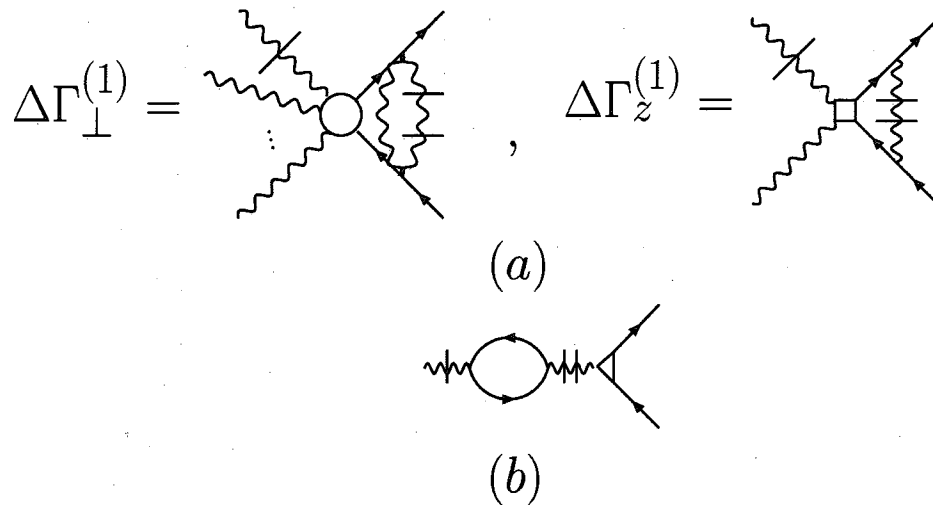
Figure 5.1 : (a) shows the lowest order corrections to the vertices Γ_z and $\Gamma_\perp$. (b) is an example of a class of diagrams that do not contribute to the beta function.

the free-field part of the QNLσM becomes:

$$\mathcal{S}_{\text{QNL}\sigma\text{M}} = \frac{c}{2g} \int d^d x d\tau \, (\partial \pi(\vec{x}, \tau))^2$$

$$= \frac{c}{2} \int d^d x d\tau \, (\partial \tilde{\pi}(\vec{x}, \tau))^2$$

Thus, the dimensions of the new fields $\tilde{\pi}$ and $\vec{\tilde{\varphi}}$ are given by:

$$[\tilde{\pi}(\vec{q}, \omega)] = -\frac{1}{2}(d+3) \tag{5.5}$$

$$\left[\vec{\tilde{\varphi}}(\vec{q}, \omega)\right] = -1 \tag{5.6}$$

$[\tilde{\pi}(\vec{q}, \omega)] = -(d+3)/2$ and $\left[\vec{\tilde{\varphi}}(\vec{q}, \omega)\right] = -1$. There are an infinite number of interaction vertices involving an increasing number of $\tilde{\pi}$ fields, always coupled to exactly two fermion fields; see Fig. 3.2. However, we only need to consider one representative vertex and all its loop corrections; other vertices renormalize in the same way, as dictated by symmetry. For further details on this point, see page 343 of the textbook by Chaikin and Lubensky [76].

We describe in some detail one example of a one-loop correction, that of $\Delta\Gamma_z^{(1)}$

outer fermionic shell

Fermi Surface

inner fermionic shell

$\Lambda - \Lambda/s \equiv d\Lambda$

$\approx \Lambda \log s$

$\vec{K}$

$\vec{P}$

allowed
phase space

bosonic shell

$K_F - \Lambda$

K_F

$K_F + \Lambda$
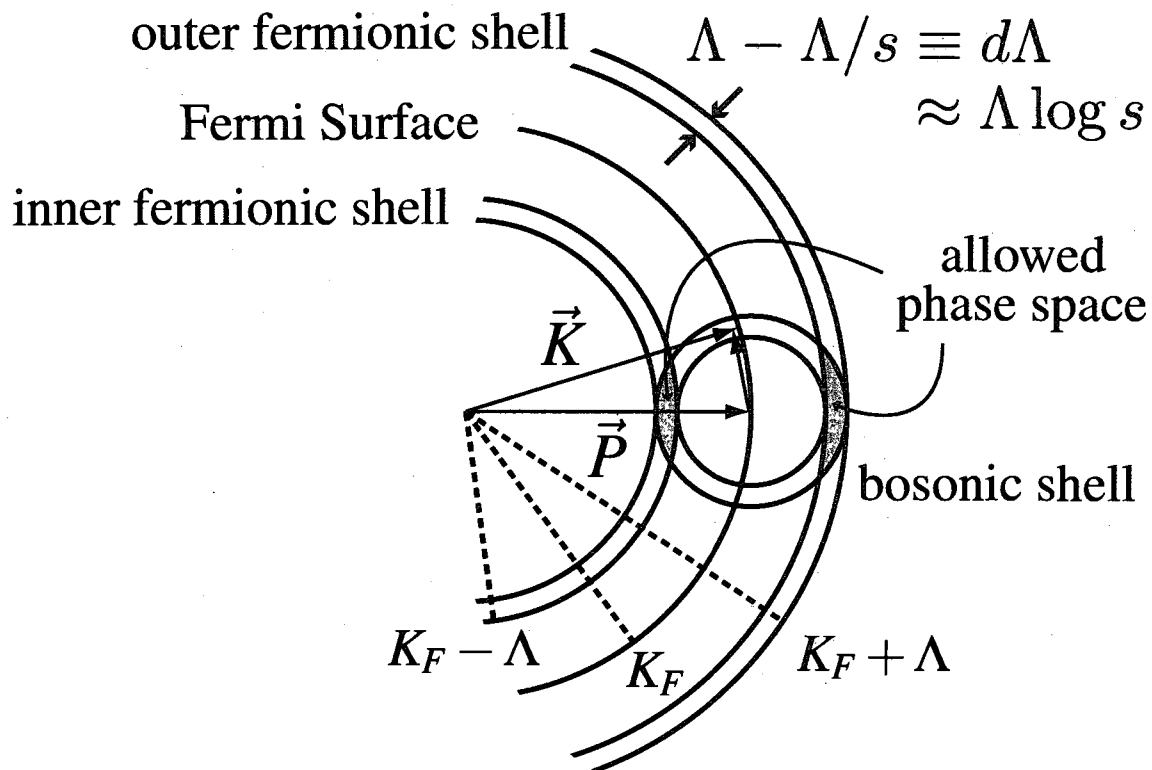
Figure 5.2 : In a combined bosonic/fermionic RG, we require the propagator momenta to live inside the appropriate shells being eliminated, but we also need to conserve momentum. This constrains the phase space so severely that only the shaded region of the figure is integrated over. Straightforward geometric analysis shows that the phase space area is proportional to $d\Lambda\sqrt{\Lambda d\Lambda} \propto (\log s)^{3/2}$.

shown in Fig. 5.1a which we call $\Delta\Gamma_z$. Other corrections are of a similar form and the conclusions are the same.

The conduction-electron propagator is $G^0(\vec{K}, i\varepsilon) = (i\varepsilon - \xi_K)^{-1}$ and the magnon propagator is $D_0(\vec{q}, i\omega) = (i\omega)^2/[(i\omega)^2 - w_{\vec{q}}^2]$, where $w_{\vec{q}} \equiv cq$ and c is the spin-wave velocity.

$$
\begin{aligned}
\Delta\Gamma_z(\vec{q}, i\omega; \vec{P}, ip_l) &= -g^2\lambda_\perp^2\lambda_z i\omega \sum_{i\varepsilon} \int d^d K\, G^0_{\psi_\uparrow^\dagger\psi_\downarrow}(\vec{K}, i\varepsilon)G^0_{\psi_\downarrow^\dagger\psi_\uparrow}(\vec{K}+\vec{q}, i\varepsilon + i\omega) \\
&\quad \times D^0_{\tilde{\pi}_- \tilde{\pi}_+}(\vec{P}-\vec{K}, ip_l - i\varepsilon) \\
&= g^2\lambda_\perp^2\lambda_z \sum_{i\varepsilon} \int d^d K\, \frac{1}{i\varepsilon - \xi_K}\frac{1}{i\varepsilon + i\omega - \xi_{K+q}} \\
&\quad \times \frac{(ip_l - i\varepsilon)^2}{(ip_l - i\varepsilon)^2 - c^2|\vec{P}-\vec{K}|^2}
\end{aligned}
\tag{5.7}
$$

The bosonic momentum $\vec{q}$ is the difference between the momenta of the two external boson lines. Similarly $i\omega$ is the difference in Matsubara frequency of the two external boson lines. Thus, $(\vec{q}, i\omega)$ represents the energy-momentum transfer of the spin-wave fluctuation. The factor $(ip_l - i\varepsilon)^2$ comes from the time derivatives of the *internal* boson propagator.

Summing over the Matsubara frequency leads to

$$
\Delta\Gamma_z(\vec{q}, i\omega; \vec{P}, ip_l) = g^2\lambda_\perp^2\lambda_z i\omega \left[\int_{\text{inner shell}} \gamma_z^{(1)} - \frac{1}{2} \int_{\text{inner+outer shells}} \gamma_z^{(2)} \right]
\tag{5.8}
$$

where

$$
\begin{aligned}
\gamma_z^{(1)} &= \frac{w_{P-K}^2(-2ip_l - i\omega + \xi_K + \xi_{K+q})}{\left[(ip_l - \xi_K)^2 - w_{P-K}^2\right]\left[(ip_l + i\omega - \xi_{K+q})^2 - w_{P-K}^2\right]} \\
\gamma_z^{(2)} &= \frac{1}{[ip_l - w_{P-K} - \xi_K]}\frac{w_{P-K}}{[ip_l + i\omega - w_{P-K} - \xi_{K+q}]}.
\end{aligned}
\tag{5.9}
$$

Here, $(\vec{P}, ip_l)$ label the energy-momentum of one of the two external fermions, while $(\vec{q}, i\omega)$ denotes the energy-momentum transfer between the two external bosons (or,

equivalently, between the two external fermions). The magnon energy is $w_{P-K} = c|\vec{P} - \vec{K}|$. The derivation of this form is given in Appendix 5A. We would normally expect $\Delta\Gamma_z$ to be a function of the four external four-momenta. Conservation of momentum reduces this number to 3, and we denote the difference of the two external boson lines by energy-momentum transfer variables $(\vec{q}, i\omega)$, thus bringing the number to 2.

We can now consider the kinematics of these one-loop corrections. Three momenta, $\vec{P}$, $\vec{K}$, and $\vec{q}$, are involved in the integral for $\Delta\Gamma_z$. The external fermion momentum $\vec{P}$ can be set to the Fermi momentum, $|\vec{P}| \approx K_F$, since any difference would be irrelevant in the RG sense. Likewise, the external boson momentum transfer $\vec{q}$ can be set to zero. The fermionic loop momentum, $\vec{K}$, is restricted to the inner and outer shells straddling the Fermi surface:

$$K_F + \Lambda/s < |\vec{K}| < K_F + \Lambda \tag{5.10}$$

$$K_F - \Lambda < |\vec{K}| < K_F - \Lambda/s \tag{5.11}$$

which is equivalent to:

$$\Lambda/s < k < \Lambda \tag{5.12}$$

$$-\Lambda < k < -\Lambda/s \tag{5.13}$$

Finally, the bosonic momentum $\vec{P} - \vec{K}$ must be contained inside the circle defined by its cutoff: $|\vec{P} - \vec{K}| < \Lambda$.

These restrictions on $\vec{P}$ and $\vec{K}$ lead to the construction shown in Fig. 5.2. The only phase space allowed by momentum conservation is the shaded region in the figure. This limits the loop integration over $\vec{K}$ to the small angular interval from $-\Lambda/K_F$ to $+\Lambda/K_F$, and two radial shells of width $d\Lambda \equiv \Lambda - \Lambda/s \approx \Lambda \log s$ (where $s \gtrsim 1$).

A simple geometric analysis shows that the allowed phase space (shaded region) is proportional to $\Lambda^2 (\log s)^{3/2}$, therefore $\Delta\Gamma_z \propto (\log s)^{3/2}$. The vertex correction is superlinear in $\log s$, so *it does not contribute to the beta function*! Therefore, the Kondo coupling is still marginal at the one-loop level.

We note that if instead of eliminating modes within the momentum shell scheme, we were to integrate over the entire phase space in a field theory approach, then the vertex correction would be of order $g^2 \lambda_\perp^2 \lambda_z \frac{\Lambda}{K_F}$, which is suppressed to zero in the limit $\Lambda/K_F \to 0$. This is shown explicitly in the Appendix 5A.

Finally, there are also vertex corrections due to the interactions purely among the fermion fields or purely among the QNLσM fields. The former do not yield loop corrections in the forward-scattering channel [63]. The latter are irrelevant since g renormalizes to 0.

Let us briefly summarize what has been done so far. We have examined the tree-level and one-loop contributions to the beta function:

$$\beta(J_K) \;=\; b_0 J_K + b_1 J_K^3 + O(J_K^5) \tag{5.14}$$

Tree level marginality means $b_0 = 0$, while the vanishing contribution at one-loop means $b_1 = 0$. This can be seen in the momentum-shell scheme from a simple phase-space analysis which shows that the loop integral is confined to a region of size $(\log s)^{3/2}$. Thus, the one-loop contribution is proportional to $\frac{d}{d\log s}(\log s)^{3/2}\big|_{s=1} = 0$. In a field theory approach, this results from the fact that the one-loop contribution is proportional to a positive power of $\Lambda/K_F \equiv 1/N_\Lambda$.

In the next section we will show that higher order terms are even smaller, thus establishing a sort of Migdal's Theorem which states that the tree-level result is the entire story. Since we found marginality at the tree-level, this is the exact answer to all orders in the limit where $\Lambda/K_F \to 0$.

5.3 Infinite Loops

The kinematic arguments so far are similar to what happens to the renormalization of the forward-scattering interactions in the pure fermion problem, where momentum conservation combined with cutoff considerations severely limit the available phase space [63]. A very similar picture can be extended to the RG beyond one loop. Again, we will describe in detail the d=2 case but the generalization to any other $d > 1$ dimensions is straightforward leading to the same conclusions. See Appendix 5B. We begin by decomposing the Fermi surface into $N_\Lambda \equiv \pi K_F/\Lambda$ patches, and rescale the momentum and energy variables for each patch in terms of Λ: $\bar{\varepsilon} = \varepsilon/\Lambda$, $\bar{k} = k/\Lambda$, and so on. We also absorb a factor of Λ^2 into the fermion field so that the kinetic term for the fermions becomes

$$\mathcal{S}_2^f = \sum_i^{N_\Lambda} \int d^2\bar{k}_i d\bar{\varepsilon}_i \psi_i^\dagger (i\bar{\varepsilon}_i - v_F\bar{k}_i)\psi_i \tag{5.15}$$

and i is the patch index. Likewise, we absorb a factor $\Lambda^{5/2}$ into the $\widetilde{\pi}$ field, so that the kinetic part of the QNLσM is

$$\mathcal{S}_{\mathrm{QNL}\sigma\mathrm{M}} = \int d^2\bar{q} d\bar{\omega} (\bar{q}^2 + \bar{\omega}^2)\widetilde{\pi}^2 \tag{5.16}$$

We then find that the spin-flip Kondo coupling ($\Gamma_\perp$) contains a factor $\Lambda^{1/2}$, and the longitudinal Kondo coupling (Γ_z) contains a factor Λ. In other words, the Kondo couplings are of the order of $(1/\sqrt{N_\Lambda})\lambda_\perp \sum_i \int \varphi\psi^\dagger\psi$ and $(1/N_\Lambda)\lambda_z \sum_i \int \varphi\psi^\dagger\psi$, respectively. This is shown in more detail in Appendix 5B. These extra $1/\sqrt{N_\Lambda}$ and $1/N_\Lambda$ factors make their contributions negligible to infinite loops, except for a chain of particle-hole bubbles (in the spin-flip channel), the lowest order of which is shown in Fig. 5.1b. These iterates of the bubble do not contribute to the beta function, since the two conduction electron poles are located on the same side of the real axis [63].

The Kondo coupling is therefore marginal to infinite loops. This should be contrasted to what happens in the single-impurity Kondo problem. There, the Kondo coupling is relevant and flows to infinity, which signifies singlet formation in the ground state and a concomitant Kondo resonance in the excitation spectrum. In the paramagnetic phase of the Kondo lattice, the Kondo coupling is believed to flow to a related strong coupling fixed point where, again, Kondo resonances are generated and the Fermi surface becomes large.

What we have shown is that inside the antiferromagnet phase an exactly marginal Kondo coupling prevails, implying that there is no Kondo singlet formation and the Fermi surface will remain small in the sense defined earlier.

5.4 Implications

We now turn from the asymptotically exact results to their implications. It is well accepted that two other phases occur in the zero-temperature phase diagram of the Kondo lattice: a paramagnetic phase with a large Fermi surface, PM_L, and an antiferromagnetic phase with a large Fermi surface, AF_L. The existence of PM_L has been most explicitly seen in the large-N limit of the SU(N) generalization of the model [24, 78] [where $\Sigma(\vec{K}, \omega) = (v^*)^2/(\omega - \epsilon_f^*)$ contains a pole and, correspondingly, $G(\vec{K}, \omega)$ yields a large Fermi surface]. Our results demonstrate that the antiferromagnetic part of the phase diagram in principle accommodates a genuine phase transition from AF_S to AF_L. For commensurate antiferromagnetic ordering this corresponds to a Lifshitz transition with a change of Fermi surface topology. Such a transition has been heuristically discussed in the past [42, 18]; our exact result on the stability of the AF_S phase provides evidence for the existence of this Lifshitz transition.

In addition, the existence of the AF_S phase opens the possibility for a direct

quantum transition from the AF$_S$ to the PM$_L$ phases. This is a "Kondo Breakdown" QCP. For this transition to be continuous, the quasiparticle residues z_S and z_L must vanish when the QCP is approached from the two respective sides. The quantum critical point is then a non-Fermi liquid with a divergent effective mass; local quantum criticality [17, 42] is one such example. The results reported here, therefore, provide a new perspective to view local quantum criticality.

5.5   Appendix 5A: One-Loop Vertex Correction

This appendix gives some details about the one-loop vertex correction. The diagram considered earlier in the chapter can be expressed in position space by

$$
\begin{aligned}
\Delta\Gamma &= -\int d^d x_1 d\tau_1 \int d^d x_2 d\tau_2 \int d^d x_3 d\tau_3 \\
&\quad \times \left\langle g\lambda_z \left(\dot{\pi}_-\pi_+\psi_\uparrow^\dagger\psi_\uparrow\right)_{x_1\tau_1} \sqrt{g}\lambda_+ \left(\dot{\pi}_-\psi_\uparrow^\dagger\psi_\downarrow\right)_{x_2\tau_2} \sqrt{g}\lambda_- \left(\dot{\pi}_+\psi_\downarrow^\dagger\psi_\uparrow\right)_{x_3\tau_3}\right\rangle \\
&= -g^2\lambda_+\lambda_-\lambda_z \int d^d x_1 d\tau_1 \int d^d x_2 d\tau_2 \int d^d x_3 d\tau_3 \\
&\quad \times \dot{\pi}_-(\vec{x}_1,\tau_1)\pi_+(\vec{x}_1,\tau_1)\psi_\uparrow^\dagger(\vec{x}_3,\tau_3)\psi_\uparrow(\vec{x}_2,\tau_2) \\
&\quad \times G^0_{\psi_\uparrow^\dagger\psi_\downarrow}(\vec{x}_1,\tau_1|\vec{x}_2,\tau_2)G^0_{\psi_\downarrow^\dagger\psi_\uparrow}(\vec{x}_1,\tau_1|\vec{x}_3,\tau_3)D^0_{\dot{\pi}_-\dot{\pi}_+}(\vec{x}_2,\tau_2|\vec{x}_3,\tau_3)
\end{aligned} \tag{5.17}
$$

We take G^0 to be the bare free-electron propagator, and D^0 to be the propagator for the π field of the nonlinear sigma model. If we translate to momentum space, this defines the vertex correction

$$
\begin{aligned}
\Delta\Gamma(\vec{Q},iq_m;\vec{P},ip_l) &= -g^2\lambda_+\lambda_-\lambda_z iq_m \sum_{ik_n} \int d^d K \, G^0_{\psi_\uparrow^\dagger\psi_\downarrow}(\vec{K},ik_n) \\
&\quad \times G^0_{\psi_\downarrow^\dagger\psi_\uparrow}(\vec{K}+\vec{Q},ik_n+iq_m)D^0_{\dot{\pi}_-\dot{\pi}_+}(\vec{P}-\vec{K},ip_l-ik_n) \quad (5.18) \\
&= -g^2\lambda_+\lambda_-\lambda_z iq_m \sum_{ik_n} \int d^d K \, \frac{1}{ik_n-\xi_K}\frac{1}{ik_n+iq_m-\xi_{K+Q}} \\
&\quad \times \frac{(ip_l-ik_n)^2}{(ip_l-ik_n)^2-c^2|\vec{P}-\vec{K}|^2}
\end{aligned} \tag{5.19}
$$

The factor iq_m comes from the time derivative on the *external* boson line $\dot{\pi}_-$, while the two factors $(ip_l - ik_n)^2$ come from the time derivatives of the *internal* boson propagator. In this appendix iq_m corresponds to the variable $i\omega$ written in the main part of this chapter.

We can do the Matsubara sum over ik_n by standard methods:

$$
\Delta\Gamma(\vec{Q}, iq_m, \vec{P}, ip_l) = -g^2\lambda_+\lambda_-\lambda_z iq_m \int d^dK \Bigg\{
$$

$$
\frac{n_F(\xi_K)}{[iq_m + \xi_K - \xi_{K+Q}]} \frac{(ip_l - \xi_K)^2}{[(ip_l - \xi_K)^2 - \omega_{P-K}^2]}
$$

$$
+ \frac{n_F(\xi_{K+Q} - iq_m)}{[-iq_m + \xi_{K+Q} - \xi_K]} \frac{(ip_l - \xi_{K+Q} + iq_m)^2}{[(ip_l - \xi_{K+Q} + iq_m)^2 - \omega_{P-K}^2]}
$$

$$
+ \frac{1}{2} \frac{n_F(ip_l - \omega_{P-K})}{[ip_l - \omega_{P-K} - \xi_K]} \frac{\omega_{P-K}}{[ip_l - c|\vec{P} - \vec{K}| + iq_m - \xi_{K+Q}]}
$$

$$
- \frac{1}{2} \frac{n_F(ip_l + \omega_{P-K})}{[ip_l + \omega_{P-K} - \xi_K]} \frac{\omega_{P-K}}{[ip_l + c|\vec{P} - \vec{K}| + iq_m - \xi_{K+Q}]} \Bigg\}
$$

$$
\tag{5.20}
$$

Note that we have used the following forms of the boson propagator:

$$
D^0_{\dot{\pi}_-\dot{\pi}_+}(\vec{P} - \vec{K}, ip_l - ik_n) = \frac{(ip_l - ik_n)^2}{(ip_l - ik_n)^2 - \omega_{P-K}^2} \tag{5.21}
$$

$$
= \frac{1}{2}\left(\frac{ip_l - ik_n}{(ip_l - ik_n) + \omega_{P-K}} + \frac{ip_l - ik_n}{(ip_l - ik_n) - \omega_{P-K}}\right) \tag{5.22}
$$

where the bosonic dispersion is defined as usual: $\omega_Q \equiv c|\vec{Q}|$. We can make further simplifications by noting that $n_F(x \pm iq_m) = n_F(x)$ for bosonic frequency $iq_m = i2\pi m/\beta$, and $n_F(x \pm ip_l) = -n_B(x)$ for fermionic frequency $ip_l = i\pi(2l + 1)/\beta$.

The vertex correction is now given by

$$
\Delta\Gamma(\vec{Q}, iq_m, \vec{P}, ip_l) = -g^2 \lambda_+ \lambda_- \lambda_z iq_m \int d^d K \Bigg\{
$$

$$
\frac{\Theta(-\xi_K)}{[iq_m + \xi_K - \xi_{K+Q}]} \frac{(ip_l - \xi_K)^2}{[(ip_l - \xi_K)^2 - \omega_{P-K}^2]}
$$

$$
+ \frac{\Theta(-\xi_{K+Q})}{[-iq_m + \xi_{K+Q} - \xi_K]} \frac{(ip_l + iq_m - \xi_{K+Q})^2}{[(ip_l + iq_m - \xi_{K+Q})^2 - \omega_{P-K}^2]}
$$

$$
+ \frac{1}{2} \frac{\Theta(\omega_{P-K})}{[ip_l - \omega_{P-K} - \xi_K]} \frac{\omega_{P-K}}{[ip_l - c|\vec{P} - \vec{K}| + iq_m - \xi_{K+Q}]}
$$

$$
- \frac{1}{2} \frac{\Theta(-\omega_{P-K})}{[ip_l + \omega_{P-K} - \xi_K]} \frac{\omega_{P-K}}{[ip_l + c|\vec{P} - \vec{K}| + iq_m - \xi_{K+Q}]} \Bigg\}
$$

$$(5.23)$$

Due to the absolute values in the argument of the last two step functions we have $\Theta(\omega_{P-K}) = \Theta(c|\vec{P} - \vec{K}|) = 1$ and $\Theta(-\omega_{P-K}) = \Theta(-c|\vec{P} - \vec{K}|) = 0$.

$$
\Delta\Gamma(\vec{Q}, iq_m, \vec{P}, ip_l) = -g^2 \lambda_+ \lambda_- \lambda_z iq_m \int d^d K \Bigg\{
$$

$$
\frac{\Theta(-\xi_K)}{[iq_m + \xi_K - \xi_{K+Q}]} \frac{(ip_l - \xi_K)^2}{[(ip_l - \xi_K)^2 - \omega_{P-K}^2]}
$$

$$
+ \frac{\Theta(-\xi_{K+Q})}{[-iq_m + \xi_{K+Q} - \xi_K]} \frac{(ip_l + iq_m - \xi_{K+Q})^2}{[(ip_l + iq_m - \xi_{K+Q})^2 - \omega_{P-K}^2]}
$$

$$
+ \frac{1}{2} \frac{\omega_{P-K}}{[ip_l - \omega_{P-K} - \xi_K]} \frac{1}{[ip_l - c|\vec{P} - \vec{K}| + iq_m - \xi_{K+Q}]} \Bigg\}
$$

$$(5.24)$$

At this point we would like to simplify the second term by shifting variables $\vec{K}' \equiv \vec{K} + \vec{Q}$. However, this is not possible because we are using a regularization with an explicit ultraviolet cutoff. Remember, though, that we are interested in the limit $Q \to 0$. Unless $Q > \Lambda$, within the momentum-shell approach the only effect of $\Theta(-\xi_K)$ and $\Theta(-\xi_{K+Q})$ is to restrict the integration region to the inner shell only. Therefore we can combine the first two terms. Since the third term has no Θ function,

we must integrate over both inner and outer shells for that term.

$$
\begin{aligned}
\Delta\Gamma(\vec{Q}, iq_m, \vec{P}, ip_l) \;=\; &-\int\limits_{\text{inner shell}} \frac{g^2\lambda_+\lambda_-\lambda_z iq_m}{[iq_m + \xi_K - \xi_{K+Q}]}\Bigg\{ \frac{(ip_l - \xi_K)^2}{[(ip_l - \xi_K)^2 - \omega_{P-K}^2]} \\
&-\frac{(ip_l + iq_m - \xi_{K+Q})^2}{[(ip_l + iq_m - \xi_{K+Q})^2 - \omega_{P-K}^2]}\Bigg\} \quad\quad (5.25)
\end{aligned}
$$

$$
\begin{aligned}
&-\; g^2\lambda_+\lambda_-\lambda_z\frac{iq_m}{2}\int\limits_{\text{inner+outer shells}}\Bigg\{\frac{1}{[ip_l - \omega_{P-K} - \xi_K]} \\
&\times\frac{\omega_{P-K}}{[ip_l + iq_m - c|\vec{P} - \vec{K}| - \xi_{K+Q}]}\Bigg\} \quad\quad (5.26)
\end{aligned}
$$

Remember that the above equation is only valid in the limit $Q \ll \Lambda$. We can also re-express this by combining terms in the curly brackets.

$$
\begin{aligned}
\Delta\Gamma(\vec{Q}, iq_m, \vec{P}, ip_l) \;=\; &g^2\lambda_+\lambda_-\lambda_z\int\limits_{\text{inner shell}}\Bigg[\frac{iq_m\omega_{P-K}^2}{[(ip_l - \xi_K)^2 - \omega_{P-K}^2]} \\
&\times\frac{(-2ip_l - iq_m + \xi_K + \xi_{K+Q})}{[(ip_l + iq_m - \xi_{K+Q})^2 - \omega_{P-K}^2]}\Bigg] \\
&-\; g^2\lambda_+\lambda_-\lambda_z\int\limits_{\text{inner+outer shells}}\Bigg[\frac{iq_m/2}{[ip_l - \omega_{P-K} - \xi_K]} \\
&\times\frac{\omega_{P-K}}{[ip_l + iq_m - c|\vec{P} - \vec{K}| - \xi_{K+Q}]}\Bigg] \quad\quad (5.27)
\end{aligned}
$$

With $\lambda_+ = \lambda_- \equiv \lambda_\perp$, this is the form of the vertex correction claimed earlier in the chapter.

5.6 Appendix 5B: Large-N_Λ

In this appendix we discuss the details of the large-N_Λ sketched in the chapter. There are two ways in which we can show that the Kondo coupling is a positive power of $1/N_\Lambda$ relative to the kinetic term. First, the patch argument. Decompose the Fermi surface integral into a sum over $N_\Lambda = \pi K_F/\Lambda$ patches each of approximate size Λ^d.

We have something like:

$$\int d^d K d\varepsilon \;=\; \sum_j^{N_\Lambda} \int_{\Lambda^d} d^d k_j \int_{-\infty}^{\infty} d\varepsilon_j \tag{5.28}$$

where j labels the patch index. The integration variables each range over regions on the order of Λ, so let us define new dimensionless variables

$$\varepsilon_j \;\equiv\; \bar{\varepsilon}_j \Lambda \tag{5.29}$$

$$k_j \;\equiv\; \bar{k}_j \Lambda \tag{5.30}$$

such that, for example, k_j is dimensionful while $\bar{k}_j$ is dimensionless. Consider the kinetic term

$$\mathcal{S}_c \;=\; \sum_j^{N_\Lambda} \int_{\Lambda^d} d^d k_j d\varepsilon_j \; \psi_j^\dagger (i\varepsilon_j - v_F k_j)\psi_j \tag{5.31}$$

$$=\; \Lambda^{d+2} \sum_j^{N_\Lambda} \int_1 d^d \bar{k}_j d\bar{\varepsilon}_j \; \psi_j^\dagger (i\bar{\varepsilon} - v_F \bar{k})\psi_j \tag{5.32}$$

The integrals are now over dimensionless regions, so the factor out front gives the overall dimension of the expression (remember that the sum over patches brings in a factor N_Λ). To define this part of the action as our reference point, let us absorb the leading factor into the definition of the field: $\Lambda^{d+2}\psi_j^\dagger\psi_j = \bar{\psi}_j^\dagger\bar{\psi}_j$. This tells us that the fermion fields are of order

$$\psi \propto \Lambda^{-(d+2)/2} \tag{5.33}$$

We do a similar exercise for the QNLσM component of the action (no patching necessary here):

$$\mathcal{S}_{\text{QNL}\sigma\text{M}} \;=\; \int d^d q d\omega (\omega^2 + q^2)|\pi|^2 \tag{5.34}$$

$$=\; \Lambda^{d+3} \int d^d \bar{q} d\bar{\omega} (\bar{\omega}^2 + \bar{q}^2)|\pi|^2 \tag{5.35}$$

To fix this reference point, we define new bosonic fields $\bar{\pi}$ such that

$$\pi \propto \Lambda^{-(d+3)/2} \qquad (5.36)$$

Now we are in a position to determine the dimension of the Kondo interaction relative to these kinetic parts of the action. For the spin-flip part,

$$\Gamma_\perp \;=\; \lambda_\perp \sum_j^{N_\Lambda} \int d^d k \, d\varepsilon \, d^d q \, d\omega [\psi^\dagger \psi (\omega \pi)] \qquad (5.37)$$

Recall that the time derivative on the π field brings in an additional factor of frequency. Re-expressing in terms of our new variables we find:

$$\Gamma_\perp \;=\; \Lambda^{d+1+d+1+2\frac{(-d-2)}{2}+1+\frac{(-d-3)}{2}} \lambda_\perp \sum_j^{N_\Lambda} \int d^d \bar{k} \, d\bar{\varepsilon} \, d^d \bar{q} \, d\bar{\omega} [\bar{\psi}^\dagger \bar{\psi} (\bar{\omega} \bar{\pi})] \qquad (5.38)$$

$$=\; \Lambda^{(d-1)/2} \lambda_\perp \sum_j^{N_\Lambda} \int d^d \bar{k} \, d\bar{\varepsilon} \, d^d \bar{q} \, d\bar{\omega} [\bar{\psi}^\dagger \bar{\psi} (\bar{\omega} \bar{\pi})] \qquad (5.39)$$

We thus find for $d = 2$,

$$\frac{\Gamma_\perp}{\mathcal{S}_c} \;\propto\; \sqrt{\Lambda} \propto \frac{1}{\sqrt{N_\Lambda}} \qquad (5.40)$$

For the non-spin-flip channel we obtain:

$$\Gamma_z \;=\; \lambda_z \sum_j^{N_\Lambda} \int d^d k \, d\varepsilon \, d^d q_1 \, d\omega_1 \, d^d q_2 \, d\omega_2 [\psi^\dagger \psi (\omega \pi \pi)] \qquad (5.41)$$

$$=\; \Lambda^{d+1+d+1+d+1+2\frac{(-d-2)}{2}+1+2\frac{(-d-3)}{2}} \lambda_z \sum_j^{N_\Lambda} \int d^d \bar{k} \, d\bar{\varepsilon} \, d^d \bar{q}_1 \, d\bar{\omega}_1 \, d^d \bar{q}_2 \, d\bar{\omega}_2 [\bar{\psi}^\dagger \bar{\psi} (\bar{\omega} \bar{\pi} \bar{\pi})]$$

$$=\; \Lambda^{d-1} \lambda_z \sum_j^{N_\Lambda} \int d^d \bar{k} \, d\bar{\varepsilon} \, d^d \bar{q}_1 \, d\bar{\omega}_1 \, d^d \bar{q}_2 \, d\bar{\omega}_2 [\bar{\psi}^\dagger \bar{\psi} (\bar{\omega} \bar{\pi} \bar{\pi})] \qquad (5.42)$$

For $d = 2$,

$$\frac{\Gamma_z}{\mathcal{S}_c} \;\propto\; \Lambda \propto \frac{1}{N_\Lambda} \qquad (5.43)$$

There is an alternative way to arrive at the same conclusion without appealing to patching arguments. For a spherical Fermi surface we can write the Fermi momentum integral in terms of spherical coordinates:

$$\int d^d K \;=\; \int_{K_F-\Lambda}^{K_F+\Lambda} K^{d-1} dK \int d^{d-1}\Omega_K \qquad (5.44)$$

$$=\; \int_{-\Lambda}^{\Lambda} (k + K_F)^{d-1} dk \int d^{d-1}\Omega_K \qquad (5.45)$$

The most relevant part of the above is

$$\int d^d K \;=\; K_F^{d-1} \int_{-\Lambda}^{\Lambda} dk \int d^{d-1}\Omega_K \qquad (5.46)$$

Now the kinetic part of the fermions can be written,

$$\mathcal{S}_c \;=\; K_F^{d-1} \int dk\, d^{d-1}\Omega_K\, d\varepsilon\; \psi^\dagger (i\varepsilon - v_F k)\psi \qquad (5.47)$$

We define new dimensionless variables:

$$\varepsilon \;=\; \Lambda\bar{\varepsilon} \qquad (5.48)$$

$$k \;=\; \Lambda\bar{k} \qquad (5.49)$$

$$\Omega_K \;=\; \bar{\Omega}_K \qquad (5.50)$$

$$K_F^{d-1}\Lambda^3 \psi^\dagger\psi \;=\; \bar{\psi}^\dagger\bar{\psi} \qquad (5.51)$$

Note that the angular components of fermionic momenta are untouched. We now have:

$$\mathcal{S}_c \;=\; \int d\bar{k}\, d^{d-1}\bar{\Omega}_K\, d\bar{\varepsilon}\; \bar{\psi}^\dagger (i\bar{\varepsilon} - v_F\bar{k})\bar{\psi} \qquad (5.52)$$

The important difference from the previous patching argument is that now the fermionic fields contain factors of K_F. Plugging this into the Kondo couplings we find (note

that the QNLσM rescaling is identical to what we did previously)

$$\Gamma_\perp = K_F^{1-d}\Lambda^{1+1+d+1-3+1-(d+3)/2}\lambda_\perp \int d\bar{k}d^{d-1}\bar{\Omega}_K d\bar{\varepsilon}d^d\bar{q}d\bar{\omega}[\bar{\psi}^\dagger\bar{\psi}(\bar{\omega}\bar{\pi})] \quad (5.53)$$

$$= \frac{\Lambda^{(d-1)/2}}{K_F^{d-1}}\lambda_\perp \int d\bar{k}d^{d-1}\bar{\Omega}_K d\bar{\varepsilon}d^d\bar{q}d\bar{\omega}[\bar{\psi}^\dagger\bar{\psi}(\bar{\omega}\bar{\pi})] \quad (5.54)$$

For $d = 2$ we have

$$\frac{\Gamma_\perp}{\mathcal{S}_c} \propto \frac{\sqrt{\Lambda}}{K_F} = \frac{1}{\sqrt{N_\Lambda}}\frac{1}{\sqrt{K_F}} \quad (5.55)$$

In the non-spin-flip channel:

$$\Gamma_z = K_F^{1-d}\Lambda^{1+1+d+1+d+1-3+1-2((d+3)/2)}\lambda_z \int d\bar{k}d^{d-1}\bar{\Omega}_K d\bar{\varepsilon}d^d\bar{q}_1 d\bar{\omega}_1 d^d\bar{q}_2 d\bar{\omega}_2[\bar{\psi}^\dagger\bar{\psi}(\bar{\omega}\bar{\pi}\bar{\pi})]$$

$$= \frac{\Lambda^{d-1}}{K_F^{d-1}}\lambda_z \int d\bar{k}d^{d-1}\bar{\Omega}_K d\bar{\varepsilon}d^d\bar{q}_1 d\bar{\omega}_1 d^d\bar{q}_2 d\bar{\omega}_2[\bar{\psi}^\dagger\bar{\psi}(\bar{\omega}\bar{\pi}\bar{\pi})] \quad (5.56)$$

For $d = 2$,

$$\frac{\Gamma_z}{\mathcal{S}_c} \propto \frac{\Lambda}{K_F} = \frac{1}{N_\Lambda} \quad (5.57)$$

We have thus shown that for any $d > 1$ the Kondo vertex will have associated with it positive powers of $1/N_\Lambda$. Because of this, as the number of powers of J_K increases, so does the suppression factor $1/N_\Lambda$. Thus, the tree-level result is the whole story.

5.7 Appendix 5C: Intersection of the Antiferromagnetic Brillouin Zone

This appendix treats the case where the Fermi surface intersects the antiferromagnetic Brillouin zone (AFBZ) boundary. In this case, the linear coupling $\vec{n} \cdot \vec{s}_c$ between the local moments and conduction electron spin cannot be neglected. Until now, we have only considered the term $\vec{L} \cdot \vec{s}_c$ because our assumption has been that the Fermi surface does not intersect the AFBZ boundary, i.e. $Q > 2K_F$. See Fig 3.1 and the comments

following equation (3.47). When $Q < 2K_F$, the conduction electrons see the AF order parameter of the local moments as a staggered scattering potential, resulting in a reconstruction of their Fermi surface. The hot spots of the Fermi surface therefore become gapped out, as shown in Fig. 5.3. At the mean field level, the conduction electron component now becomes:

$$\mathcal{H}_c^{\text{MF}} = \sum_{k\alpha\beta}^{AFBZ} \left(c_{k,\alpha}^\dagger, \ c_{k+Q,\alpha}^\dagger \right) \begin{pmatrix} \tau_{\alpha\beta}^0 \epsilon_k & \tau_{\alpha\beta}^z \Delta \\ \tau_{\alpha\beta}^z \Delta & \tau_{\alpha\beta}^0 \epsilon_{k+Q} \end{pmatrix} \begin{pmatrix} c_{k,\beta} \\ c_{k+Q,\beta} \end{pmatrix}$$

where the sum on k only runs over the AFBZ, $\vec{Q} = (\pi/a, \pi/a)$ is the AF ordering wavevector, τ^μ are the 2×2 Pauli matrices, and the gap is given by the product of the Kondo coupling and expectation value of the massive field of the QNLσM: $\Delta = \lambda\langle\sigma\rangle$. In this mean-field picture, the quadratic Hamiltonian can be simply diagonalized by a unitary transformation:

$$\begin{pmatrix} a_{k\alpha} \\ b_{k\alpha} \end{pmatrix} = \begin{pmatrix} u_k \sigma_{\alpha\beta}^0 & v_k \sigma_{\alpha\beta}^z \\ v_k \sigma_{\alpha\beta}^z & -u_k \sigma_{\alpha\beta}^0 \end{pmatrix} \begin{pmatrix} c_{k\beta} \\ c_{k+Q,\beta} \end{pmatrix}. \tag{5.58}$$

Using these new quasiparticles, the effective spin-flip Kondo couplings become

$$-\frac{J_K}{2} \sum_k^{AFBZ} \sum_q^{BZ} \left[\Gamma^{\sigma\bar\sigma}(k,q) \left(a_{k\sigma}^\dagger a_{k+q,\bar\sigma} - b_{k\sigma}^\dagger b_{k+q,\bar\sigma} \right) n_q^{\bar\sigma} \right] \tag{5.59}$$

where $\Gamma^{\sigma\bar\sigma}(k,q) = u_k v_{k+q} - v_k u_{k+q}$ is the coherence factor. See the next section. The other terms, such as inter-band interactions (e.g. $a^\dagger b$) are gapped out at low energies. Near the ordering wavevector the vertex is linear in momentum: $\Gamma^{\uparrow\downarrow}(k,q) \propto q$, where $\vec{q}$ is the deviation from the AF ordering wavevector $\vec{Q}$. (See e.g., Ref. [79].) The form of this linear-momentum suppression factor survives beyond the mean-field treatment of the conduction electron band, as dictated by Adler's Theorem [80]. Within the RG analysis, the linear-momentum factor serves the same function as the time derivative in $\vec{\varphi}$ to preserve the marginality of the transverse Kondo coupling.

The next section will show how we obtain the momentum dependence of the coherence factor.
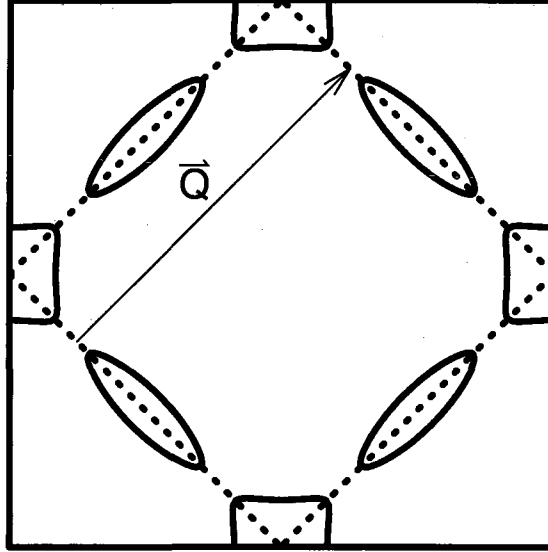
Figure 5.3 : When the Fermi surface of the conduction electrons intersects the AFBZ boundary (the dashed lines), the Kondo coupling connects the re-diagonalized fermions (whose Fermi surfaces are given by the solid lines) to the QNLσM fields.

5.7.1 Kondo coupling coherence factors

We are interested in the following spin-fermion coupling:

$$\Gamma_\perp = \frac{J_K}{2} \sum_r c_{r\alpha}^\dagger \sigma_{\alpha\beta} c_{r\beta} \cdot \mathbf{S}_r = \frac{J_K}{2} \sum_r \sum_{k_1,k_2,q} e^{i(k_1-k_2+q)\cdot r} c_{k_1\alpha}^\dagger \sigma_{\alpha\beta} c_{k_2\beta} \cdot \mathbf{S}_q \quad (5.60)$$

For the local moment spin we write $\mathbf{S}_q \approx \mathbf{n}_q e^{iQ\cdot r} + \mathbf{L}_q$. Plugging in:

$$\Gamma_\perp = \frac{J_K}{2} \sum_r \sum_{k_1,k_2,q} e^{i(k_1-k_2+q)\cdot r} c_{k_1\alpha}^\dagger \sigma_{\alpha\beta} c_{k_2\beta} \cdot \left(\mathbf{n}_q e^{iQ\cdot r} + \mathbf{L}_q \right) \qquad (5.61)$$

$$= \frac{J_K}{2} \sum_{k,q} \left(c_{k\alpha}^\dagger \sigma_{\alpha\beta} c_{k+q+Q,\beta} \cdot \mathbf{n}_q + c_{k\alpha}^\dagger \sigma_{\alpha\beta} c_{k+q,\beta} \cdot \mathbf{L}_q \right) \qquad (5.62)$$

Now we need to rewrite the sum over fermion wavevectors in the full Brillouin zone as a sum over only the magnetic Brillouin zone:

$$
\Gamma_\perp = \frac{J_K}{2} \sum_{\alpha\beta} \sigma_{\alpha\beta} \cdot \left\{ \sum_k^{BZ} \sum_q^{BZ} \left[c_{k\alpha}^\dagger c_{k+q+Q,\beta} \mathbf{n}_q + c_{k\alpha}^\dagger c_{k+q,\beta} \mathbf{L}_q \right] \right\} \tag{5.63}
$$

$$
= \frac{J_K}{2} \sum_{\alpha\beta} \sigma_{\alpha\beta} \cdot \left\{ \sum_k^{AFBZ} \sum_q^{BZ} \right] \left(c_{k\alpha}^\dagger c_{k+q+Q,\beta} + c_{k+Q,\alpha}^\dagger c_{k+q+2Q,\beta} \right) \mathbf{n}_q
$$
$$
+ \left(c_{k\alpha}^\dagger c_{k+q,\beta} + c_{k+Q,\alpha}^\dagger c_{k+q+Q,\beta} \right) \mathbf{L}_q \right] \right\} \tag{5.64}
$$

$$
= \frac{J_K}{2} \sum_{\alpha\beta} \sigma_{\alpha\beta} \cdot \left\{ \sum_k^{AFBZ} \sum_q^{BZ} \left[\left(c_{k\alpha}^\dagger d_{k+q,\beta} + d_{k\alpha}^\dagger c_{k+q,\beta} \right) \mathbf{n}_q + \left(c_{k\alpha}^\dagger c_{k+q,\beta} \right. \right. \right.
$$
$$
\left. \left. \left. + d_{k\alpha}^\dagger d_{k+q,\beta} \right) \mathbf{L}_q \right] \right\} \tag{5.65}
$$

where $d_{k\alpha}^\dagger \equiv c_{k+Q,\alpha}^\dagger$. From here we need to substitute the inverse Bogoliubov transformation:

$$
c_{k,\alpha} = u_k \sigma_{\alpha\beta}^0 a_{k\beta} + v_k \sigma_{\alpha\beta}^z b_{k\beta} \tag{5.66}
$$

$$
d_{k,\alpha} = v_k \sigma_{\alpha\beta}^z a_{k\beta} - u_k \sigma_{\alpha\beta}^0 b_{k\beta} \tag{5.67}
$$

According to Adler's Principle, the effective vertices between the Bogoliubov fermions a_k, b_k and the spin variables $\mathbf{n}_q, \mathbf{L}_q$ should give us something that vanishes when $q = Q$ for vertices involving $\mathbf{n}$ fields, though the situation is not so clear for vertices with $\mathbf{L}$

fields.

$$
\begin{aligned}
\Gamma_\perp \;=\; & \frac{J_K}{2} \sum_{\alpha\beta} \sigma_{\alpha\beta} \cdot \Bigg\{ \sum_k^{AFBZ} \sum_q^{BZ} \Bigg[\Bigg(\\
& \left[u_k \sigma_{\alpha\delta}^0 a_{k\delta}^\dagger + v_k \sigma_{\alpha\delta}^z b_{k\delta}^\dagger \right] \left[v_{k+q} \sigma_{\beta\gamma}^z a_{k+q,\gamma} - u_{k+q} \sigma_{\beta\gamma}^0 b_{k+q,\gamma} \right] \\
+\; & \left[v_k \sigma_{\alpha\delta}^z a_{k\delta}^\dagger - u_k \sigma_{\alpha\delta}^0 b_{k\delta}^\dagger \right] \left[u_{k+q} \sigma_{\beta\gamma}^0 a_{k+q,\gamma} + v_{k+q} \sigma_{\beta\gamma}^z b_{k+q,\gamma} \right] \Bigg) \mathbf{n}_q \\
+\; & \Bigg(\left[u_k \sigma_{\alpha\delta}^0 a_{k\delta}^\dagger + v_k \sigma_{\alpha\delta}^z b_{k\delta}^\dagger \right] \left[u_{k+q} \sigma_{\beta\gamma}^0 a_{k+q,\gamma} + v_{k+q} \sigma_{\beta\gamma}^z b_{k+q,\gamma} \right] \\
+\; & \left[v_k \sigma_{\alpha\delta}^z a_{k\delta}^\dagger - u_k \sigma_{\alpha\delta}^0 b_{k\delta}^\dagger \right] \left[v_{k+q} \sigma_{\beta\gamma}^z a_{k+q,\gamma} - u_{k+q} \sigma_{\beta\gamma}^0 b_{k+q,\gamma} \right] \Bigg) \mathbf{L}_q \Bigg] \Bigg\} \quad (5.68)
\end{aligned}
$$

$$
\begin{aligned}
=\; & \frac{J_K}{2} \sum_{\alpha\beta} \sigma_{\alpha\beta} \cdot \Bigg\{ \sum_k^{AFBZ} \sum_q^{BZ} \Bigg[\\
& \Bigg(V_{aa}^{\alpha\beta}(k,q) a_{k\alpha}^\dagger a_{k+q,\beta} + V_{bb}^{\alpha\beta}(k,q) b_{k\alpha}^\dagger b_{k+q,\beta} + V_{ab}^{\alpha\beta}(k,q) a_{k\alpha}^\dagger b_{k+q,\beta} \\
& + V_{ba}^{\alpha\beta}(k,q) b_{k\alpha}^\dagger a_{k+q,\beta} \Bigg) \mathbf{n}_q \\
& \Bigg(W_{aa}^{\alpha\beta}(k,q) a_{k\alpha}^\dagger a_{k+q,\beta} + W_{bb}^{\alpha\beta}(k,q) b_{k\alpha}^\dagger b_{k+q,\beta} + W_{ab}^{\alpha\beta}(k,q) a_{k\alpha}^\dagger b_{k+q,\beta} \\
& + W_{ba}^{\alpha\beta}(k,q) b_{k\alpha}^\dagger a_{k+q,\beta} \Bigg) \mathbf{L}_q \Bigg] \Bigg\} \quad (5.69)
\end{aligned}
$$

The vertices are defined as follows:

$$
V_{aa}^{\alpha\beta}(k,q) \;=\; (\beta u_k v_{k+q} + \alpha v_k u_{k+q}) \quad (5.70)
$$

$$
V_{bb}^{\alpha\beta}(k,q) \;=\; -(\alpha u_k v_{k+q} + \beta v_k u_{k+q}) \quad (5.71)
$$

$$
V_{ab}^{\alpha\beta}(k,q) \;=\; (-u_k u_{k+q} + v_k v_{k+q}) \quad (5.72)
$$

$$
V_{ba}^{\alpha\beta}(k,q) \;=\; (v_k v_{k+q} - u_k u_{k+q}) \quad (5.73)
$$

$$
W_{aa}^{\alpha\beta}(k,q) \;=\; (u_k u_{k+q} + \alpha\beta v_k v_{k+q}) \quad (5.74)
$$

$$
W_{bb}^{\alpha\beta}(k,q) \;=\; (\alpha\beta v_k v_{k+q} + u_k u_{k+q}) \quad (5.75)
$$

$$
W_{ab}^{\alpha\beta}(k,q) \;=\; (\beta u_k v_{k+q} - \alpha v_k u_{k+q}) \quad (5.76)
$$

$$
W_{ba}^{\alpha\beta}(k,q) \;=\; (\alpha v_k u_{k+q} - \beta u_k v_{k+q}) \quad (5.77)
$$

The important interaction terms are those which do not involve an energy gap (from band a to a, or b to b, but not a to b), and flip the spin of the fermion ($\alpha = -\beta$). These are:

$$V_{aa}^{\alpha\bar{\alpha}}(k,q) = -V_{bb}^{\alpha\bar{\alpha}}(k,q) = -\alpha\left(u_k v_{k+q} - v_k u_{k+q}\right) \tag{5.78}$$

$$W_{aa}^{\alpha\bar{\alpha}}(k,q) = W_{bb}^{\alpha\bar{\alpha}}(k,q) = \left(u_k u_{k+q} - v_k v_{k+q}\right) \tag{5.79}$$

These expression agree with Vekhter and Chubukov [79]. The explicit momentum dependence of these quantities can be further simplified for small q:

$$u_{k+q} = u_k + A(k,Q) + O(q^2) \tag{5.80}$$

$$A(k,Q) = \frac{\Delta\sqrt{2}\left[2\Delta^2 + \delta_k(\delta_k + D_k)\right](\epsilon'_k - \epsilon'_{k+Q})}{D_k^{5/2}(\delta_k + D_k)^{3/2}} \tag{5.81}$$

$$v_{k+q} = v_k + B(k,Q)q + O(q^2) \tag{5.82}$$

$$B(k,Q) = \frac{\Delta^2\sqrt{2}(\epsilon'_k - \epsilon'_{k+Q})}{D_k^{5/2}\sqrt{\delta_k + D_k}} \tag{5.83}$$

where we have used the shorthand $\epsilon'_k \equiv \left.\frac{\partial \epsilon_{k+q}}{\partial q}\right|_{q=0}$. This approximation shows that the interaction vertex involving the Goldstone mode is:

$$V_{aa}^{\alpha\bar{\alpha}}(k,q) = -V_{bb}^{\alpha\bar{\alpha}}(k,q) = -\alpha\left[(u_k v_k - v_k u_k) + q(Bu_k - Av_k) + O(q^2)\right] \tag{5.84}$$

$$= -\alpha\left[q(Bu_k - Av_k) + O(q^2)\right] \tag{5.85}$$

Thus, the leading order term is linear in q and the vertex vanishes for $q \to 0$. This is in accord with Adler's Theorem. Note that here we are measuring q from Q rather than from zero. This is clear because we have:

$$S_r = n_r e^{\pm iQ \cdot r} + L_r \tag{5.86}$$

$$\implies S_q = n_{q\pm Q} + L_q \tag{5.87}$$

where we've noted that for a general function $\phi(t)$ and its Fourier transform $\Phi(\omega)$, the Fourier transform of $\phi(t)e^{i\Omega t}$ is simply $\Phi(\omega + \Omega)$. So multiplying by exponentials

in real space merely shifts the argument of the Fourier transform in reciprocal space.

To summarize, this appendix has shown that when the Fermi surface intersects the AFBZ boundary the coherence factors produced in the re-diagonalization of fermions induce an additional factor of q in the effective coupling. This can be viewed as a kinematic suppression similar to the deformation potential problem of the electron-phonon system [80]. From the RG perspective, the additional factor of q represents a decrease in the dimension of the coupling which has the same effect as a derivative coupling: $\vec{s}_c \cdot \vec{n}_q \rightarrow q a^\dagger a \vec{\sigma} \cdot \vec{n}_q$. Now the conduction electron spin is coupled directly to $\vec{n}_q$ which has dimension $[\pi_q] = -d - 1$, but the additional factor of q brings the dimension to $[q\, \vec{n}_q] = -d$ which has the same value as the vector field $[\vec{\varphi}_q] = -d$ we considered earlier for the case where the Fermi surface does not intersect the AFBZ boundary. Therefore, our previous result on the marginality of the Kondo coupling is not spoiled when the Fermi surface intersects the magnetic zone boundary.

Chapter 6

Ferromagnetism in the Kondo Lattice

6.1 Introduction and Motivations

We now turn our attention from antiferromagnetic to ferromagnetic order in heavy fermion materials. The next few chapters are based on work submitted for publication and currently posted on the arXiv [81]. Surprisingly, a rigorous theoretical basis for metallic ferromagnetism is still largely missing [82]. The Stoner approach perturbatively treats Coulomb interactions when the latter need to be large [2], while the Nagaoka approach incorporates thermodynamically negligible holes into a half-filled band [83]. We will show that the ferromagnetic order of the Kondo lattice is amenable to an asymptotically exact analysis over a range of interaction parameters. In the ferromagnetic phase, the conduction electrons and local moments are strongly coupled but the Fermi surface does not enclose the latter (*i.e.*, it is "small"). Moreover, non-Fermi liquid behavior appears over a range of frequencies and temperatures, which will be demonstrated in the next chapter. Our results provide the basis to understand some long-standing puzzles [84, 85, 86] in the ferromagnetic heavy fermion metals, and raises the prospect for a new class of ferromagnetic quantum phase transitions.

The vast majority of theoretical work on magnetic heavy fermions has focused on antiferromagnetism [46, 6]. Nonetheless, the list of heavy fermion metals which are known to exhibit ferromagnetic order continues to grow. An early example subjected to extensive studies is $CeRu_2Ge_2$ (ref. [87] and references therein). Other ferromagnetic heavy fermion metals include CePt [88], $CeSi_x$ [89], $CeAgSb_2$ [90], and $URu_{2-x}Re_xSi_2$ at x > 0.3 [91]. More recently discovered materials include

CeRuPO [92] and UIr_2Zn_{20} [30]. Finally, systems such as UGe_2 [93] and URhGe [94] are particularly interesting because they exhibit a superconducting dome as their metallic ferromagnetism is tuned toward its border. Some fascinating and general questions have emerged, yet they have hardly been addressed theoretically. One central issue concerns the nature of the Fermi surface: Is it "large," encompassing both the local moments and conduction electrons as in paramagnetic heavy fermion metals [16, 26], or is it "small," incorporating only conduction electrons? Measurements of the de Haas-van Alphen (dHvA) effect have suggested that the Fermi surface is small in $CeRu_2Ge_2$ [84, 85, 86], and have provided evidence for Fermi surface reconstruction as a function of pressure in UGe_2 [95]. At the same time, it is traditional to consider the heavy fermion ferromagnets as having a large Fermi surface when their relationship with unconventional superconductivity is discussed [93, 94]; an alternative form of the Fermi surface in the ordered state could give rise to a new type of superconductivity near its phase boundary. All these point to the importance of theoretically understanding the ferromagnetic phases of heavy fermion metals, and this will be the focus of the next few chapters. The derivation of the effective field theory will closely parallel the antiferromagnetic case, but the resulting form will be slightly different. Moreover, the scaling analysis will require significant modification due to the presence of a Stoner gap in the excitation spectrum and a different form of the dynamics, corresponding to $z \neq 1$. This chapter has the modest goal of establishing the effective field theory appropriate for the ferromagnetically ordered phase, while the next chapter will present its analysis.

6.2 Field Theory for the Ferromagnetic Phase

As before, we begin with the Kondo lattice model in which a periodic array of local moments interact with each other and with a conduction-electron band. Kondo lattice systems are normally studied in the paramagnetic state, where Kondo screening leads to heavy quasiparticles in the single-electron excitation spectrum [16]. The Stoner mean field treatment of these heavy quasiparticles may then lead to an itinerant ferromagnet [96]. With the general limitations of the Stoner approach in mind, here we carry out an asymptotically exact analysis of the ferromagnetic state. We are able to do so by using a reference point that differs from both the Stoner or Nagaoka limits.

The model contains a lattice of spin-$\frac{1}{2}$ local moments ($\mathbf{S}_i$ for each site i) with a ferromagnetic exchange interaction ($I < 0$), a band of conduction electrons ($c_{\vec{K}\sigma}$, where $\vec{K}$ is the wavevector and σ the spin index) with a dispersion $\epsilon_{\vec{K}}$ and a characteristic bandwidth W, and an on-site antiferromagnetic Kondo exchange interaction ($J_K > 0$) between the local moments and the spin of the conduction electrons. The corresponding Hamiltonian is

$$H = \sum_{\vec{K}} \epsilon_{\vec{K}} c_{\vec{K}\sigma}^{\dagger} c_{\vec{K}\sigma} + I \sum_{\langle ij \rangle} S_i^a S_j^a + \sum_i J_K^a S_i^a c_{i\sigma}^{\dagger} \frac{T_{\sigma\sigma'}^a}{2} c_{i\sigma'}. \qquad (6.1)$$

Here I represents the sum of direct exchange interaction between the local moments and the effective exchange interaction generated by the conduction electron states that are not included in Eq. 6.1. Incorporating this explicit exchange interaction term allows the study of the global phase diagram of the Kondo lattice systems, and tuning a control parameter in any specific heavy fermion material represents taking a cut within this phase diagram. As a side remark, a distinction should be made between this problem and what is sometimes called the "ferromagnetic Kondo lattice" in the

literature [97]. Such double-exchange ferromagnet studies are typically focused on the manganites where the local moments belong to the lowest submanifold of a crystal-field-split d-shell (say, t_{2g}), while the conduction electrons live in the higher manifold of the same d-shell (e_g). Due to Hund's rules, the coupling between the local moment and conduction electron is necessarily ferromagnetic. This is *not* the situation under investigation here. We consider local moments which belong to the f-orbitals of a rare-earth element, such as Ce, which couple antiferromagnetically to conduction electrons residing in metallically hybridized d- or s-orbitals. Of course the J-multiplet will also be split by the crystal field, often resulting in a ground state doublet for Kramers ions, but the essential difference we care about is the antiferromagnetic spin exchange coupling between the local moment ground state doublet and the conduction electron spin. We usually refer to this spin exchange as a "Kondo coupling."

The parameter region we will focus on is $J_K \ll |I| \ll W$. Here we can use the limit $J_K = 0$ as the reference point where local moments represent f-electrons with strong Coulomb repulsion and are decoupled from the conduction electrons. As illustrated in Fig. 6.1, the local moments order in a ferromagnetic ground state because $I < 0$, whereas the conduction electrons form a Fermi sea with a Fermi surface. A finite but small J_K will couple these two components, and its effect is analyzed in terms of a fermion+boson renormalization group (RG) procedure [81, 49, 68, 63] described in the next chapter. Though our analysis will focus on this weak J_K regime, the results will be germane to a more extended parameter regime through continuity.

The Heisenberg part of the Hamiltonian, describing the local moments alone, is mapped to a continuum field theory [98] in the form of a Quantum Nonlinear Sigma Model (QNLσM). In this framework, the local moments are represented by an O(3) field, $\vec{m}$, which is constrained non-linearly with the following continuum partition
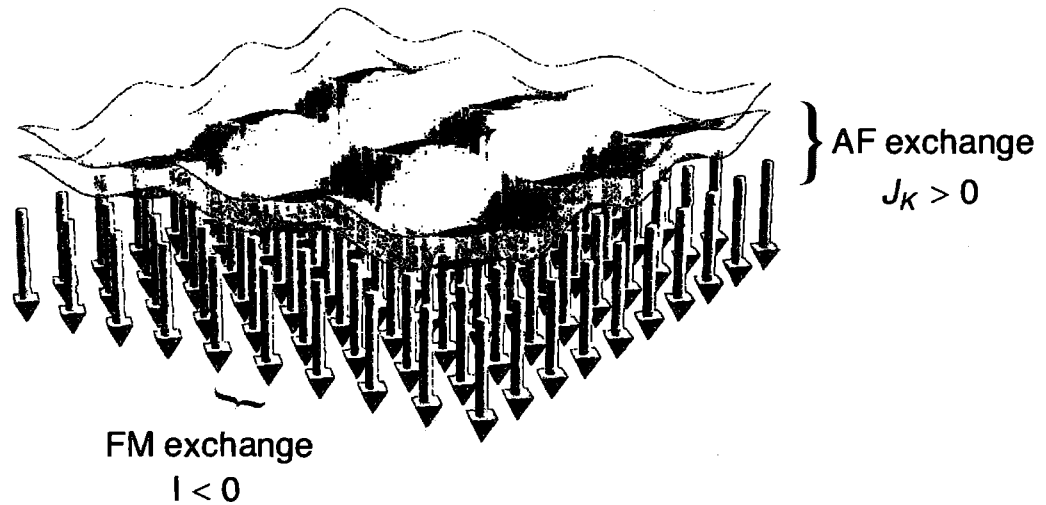
Figure 6.1 : An illustration of the Kondo lattice. Local moments from f-orbitals are in green, and are depicted here to be spin down. Spin-up conduction electrons are in red, which have a higher probability density than the spin-down conduction electrons in blue. The Hamiltonian for the model is given in Eq. (6.1) where σ is the spin index and a refers to the three spin directions. Note that the Einstein summation convention is used on indices. For simplicity, we assume $\epsilon_{\vec{K}} = \frac{K^2}{2m_e}$. The characteristic kinetic energy, W, is defined as $W \equiv 1/\rho_0$, where $\rho_0 \equiv \sum_{\vec{K}} \delta(E_F - \epsilon_{\vec{K}})$ is the single-particle density of states at the Fermi energy (E_F). Both E_F and the chemical potential, μ, scale like W. We use the Shankar notation with $K = |\vec{K}|$ measured from the center of the Brillouin zone.

function.

$$Z = \int \mathcal{D}\vec{m} \mathcal{D}[\bar{\psi}, \psi] \, \delta(\vec{m}^2(\vec{x}, \tau) - 1)e^{-\mathcal{S}} \quad .$$

$$\mathcal{S} \equiv \mathcal{S}'_m + \mathcal{S}_{\text{Berry}} + \mathcal{S}'_c + \mathcal{S}_K$$

$$\mathcal{S}'_m = \frac{\rho_s}{2} \int d^d x d\tau \, \frac{\partial m^a(\vec{x}, \tau)}{\partial x^\mu} \frac{\partial m^a(\vec{x}, \tau)}{\partial x^\mu}$$

$$\mathcal{S}_{\text{Berry}} = iM_0 \int d^d x d\tau \, A^a[\vec{m}] \frac{\partial m^a(\vec{x}, \tau)}{\partial \tau}$$

$$\mathcal{S}'_c = \int d^d x d\tau \, \bar{\psi}_\sigma(\vec{x}, \tau) \left(\partial_\tau - \frac{\nabla^2}{2m_e} - \mu \right) \psi_\sigma(\vec{x}, \tau)$$

$$\mathcal{S}_K = J_K^a \int d^d x d\tau \, s_c^a(\vec{x}, \tau) m^a(\vec{x}, \tau) \tag{6.2}$$

where, as usual, $s_c^a \equiv \bar{\psi}_{i\sigma} \frac{\tau_{\sigma\sigma'}^a}{2} \psi_{i\sigma'}$. The topological Berry phase term is crucial to capture the dynamics correctly [99]. If we define the z-axis as the direction of magnetization, we have $\nabla_m \times \vec{A} = (0, 0, 1) = \langle \vec{m} \rangle$ (note that the curl is in field space, not real space). Thus, in a linearized, low-energy theory of spin fluctuations, we have $\vec{A} \approx (-m_y, m_x, 0)$. Defining $m^+ = m_x + im_y$ and $m^- = m_x - im_y$ we obtain a theory of a single complex scalar

$$\mathcal{S}_m = \mathcal{S}'_m + \mathcal{S}_{\text{Berry}} \tag{6.3}$$

$$\approx \frac{1}{2} \int d\omega d^d q \, m^+(\vec{q}, i\omega) \left(-M_0 i\omega + \rho_s q^2 \right) m^-(-\vec{q}, -i\omega)$$

$$+ g \int (\partial m)^4 \tag{6.4}$$

Here, M_0 is the magnetization density, and ρ_s the magnon stiffness constant. The magnon-magnon coupling g, schematically written above and more precisely specified in the next chapter, turns out to be irrelevant in the RG sense when fermions are also coupled to the system. Finally, the Kondo coupling can be separated into static and dynamic parts. The static order of the local moments induces a splitting of the conduction electron band on the order of $\Delta \sim J_K^z \langle m^z \rangle \sim J_K^z$, which modifies $\mathcal{S}'_c$ into

the following action for the conduction electrons

$$\mathcal{S}_c = \int d^d K d\epsilon \, \bar{\psi}_\sigma(\vec{K}, \epsilon) \left(-i\epsilon + \frac{K^2}{2m_e} - \mu + \sigma\Delta \right) \psi_\sigma(\vec{K}, \epsilon) \tag{6.5}$$

The dynamical part couples the magnons with the conduction electrons, leading to

$$\mathcal{S}_K^\pm = J_K^\pm \int d^d q d\omega d^d K d\varepsilon \left(\psi^\dagger_{K+q,\uparrow} \psi_{K,\downarrow} m_q^- + \psi^\dagger_{K+q,\downarrow} \psi_{K,\uparrow} m_q^+ \right) \tag{6.6}$$

$$\mathcal{S}_K^z = -\frac{J_K^z}{2} \int d^d q_1 d\omega_1 d^d q_2 d\omega_2 d^d K d\varepsilon \left(\psi^\dagger_{K+q_1-q_2,\sigma} \tau^z_{\sigma\sigma'} \psi_{K,\sigma'} m_{q_1}^- m_{q_2}^+ \right) \tag{6.7}$$

The mapping from the microscopic model in Eq. (6.1) to the field theory in (6.3)-(6.7) is similar to the antiferromagnetic case [49], but differs from the latter in several important ways. One simplification is that translational symmetry is preserved in the ferromagnetic phase. At the same time, two complications arise. Ferromagnetic order breaks time-reversal symmetry, which is manifested in the Zeeman splitting of the spin up and down bands. In addition, the effective field theory for a local-moment quantum ferromagnet involves a Berry phase term [98] such that Lorentz invariance is broken, even in the continuum limit; the dynamic exponent, connecting ω and q in Eq. (6.3), is $z = 2$ instead of 1. The effective field theory, comprising Eqs. (6.3)-(6.7), is subjected to a two-stage RG analysis as detailed in the next chapter.

Chapter 7

Fermi Surface, non-Fermi Liquid, and Ferromagnetism in the Kondo Lattice

The previous chapter presented the derivation of the QNLσM representation of the ferromagnetic Kondo lattice. This chapter is devoted to its analysis for the purpose of answering the same question posed earlier for the antiferromagnetic phase: Is the Fermi surface large or small? The analysis will prove to be significantly more complicated than the antiferromagnetic phase as the length of this chapter testifies. For the sake of clarity, a summary of all the results and their implications are presented in the next subsection. The rest of the chapter will provide the details explaining how those conclusions can be derived. The contents of this chapter will appear in a future publication [81].

7.1 Summary of Results and Implications

The most important concepts to physically understand about the ferromagnetic phase of the Kondo lattice are depicted in figure 7.1. This displays the spin-subband splitting of the conduction electrons induced by the local-moment ferromagnetic order, and the resulting effect on the excitation spectrum which is a gap in the spin-flip continuum. As mentioned at the end of the last chapter, this splitting will lead to a separation of the problem into two kinematic regimes. At the lowest energy scales, the local-moment magnon is undamped and propagates with $z = 2$. At higher energies, it enters the damping continuum and transforms into $z = 3$. This can be seen by incorporating self-energy corrections as detailed in later subsections of this chapter.

From the perspective of the RG, it is perhaps more sensible to think about the high energy regime first, and scale down (integrate out high energy modes) to lower energies to see how the behavior changes. We refer to the energy and momentum where the magnon enters the continuum as cutoffs, (q_c, ω_c), since this divides the problem into two dynamical regimes which call for separate analyses.
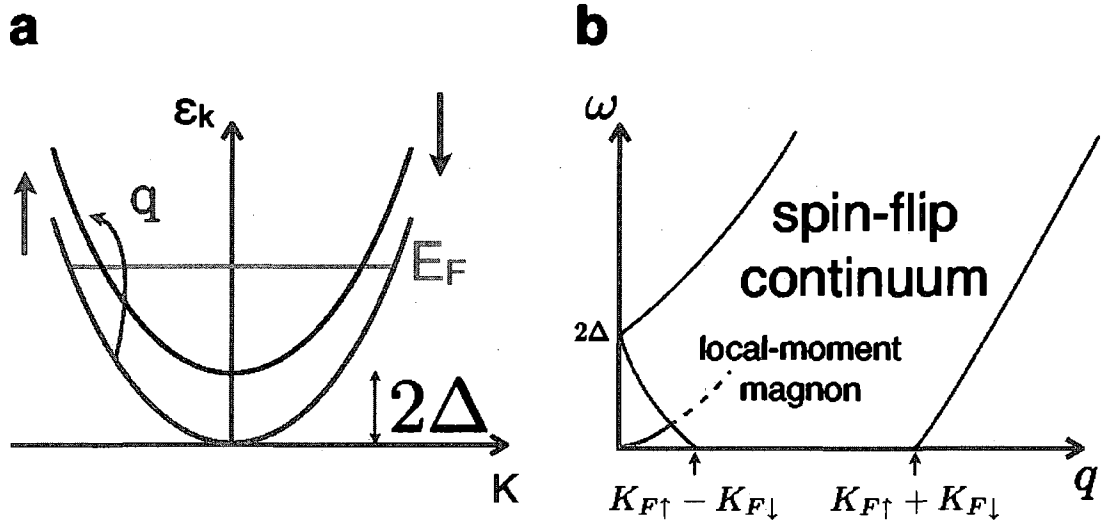
Figure 7.1 : Phase space for the Kondo coupling. **a,** The spin-splitting of the conduction electron band, which kinematically suppresses interband processes associated with the Kondo spin-flip coupling to the local-moment magnons. **b,** The kinematics for the spin-flip Kondo coupling. The low-lying excitations of the local-moment system are the magnons which enter the continuum at finite ω and q. Those of the conduction electrons are expressed in terms of the spin-flip continuum, whose Kondo-coupling to the local-moment magnons is cut off below the cutoff energy, $\omega_c \approx (I/W^2)\Delta^2$, and the cutoff momentum, $q_c \approx K_{F\uparrow} - K_{F\downarrow} \approx (K_F/W)\Delta$.

For energies and momenta above their respective cutoffs, $\omega_c \sim (I/W^2)\Delta^2$ and $q_c \sim K_{F\uparrow} - K_{F\downarrow} \approx (K_F/W)\Delta$, the magnons are coupled to the continuum part of the transverse spin excitations of the conduction electrons. Here, the Kondo coupling is relevant in the RG sense below three dimensions. This implies strong coupling between the conduction electrons and the local moments, and both the QNLσM

as well as the action for the conduction electrons will be modified. Explicitly, the correction to the quadratic part of the QNLσM is

$$\Pi(\vec{q},\omega) \approx J_K^2 \rho_0 \left(1 + i\gamma \frac{\omega}{v_F q} \right) \tag{7.1}$$

where γ is a dimensionless constant prefactor. At the same time, the conduction electrons acquire the following self-energy:

$$\Sigma(K_F, \epsilon) = \begin{cases} -A_2(\rho_0 J_K^4/I^2)^{1/3} \, (-i\epsilon)^{2/3} & d = 2 \\ -A_3(\rho_0 J_K^2/I) \, \epsilon \log(-i\epsilon) & d = 3 \end{cases} \tag{7.2}$$

where A_2 and A_3 are dimensionless constants of order unity. Similar forms for the self-energies appear in other contexts, notably the gauge-fermion problem and the spin-fluctuation-based quantum critical regime. The formal similarities as well as some of the important differences are discussed in later subsections.

With these damping corrections incorporated, the effective transverse Kondo coupling, $J_K^\pm$, becomes marginal in the RG sense in both two and three dimensions; the marginality is exact in the sense that it extends to infinite loops. This signals the stability of the form of damping for both the magnons and conduction electrons [68, 66]. At the same time, the effective longitudinal Kondo coupling, J_K^z, as well as the nonlinear coupling among the magnons, g, are irrelevant in the RG sense.

The exactly marginal nature of the Kondo coupling in the continuum part of the phase space implies that the effective coupling remains small as we scale down to the energy cutoff $\omega \sim \omega_c$ and, correspondingly, the momentum cutoff $q \sim q_c$. Below these cutoffs, the transverse Kondo coupling, which involves spin flips of the conduction electrons, cannot connect two points near the up-spin and down-spin Fermi surfaces; see Fig. 7.1. Although there is no gap in the density of states, as far as the spin-flip Kondo coupling is concerned, the system behaves as if the lowest energy excitations

have been gapped out. The important conclusion, then, is that the effective transverse Kondo coupling renormalizes to zero in the zero-energy and zero-momentum limit. This establishes the absence of static Kondo screening. Hence, the Fermi surface is small, and this is illustrated in Fig. 7.2a.

Our result is surprising given that the ratio $J_K/\omega_c \sim W^2/\left(IJ_K\langle m^z\rangle^2\right) \gg 1$. By contrast, the standard Kondo impurity problem with a pseudo-gap of order $\Delta_{pg} \ll J_K$ in the conduction electron density of states near the Fermi energy would be Kondo-screened [100, 101]. The difference is that, in the latter case, the Kondo coupling renormalizes to stronger values as the energy is lowered in the range $\Delta_{pg} \ll \omega \ll W$; for $J_K/\Delta_{pg} \gg 1$, the renormalized Kondo coupling is already large by the time the energy is lowered to $\omega \sim \Delta_{pg}$.

The small Fermi surface we have established is to be contrasted with the large Fermi surface of a ferromagnetic heavy fermion metal in the Stoner treatment, illustrated in Fig. 7.2b. In the latter case, the local moments become entangled with the conduction electrons as a result of the static Kondo screening. Kondo resonances develop and the local moments become incorporated into a large Fermi surface. This Fermi surface comes from a Zeeman-splitting of an underlying Fermi surface for the paramagnetic phase. That the paramagnetic Fermi surface is large can be seen through a non-perturbative proof [26] that relies upon time-reversal invariance.

The region of validity of Eqs. (7.1,7.2) corresponds to $\omega_c \ll \omega \ll |I|$ and $q_c \ll q \ll 2K_F$. This range is well-defined given that $\Delta \approx J_K\langle m^z\rangle \leq J_K$ and that we are considering $J_K \ll |I| \ll W$. In the same energy and corresponding temperature range, other physical properties also show a non-Fermi liquid behavior. In two dimensions, the specific heat coefficient $C/T \sim T^{-1/3}$ and the electrical resistivity $\rho \sim T^{4/3}$. In three dimensions, $C/T \sim \log(1/T)$ and $\rho \sim T^{5/3}$.
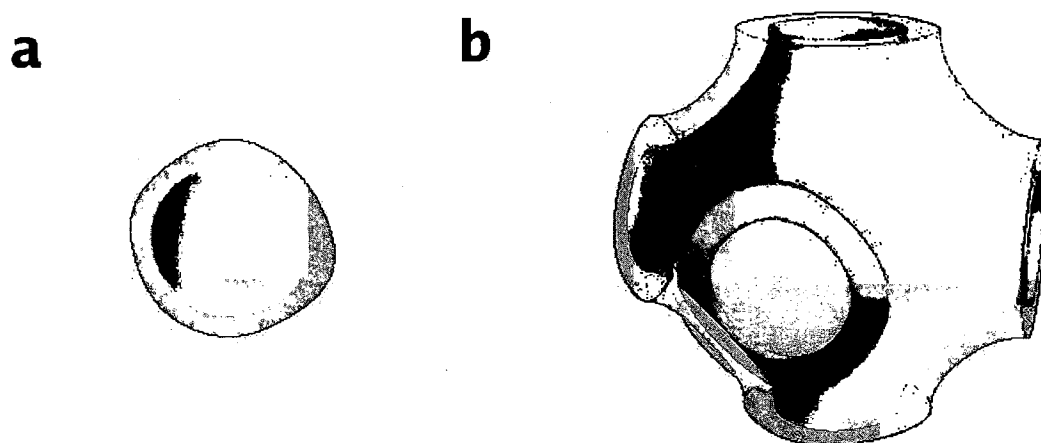
Figure 7.2 : Contrasting the small and large Fermi surfaces. The spin-up electron Fermi surface is drawn in red and larger than the spin-down electron Fermi surface in blue. The larger Fermi surface has been made slightly transparent to reveal the smaller sheet. **a**, The local moments are not part of the Fermi surface. **b**, Static Kondo screening has caused the Fermi surface to expand to accommodate the Kondo resonances associated with the local moments.

Our result of a stable ferromagnetic metal phase with a small Fermi surface provides the basis to understand the dHvA-measured [84, 85, 86] Fermi surface of $CeRu_2Ge_2$, which is ferromagnetic below $T_c = 8$ K. Our interpretation rests on a dynamical Kondo screening effect that turns increasingly weak at lower energies. This is supported by the observation of the collapsing quasielastic peak measured in the inelastic neutron-scattering cross section as the temperature is reduced [102]. It will be very instructive if the Fermi surface of UGe_2 [95] is further clarified and if systematic dHvA measurements are carried out in other ferromagnetic heavy fermion metals as well. With future experiments in mind, we note that our conclusion of a small Fermi surface also applies to ferrimagnetic order. The might be relevant to UIr_2Zn_{20} which displays an antiferromagnetic Weiss temperature, but ferromagnetic order [30]. All that is required in our theory of "ferromagnetism" is a splitting of the up and down spin Fermi surfaces as a result of the coupling to local moment order.

In the parameter regime we have considered, the non-Fermi liquid features are sizable. For instance, the non-Fermi liquid contribution to the self-energy [Eq. (7.2)] is, at the cutoff energy ω_c, larger than the standard Fermi liquid term associated with the interactions among the conduction electrons. It remains to be fully established whether the non-Fermi liquid terms in the electrical resistivity and specific heat can be readily isolated from contributions of other processes. Still, there is at least one family of materials, $URu_{2-x}Re_xSi_2$ at x > 0.3, in which non-Fermi liquid features have been shown to persist deep inside the ferromagnetic regime [91]. Whether this observed feature is indeed a property of the ferromagnetic phase, or if it is related to some quantum critical fluctuations or even certain disorder effects, remains to be clarified experimentally. We hope that our theory will provide motivation for the experimental search of non-Fermi liquid behavior in ferromagnetic heavy fermion

metals as well.

Finally, the existence of a ferromagnetic phase with a small Fermi surface raises the prospect of a direct quantum phase transition from a Kondo-destroyed ferromagnetic metal to a Kondo-screened paramagnetic metal. This, like its antiferromagnetic counterpart [46, 47, 103], in turn raises the possibility of a new type of superconductivity; the underlying quantum fluctuations would be associated with not only the development of the ferromagnetic order [93] but also the transformation of a large-to-small Fermi surface. Accessing the quantum phase transition requires that our analysis be extended to the regime where the Kondo coupling is large compared to the RKKY interaction, and this represents an important direction for the future.

To summarize, we have shown that the ferromagnetic Kondo lattice has a parameter range where static Kondo screening is destroyed and the Fermi surface is small. This conclusion is important for heavy fermion physics. It allows us to understand a long-standing puzzle on the Fermi surface, as epitomized by the dHvA measurements in $CeRu_2Ge_2$. It also sharpenes the analogy with the extensively studied antiferromagnetic heavy fermion metals, where the dichotomy between Kondo breakdown and conventional quantum criticality is well established. More broadly, this work has led to one of the very few asymptotically exact results for metallic ferromagnetism.

The remainder of this chapter will describe how the conclusions discussed above were found.

7.2   Scaling Analysis

We need to carry out an RG analysis for the field theory above several times, both before and after self-energies have been incorporated. To begin, we summarize the pure boson problem which has been done previously [98]. The dimension of the m field

is fixed by the nonlinear constraint $m^a(\vec{x}, \tau) m^a(\vec{x}, \tau) = 1$ which requires $[m^a(\vec{x}, \tau)] = 0$. In momentum space, this becomes $[m^a(\vec{q}, \omega)] = -d - z_b$. Unless indicated otherwise, we will exclusively be concerned with field dimensions in momentum space, so the arguments will often be dropped: $[m] = -d - z_b$. As usual for purely bosonic RG, the momenta and energies scale simply as $[q] = 1$ and $[\omega] = z_b$, where $z_b = 2$ is the dynamical exponent for the boson, which is consistent with $\omega \sim q^2$. The modulo 4π ambiguity in the Berry phase dictates $[M_0] = d$, and the scale invariance of $\mathcal{S}_m$ establishes $[\rho_s] = d + z_b - 2$.

Read and Sachdev were the first to point out that higher order gradient terms may be relevant.

$$\mathcal{S}_m^{(4)} = g \int d^d x d\tau \Big(\partial_\mu m_a \partial_\mu m_a \partial_\nu m_b \partial_\nu m_b - 2 \partial_\nu m_a \partial_\nu m_a \partial_\mu m_b \partial_\nu m_b \Big) \quad (7.3)$$

Using the scaling scheme described above, this coupling, representing magnon-magnon interactions, has scaling dimension $[g] = d - 2$. This indicates that, for $d \geq 2$, the magnon-magnon scattering is relevant. We will see later why this term becomes irrelevant when fermions are incorporated.

In parallel to the pure boson problem, there is a well known procedure for handling pure fermion problems within a momentum shell approach [63]. The essential difference from the bosonic RG is that the low energy manifold now consists of an extended surface, the Fermi surface, rather than a single point. Scaling should therefore be done with respect to this surface, and this may be accomplished by a clever change of coordinates for a simple spherical Fermi surface.

When the action contains both bosons and fermions, the momentum shell RG becomes much more complicated. In the special case $z_f = 1$ and $z_b = 1$, we have extended Shankar's approach in a straightforward fashion [49]. However, such an

approach does not work if $z_f \neq z_b$. Another strategy has been proposed by Altshuler, Ioffe, and Millis [68], and we adopt this method here.

Each fermion momentum space integral is decomposed into patches of size Λ_f in every direction so that each patch is locally a flat space. Scaling is accomplished locally with respect to the center of each patch. Momenta are therefore decomposed into components parallel ($k_\parallel$) and perpendicular ($k_\perp$) to the vector normal to the Fermi surface at this reference point. For example, $\int_{\text{annulus}} d^d K = \sum_{\text{patches}} \int_{-\Lambda_f}^{\Lambda_f} d^{d-1} k_\perp dk_\parallel$. Note that some authors use an opposite naming convention for components; we follow the notation of Ref. [68]. A tacit assumption of this approach is that the boson does not connect two fermions in different patches; this is only justified for forward scattering problems like the one we consider here. Bosonic momentum integrals are already constrained to a volume of linear dimension Λ_b, which we assume naturally fits inside the fermionic patch: $\Lambda_b \sim \Lambda_f \equiv \Lambda$. In this scheme, fermionic and bosonic momenta scale the same way, albeit anisotropically. The assignment of values for $[\epsilon]$, $[k_\parallel]$, and $[k_\perp]$ will depend on the form of the quadratic action, and this will be different depending on how we incorporate the corrections to the QNLσM and fermion actions. The scaling analysis will therefore need to be done anew for each case.

The introduction of fermions and the choice to use the scaling procedure outlined above has an immediate consequence on the way we scale the bosonic action. In the pure boson case, we can use $[M_0] = d$. This comes from the modulo 4π ambiguity of the Berry phase. Specifically, since $e^{i4\pi S} = 1$, we need $i4\pi S = i2\pi n$, where n is an integer. Therefore S is quantized at either an integer or half integer value, and is insensitive to the RG rescaling. However, since $S = M_0 \int d^d x = M_0 L^d$, and since $[L^d] = -d$, we must have $[M_0] = d$ [9]. But the anisotropic scalings we employ in momentum space no longer translate simply to a coordinate space analysis. We must

therefore abandon these dimension assignments for the pure boson problem. Instead, we write the action completely in momentum space and live with the understanding that after rescaling, the fields $m^a(\vec{q}, \omega)$ and $\psi(\vec{k}, \epsilon)$ no longer represent the Fourier transforms of the coordinate space fields $m^a(\vec{x}, \tau)$ and $\psi(\vec{x}, \tau)$. This is nothing new since even in the original Wilsonian RG formalism the imposition of a cutoff invalidates the interpretation of $\phi(q)$ as a true Fourier transform of $\phi(x)$.

A second reason to modify the Read-Sachdev assignments for scaling dimensions in the pure boson problem is that the addition of fermions acts as a magnetization sink for the local-moment system. Of course, the overall magnetization is still conserved in the ferromagnetic phase. Furthermore, we assume there are no valence fluctuations (an implicit assumption in writing down the microscopic Kondo-Heisenberg Hamiltonian) so we can still treat the local moments as O(3) spins attached to the lattice, and therefore work with the nonlinear field theory.

The way we fix the scaling dimensions is to define the quadratic action according to:

$$S_m = \int d\omega \, d^{d-1}q_\perp dq_\parallel \, m^+ \left(-i\omega + q_\perp^2\right) m^- \tag{7.4}$$

$$S_c = \sum_{\text{patches}} \int d\epsilon \, d^{d-1}k_\perp dk_\parallel \, \bar{\psi}_\sigma \left(i\epsilon - v_F k_\parallel - \frac{v_F}{2K_F}k_\perp^2\right) \psi_\sigma \tag{7.5}$$

where, as usual [68], $q_\perp \gg q_\parallel$. The coupling of the local-moment magnons to the fermions introduces anisotropy in momentum space; as we will see, such an anisotropic fixed point turns out to be exactly marginal. To ensure that these forms are scale

invariant, we make the assignments:

$$[\epsilon] = 1$$

$$[k_\parallel] = 1$$

$$[k_\perp] = 1/z_b = 1/2$$

$$[\psi] = -(3z_b + d - 1)/(2z_b) = -(5 + d)/4$$

$$[m] = -(2z_b + d + 1)/(2z_b) = -(5 + d)/4 \tag{7.6}$$

This information is used to count dimensions for the Kondo coupling.

$$\mathcal{S}_K^\pm = J_K^\pm \int d^{d-1}q_\perp dq_\parallel d\omega d^{d-1}k_\perp dk_\parallel d\varepsilon \left[\bar{\psi}_{k+q,\uparrow}\psi_{k,\downarrow}m_q^- + \bar{\psi}_{k+q,\downarrow}\psi_{k,\uparrow}m_q^+ \right] \tag{7.7}$$

The tree-level dimension of the Kondo coupling is now easily found.

$$[\mathcal{S}_K^\pm] = 0$$

$$= [J_K^\pm] + 2[d^{d-1}k_\perp dk_\parallel d\varepsilon] + 2[\psi] + [m]$$

$$= [J_K^\pm] + 2\frac{d - 1 + 2z_b}{z_b} - 2\frac{3z_b + d - 1}{2z_b} - \frac{2z_b + d + 1}{2z_b}$$

$$\implies [J_K^\pm] = (3 - d)/(2z_b) \tag{7.8}$$

The spin-flip Kondo coupling is relevant in two dimensions, and marginal (at the tree level) in three dimensions. Usually, when the Kondo coupling is relevant, we expect the model to flow to a strong coupling fixed point where Kondo screening sets in, destroying the magnetic order and leading to a paramagnetic phase with a large Fermi surface. This, however, would be an incorrect, and inconsistent, conclusion. A proper calculation of the self energies and subsequent re-analysis of the scaling dimensions around the appropriate fixed point will show that there will never be Kondo screening.

7.3 Damping Corrections to the QNLσM and Scaling

Our analysis so far has been a little too naive. In particular, it describes the wrong fixed point. Note that so far we have not considered the z-component of the Kondo interaction, $J_K^z \int s_c^z m^z$, which we refer to as the longitudinal channel. This coupling has two important effects. First, it introduces the effect of splitting the spin bands of the conduction electrons. Second, when the modified bosonic propagator is inserted into the fermionic self energy we will obtain a non-Fermi liquid form when the Kondo coupling is SU(2) symmetric ($J_K^+ = J_K^- = J_K^z$). What is crucial for this, of course, is that the magnons will remain gapless in the presense of the Kondo coupling to the conduction electrons, and we wish to show this explicitly. With all this in mind, we present below in some detail the calculation of the magnon self-energy, as well as an RG analysis with the modified QNLσM.
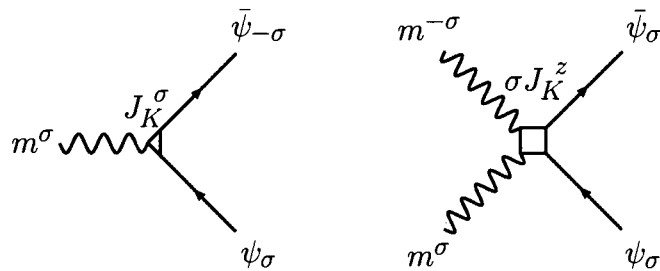
Figure 7.3 : Interaction vertices of the F$_S$ phase

The first observation is easy to demonstrate. For small fluctuations about the ordered state, the longitudinal interaction is approximately $J_K^z \int (\bar{\psi}_\uparrow \psi_\uparrow - \bar{\psi}_\downarrow \psi_\downarrow)(1 - \frac{1}{2}m^+ m^-)$. where we have used the constraint $m^z = \sqrt{1 - m^+ m^-}$. The "1" comes from the magnetization in the z-direction, and leads to a Zeeman shift in the energy of the conduction electrons. The reference point for our theory should therefore have

a quadratic action for the fermions of the form

$$\mathcal{S}_c = \int d^d x d\tau \, \bar{\psi}_\sigma(\vec{x}, \tau) \left(\partial_\tau - \frac{\nabla^2}{2m} - \mu + \sigma \Delta \right) \psi_\sigma(\vec{x}, \tau) \qquad (7.9)$$

where $\Delta \sim J_K^z \langle m^z \rangle \sim J_K^z$. We need to write this in momentum space where it has the effect of defining a spin-dependent Fermi wavevector: $K_{F\sigma} \equiv \sqrt{2m_e(\mu + \sigma\Delta)}$. Expression (7.5) is unchanged except for the new definition of $K_{F\sigma}$. We need to build an effective low-energy theory around this fixed point, where there is a gap of size 2Δ between the up-spin and down-spin bands. This form of the fermionic spectrum is essential to correctly capture the damping of magnons via the Kondo interaction. The interaction vertices are represented diagrammatically in figure 7.3, while the leading contributions to the self energies are shown in figure 7.4. The real and imaginary parts of the retarded functions can be calculated exactly. For example, the contribution from diagram Π^A is

$$\text{Re}\Pi_R^A(\vec{q}, \omega) = -\frac{mJ_K^+ J_K^-}{q\pi} \Big[q$$
$$+ K_{F\uparrow} \text{sgn}(\zeta_{-,\uparrow}) \Theta(|\zeta_{-,\uparrow}| - 1) \sqrt{\zeta_{-,\uparrow}^2 - 1}$$
$$+ K_{F\downarrow} \text{sgn}(\zeta_{+,\downarrow}) \Theta(|\zeta_{+,\downarrow}| - 1) \sqrt{\zeta_{+,\downarrow}^2 - 1} \Big]$$
$$\text{Im}\Pi_R^A(\vec{q}, \omega) = \frac{mJ_K^+ J_K^-}{q\pi} \Big[- K_{F\uparrow} \Theta(1 - |\zeta_{-,\uparrow}|) \sqrt{1 - \zeta_{-,\uparrow}^2}$$
$$+ K_{F\downarrow} \Theta(1 - |\zeta_{+,\downarrow}|) \sqrt{1 - \zeta_{+,\downarrow}^2} \Big] \qquad (7.10)$$

where we have defined $\zeta_{\pm,\sigma} \equiv \frac{\omega - 2\Delta}{v_{F\sigma} q} \pm \frac{q}{2K_{F\sigma}}$, and $\sigma \in \{+, -\}$. The region in (ω, q)-space where the imaginary part is non-zero is depicted in the main paper. A similar exact expression is also available in $d = 3$, but the approximate form is perhaps more useful. The bubble Π_R^A in the regime $\Delta \ll \omega \ll v_F q \ll \mu = K_F^2/(2m_e)$ is approximately:

$$\Pi_R^A(\vec{q}, \omega) \approx J_K^+ J_K^- \rho_0^{(d)} \left(1 + i\gamma_d \frac{\omega}{v_F q} \right) \qquad (7.11)$$

where γ_d is a constant prefactor which depends on the spatial dimension, and $\rho_0^{(d)} = \sum_\sigma \rho_{0,\sigma}^{(d)}$ is the density of states at the Fermi level. In two and three dimensions, the explicit expressions are $\rho_{0,\sigma}^{(d=2)} = \frac{m}{2\pi}$ and $\rho_{0,\sigma}^{(d=3)} = \frac{m}{2\pi^2} K_{F\sigma}$. The ω/q form of the damping is common to a variety of systems; in this case it signifies Landau damping of the magnons with spin 1 excitations of the fermions.
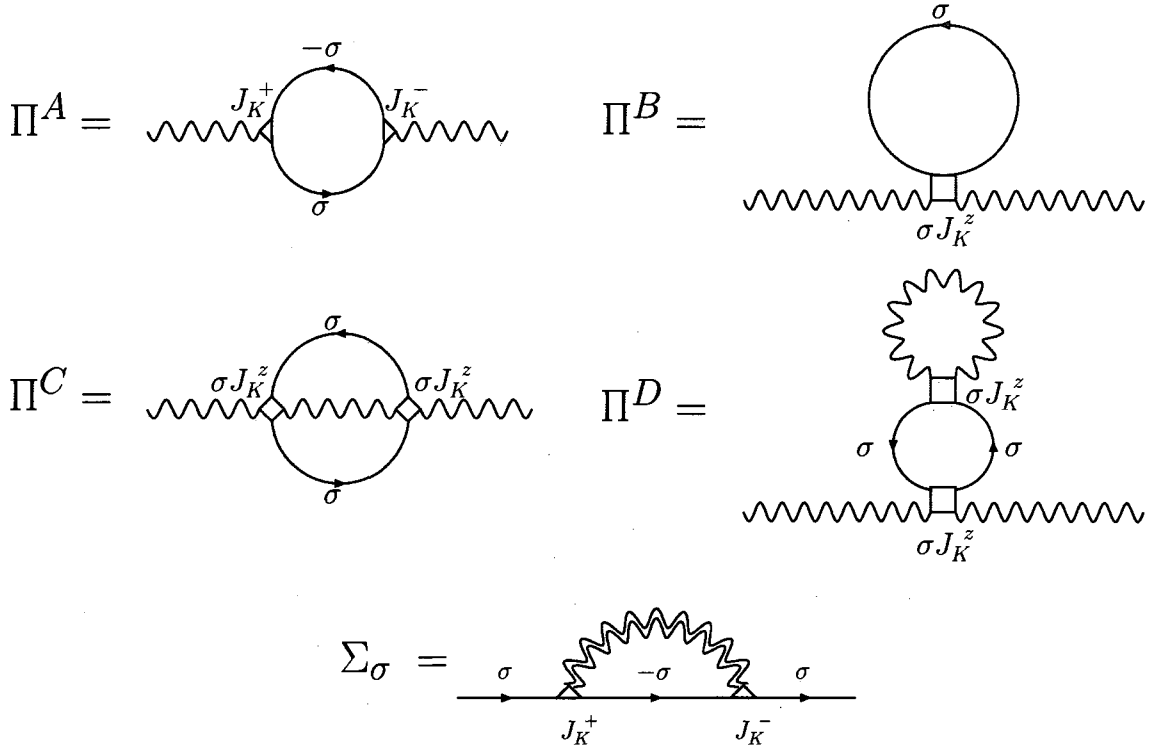
Figure 7.4 : Self energies of the F_S phase

To satisfy Goldstone's theorem, it is necessary for all the pieces of Π to cancel in such a way that the full bosonic propagator emerges in massless form. In the gauge-fermion problem, this is a consequence of gauge invariance [104]. In our case, the cancellation is somewhat more subtle. First, note that the diagrams Π^C and Π^D are explicitly $O(J_K^2)$. Diagrams Π^A and Π^B, however, are both linear in J_K. This is

obvious for Π^B, whose calculation is trivial:

$$
\begin{aligned}
\mathrm{Re}\Pi_R^B(\vec{q},\omega) &= -J_K^z(n_\uparrow - n_\downarrow) \\
\mathrm{Im}\Pi_R^B(\vec{q},\omega) &= 0
\end{aligned}
\tag{7.12}
$$

The sign difference comes from the fact that there is a four-leg vertex J_K^z for each spin, but the sign of the coupling constant depends on σ. The reason why Π^A is linear in J_K instead of $O(J_K^2)$ can be seen from a simple calculation at $(\vec{q}=0, \omega=0)$, which is non-singular due to the different spin indices. After performing the Matsubara sum,

$$
\begin{aligned}
\Pi_R^A(\vec{0},0) &= 2J_K^+ J_K^- \int \frac{d^d K}{(2\pi)^d} \frac{n(\xi_{K,\uparrow}) - n(\xi_{K,\downarrow})}{\xi_{K,\downarrow} - \xi_{K,\uparrow}} \\
&= 2J_K^+ J_K^- \int \frac{d^d K}{(2\pi)^d} \frac{n(\xi_{K,\uparrow}) - n(\xi_{K,\downarrow})}{2J_K^z} \\
&= \frac{J_K^+ J_K^-}{J_K^z}(n_\uparrow - n_\downarrow)
\end{aligned}
\tag{7.13}
$$

Therefore, when the Kondo coupling is SU(2) symmetric the mass terms cancel and $\Pi^A + \Pi^B \approx J_K^2 \gamma_d |\omega|/q$ and thus $\chi^{-1}(\vec{q}, i\omega) = q^2 + \gamma_d J_K^2 \frac{|\omega|}{q}$, where as usual we have neglected the linear in ω term because it is less relevant in the RG sense. This special form of the bosonic propagator has emerged in a number of other applications, the most famous example being the gauge-fermion problem. We will comment on its consequence a little later.

With the inclusion of damping, the quadratic action now becomes:

$$
\mathcal{S}_m = \int d\omega d^{d-1}q_\perp dq_\parallel \, m^+ \left(q_\perp^2 + b\frac{\omega}{q_\perp} \right) m^-
\tag{7.14}
$$

$$
\mathcal{S}_c = \int d\epsilon d^{d-1}k_\perp dk_\parallel \, \bar{\psi}_\sigma \left(i\epsilon - v_F k_\parallel - a_\sigma k_\perp^2 \right) \psi_\sigma
\tag{7.15}
$$

where a_σ and b are simply couplings that control the relative scaling between different components of the action. Their dimensions will be chosen to ensure the quadratic action is scale invariant. Significantly, in this $z_b = 3$ theory the Berry phase no longer

controls the dynamics, being instead overwhelmed by the damping term. Physically, this is because the magnetization of the local moment system is no longer conserved by itself once it can exchange spin flips with the conduction electrons.

The scaling analysis now needs to be redone.

$$
\begin{aligned}
[\epsilon] &= 1 \\
[k_\parallel] &= 1 \\
[k_\perp] &= 1/z_b = 1/3 \\
[a] &= 1 - 1/z_b = 2/3 \\
[b] &= 0 \\
[\psi] &= -(3z_b + d - 1)/(2z_b) = -(8 + d)/6 \\
[m] &= -(2z_b + d + 1)/(2z_b) = -(7 + d)/6
\end{aligned} \tag{7.16}
$$

Note that in principle a_σ and ψ_σ could scale differently for different spin projections, but because of the way they enter the action, we scale them identically. With these choices, all the terms in the quadratic action are scale invariant. The Kondo coupling terms,

$$
\mathcal{S}_K^\pm = J_K^\pm \int d^{d-1}q_\perp \, dq_\parallel \, d\omega \, d^{d-1}k_\perp \, dk_\parallel \, d\varepsilon \left[\bar{\psi}_{k+q,\uparrow} \psi_{k,\downarrow} m_q^- + \bar{\psi}_{k+q,\downarrow} \psi_{k,\uparrow} m_q^+ \right] \tag{7.17}
$$

$$
\begin{aligned}
\mathcal{S}_K^z = J_K^z \int d^{d-1}q_{1\perp} \, dq_{1\parallel} \, d\omega_1 \, d^{d-1}q_{2\perp} \, dq_{2\parallel} \, d\omega_2 \, d^{d-1}k_\perp \, dk_\parallel \, d\varepsilon \\
\times \left[\bar{\psi}_{k+q_1-q_2,\uparrow} \psi_{k,\uparrow} m_{q_1}^+ m_{q_2}^- + \bar{\psi}_{k+q_1-q_2,\downarrow} \psi_{k,\downarrow} m_{q_1}^+ m_{q_2}^- \right]
\end{aligned} \tag{7.18}
$$

are easily analyzed:

$$[\mathcal{S}_K^{\pm}] = 0$$

$$= [J_K^{\pm}] + 2[d^{d-1}k_\perp dk_\parallel d\varepsilon] + 2[\psi] + [m]$$

$$= [J_K^{\pm}] + 2\frac{d-1+2z_b}{z_b} - 2\frac{3z_b+d-1}{2z_b} - \frac{2z_b+d+1}{2z_b}$$

$$\implies [J_K^{\pm}] = (3-d)/(2z) \tag{7.19}$$

$$[\mathcal{S}_K^z] = 0$$

$$= [J_K^z] + 3[d^{d-1}k_\perp dk_\parallel d\varepsilon] + 2[\psi] + 2[m]$$

$$= [J_K^z] + 3\frac{d-1+2z_b}{z_b} - 2\frac{3z_b+d-1}{2z_b} - 2\frac{2z_b+d+1}{2z_b}$$

$$\implies [J_K^z] = (1-d)/z \tag{7.20}$$

The inclusions of ω/q damping into the quadratic part of the boson action has the effect of changing the dynamics from $z_b = 2$ to $z_b = 3$, however, there is no change to the dimension of the spin-flip Kondo coupling. The longitudinal Kondo coupling is irrelevant for any $d > 1$.

It turns out that a proper analysis of the fixed point requires insertion of the fermion self energy as well [68], which we turn to next.

7.4 Electron Self Energy and Non-Fermi Liquid Behavior

In addition to the scaling analysis, we have another reason to determine the electron self-energy. Anticipating that the non-Fermi liquid contribution from the Kondo coupling to the magnons will be cut off at the energy of order $\omega \sim \omega_c \sim (I/W^2)\Delta^2$, we wish to ascertain the magnitude of the non-Fermi liquid term at this cutoff scale. This will allow us to compare this term with some background Fermi liquid contributions. Since the Kondo coupling also occurs in the modified magnon propagator, we present here the calculation of the electron self-energy in some detail.

The leading order contribution to the electron self energy in $d = 2$ is given by the dressed boson, bare fermion and no vertex correction, as depicted in figure 7.4.

$$
\begin{aligned}
\Sigma_{\bar{\sigma}}(\vec{K}, i\epsilon) &= J_K^2 \int \frac{d^2q\,d\omega}{(2\pi)^3} G_{\sigma}^0(\vec{K} + \vec{q}, i\epsilon_m + i\omega_n)\chi(\vec{q}, i\omega_n) \\
&= J_K^2 \int \frac{d^2q\,d\omega}{(2\pi)^3} \frac{1}{i\epsilon + i\omega - \xi_{K+q,\sigma}} \frac{1}{q^2 - \Pi(\vec{q}, i\omega)} \\
&= J_K^2 \int \frac{d^2q\,d\omega}{(2\pi)^3} \frac{1}{i\epsilon + i\omega - \xi_{K\sigma} - \frac{Kq}{m}\cos\theta} \frac{1}{q^2 - \Pi(\vec{q}, i\omega)}
\end{aligned} \tag{7.21}
$$

From the previous section we have the result $\Pi(\vec{q}, i\omega_n) \approx -J_K^2 \gamma \frac{|\omega|}{q}$. For the integral over θ we use: $\int_0^{2\pi} \frac{1}{z + i\cos\theta} = \frac{2\pi\,\mathrm{sgn}\,\mathrm{Re}(z)}{\sqrt{z^2 + 1}}$ for any complex z.

$$
\begin{aligned}
\Sigma_{\bar{\sigma}}(\vec{K}, i\epsilon) &= J_K^2 \int \frac{q\,dq\,d\omega}{(2\pi)^3} \frac{1}{Kq/m} \frac{1}{q^2 + J_K^2\gamma\frac{|\omega|}{q}} \int d\theta \frac{1}{\frac{i\epsilon + i\omega - \xi_{K\sigma}}{\frac{Kq}{m}} - \cos\theta} \\
&= -iJ_K^2 \int \frac{q\,dq\,d\omega}{(2\pi)^3} \frac{1}{Kq/m} \frac{1}{q^2 + J_K^2\gamma\frac{|\omega|}{q}} \int d\theta \frac{1}{\frac{\epsilon + \omega + i\xi_{K\sigma}}{\frac{Kq}{m}} + i\cos\theta} \\
&= -iJ_K^2 \int \frac{q\,dq\,d\omega}{(2\pi)^3} \frac{1}{Kq/m} \frac{1}{q^2 + J_K^2\gamma\frac{|\omega|}{q}} \frac{2\pi\,\mathrm{sgn}(\epsilon + \omega)}{\sqrt{\left(\frac{\epsilon + \omega + i\xi_{K\sigma}}{\frac{Kq}{m}}\right)^2 + 1}}
\end{aligned} \tag{7.22}
$$

But in the regime of interest, and with the momentum restricted to $K \approx K_F$, we have $\frac{\epsilon + \omega + i\xi_{K\sigma}}{K_F/m} \ll 1$. The self-energy then simplifies to

$$
\begin{aligned}
\Sigma_{\bar{\sigma}}(K_F, i\epsilon) &\approx -iJ_K^2 \int \frac{q\,dq\,d\omega}{(2\pi)^3} \frac{1}{K_Fq/m} \frac{2\pi\,\mathrm{sgn}(\epsilon + \omega)}{q^2 + J_K^2\gamma\frac{|\omega|}{q}} \\
&= -J_K^2 \frac{im}{(2\pi)^2 K_F} \int_0^\Lambda dq \int_{-\infty}^\infty d\omega \frac{\mathrm{sgn}(\epsilon + \omega)}{q^2 + J_K^2\gamma\frac{|\omega|}{q}}
\end{aligned} \tag{7.23}
$$

This integral is a little tricky. First note that the frequency integral should have a cutoff, but this is complicated by the presence of the sgn function. It would be incorrect to simply shift variables $\omega \to \omega + \epsilon$. The essential identity we need is:

$$
\int_{-\Lambda}^\Lambda d\omega\, f(\omega)\mathrm{sgn}(\omega + \epsilon) = 2\int_0^\epsilon d\omega\, f(\omega) \tag{7.24}
$$

which is only true for even functions: $f(\omega) = f(-\omega)$. To see where this comes from, note first that for even functions:

$$\int_a^b d\omega f(\omega) = -\int_{-a}^{-b} d\omega f(\omega)$$

Next, to handle the sgn function we partition the integral into four regions:

$$\int_{-\Lambda}^{\Lambda} d\omega f(\omega) \mathrm{sgn}(\omega + \epsilon) = -\int_{-\Lambda}^{-\epsilon} d\omega f(\omega) + \int_{-\epsilon}^{0} d\omega f(\omega) + \int_{0}^{\epsilon} d\omega f(\omega) + \int_{\epsilon}^{\Lambda} f(\omega)$$

where the minus sign is the result of the sgn function. Now we use the identity valid for even functions:

$$\int_{-\Lambda}^{\Lambda} d\omega f(\omega) \mathrm{sgn}(\omega + \epsilon) = \int_{\Lambda}^{\epsilon} d\omega f(\omega) - \int_{\epsilon}^{0} d\omega f(\omega) + \int_{0}^{\epsilon} d\omega f(\omega) + \int_{\epsilon}^{\Lambda} f(\omega)$$

$$= 2\int_{0}^{\epsilon} d\omega f(\omega) \tag{7.25}$$

Armed with this identity, the self energy is:

$$\Sigma_{\bar{\sigma}}(K_F, i\epsilon) \approx -J_K^2 \frac{2im}{(2\pi)^2 K_F} \int_0^\infty dq \int_0^\epsilon d\omega \frac{1}{q^2 + J_K^2 \gamma \frac{|\omega|}{q}}$$

$$= -J_K^2 \frac{2im}{(2\pi)^2 K_F J_K^2 \gamma} \int_0^\infty dq\, q \log\left(1 + J_K^2 \frac{\gamma\epsilon}{q^3}\right)$$

$$= -\frac{i2m}{(2\pi)^2 K_F \gamma} \frac{\pi}{\sqrt{3}} \left(J_K^2 \gamma\epsilon\right)^{2/3} \tag{7.26}$$

Had we used a cutoff on the q-integral, we would have ended up with some unsightly hypergeometric functions whose asymptotic form is the same as above, so it is easier to just set the cutoff to infinity straight away. For convenience, we have so far dropped the stiffness (ρ_s) factor in the q^2 term of the boson propagator. Reintroducing this factor, and taking $\rho_s \propto I$, we end up with the conduction electron self-energy quoted in the main text, Eq. (6).

Redoing the calculations for $d = 3$ is relatively straightforward, although now the integral will be UV divergent. The only difference is that now we set $\vec{K}$ onto the

K_x-axis since the ϕ variable is the one that runs from $0 \to 2\pi$. This allows us to use the same identity on the ϕ integral that we used in the $d = 2$ case for the θ integral.

$$
\begin{aligned}
\Sigma_{\bar{\sigma}}(\vec{K}, i\epsilon) &= J_K^2 \int \frac{q^2 dq \sin\theta d\theta d\omega}{(2\pi)^4} \frac{1}{Kq/m} \frac{1}{q^2 + J_K^2 \gamma \frac{|\omega|}{q}} \int d\phi \frac{1}{\frac{i\epsilon + i\omega - \xi_{K\sigma}}{\frac{Kq}{m}} - \cos\phi} \\
&= -i J_K^2 \int \frac{q^2 dq \sin\theta d\theta d\omega}{(2\pi)^4} \frac{1}{Kq/m} \frac{1}{q^2 + J_K^2 \gamma \frac{|\omega|}{q}} \int d\phi \frac{1}{\frac{\epsilon + \omega + i\xi_{K\sigma}}{\frac{Kq}{m}} + i\cos\phi} \\
&= -i J_K^2 \int \frac{q^2 dq \sin\theta d\theta d\omega}{(2\pi)^4} \frac{1}{Kq/m} \frac{1}{q^2 + J_K^2 \gamma \frac{|\omega|}{q}} \frac{2\pi \operatorname{sgn}(\epsilon + \omega)}{\sqrt{\left(\frac{\epsilon + \omega + i\xi_{K\sigma}}{\frac{Kq}{m}}\right)^2 + 1}}
\end{aligned}
$$

Within the regime of interest this simplifies to

$$
\begin{aligned}
\Sigma_{\bar{\sigma}}(K_F, i\epsilon) &\approx -J_K^2 \frac{2im}{(2\pi)^3 K_F} \int q dq \int_0^\epsilon d\omega \frac{1}{q^2 + J_K^2 \gamma \frac{|\omega|}{q}} \\
&= -J_K^2 \frac{2im}{(2\pi)^3 K_F J_K^2 \gamma} \int_0^\Lambda dq q^2 \log\left(1 + \frac{J_K^2 \gamma \epsilon}{q^3}\right) \\
&= -\frac{2im}{(2\pi)^3 K_F \gamma} \left[\Lambda^3 \log\left(1 + \frac{J_K^2 \gamma \epsilon}{\Lambda^3}\right) + J_K^2 \gamma \epsilon \log\left(1 + \frac{\Lambda^3}{J_K^2 \gamma \epsilon}\right)\right] \\
&\approx -\frac{2im}{(2\pi)^3 K_F \gamma} \left[J_K^2 \gamma - J_K^2 \gamma \log\epsilon + J_K^2 \gamma \log\frac{\Lambda^3}{J_K^2 \gamma}\right] \epsilon + O(\epsilon^2) \quad (7.27)
\end{aligned}
$$

So the leading singularity in $d = 3$ is:

$$
\Sigma \propto i J_K^2 \epsilon \log\epsilon \tag{7.28}
$$

Again, recovering the stiffness factor leads to the form of the conduction electron self-energy presented in the main text, Eq. (6).

Holstein, Norton, and Pincus were the first to show that the transverse electromagnetic field coupling remains unscreened and can in principle lead to non-Fermi liquid behavior [70]. For a real electromagnetic field, the smallness of the fine structure constant suppresses this effect to extremely low temperatures. Related non-Fermi liquid form appears in the gauge-fermion problem [105, 66, 68]. More recently, similar self energies have been found near quantum critical points and the nematic fermi

fluid [106, 107, 108]. The prevalence of this self energy results from the generic presence of a massless $z_b = 3$ boson coupled to a system with a Fermi surface. The problem we have considered here has some important formal differences from the gauge-fermion and critical Fermi liquid cases, even in the $z_b = 3$ continuum regime. One difference is in the mechanism by which the boson propagators are gapless. In the gauge-fermion problem, gauge invariance guarantees the cancellation of the mass term upon adding the bubble and tadpole diagrams in a large-N calculation of the self energy of the vector potential [104]. At the ferromagnetic QCP, the divergence of the correlation length ($\xi^{-2} \to 0$) leads to gapless quantum critical fluctuations. In our case, it is the SU(2) spin symmetry of the Kondo interaction which dictates that the contribution from the longitudinal channel exactly cancels that from the transverse channel. A similar effect from the longitudinal mode of the ordered itinerant antiferromagnet was recently discussed by [79], and we suspect that the cancellation argument we advance here may apply to their case as well. Another feature that is unique to our problem corresponds to the specific non-linear terms [Eq. 7.3] that occur here, which come into play in our RG analysis. We have shown that these terms, while relevant for the pure Heisenberg problem, become irrelevant when the Kondo coupling to the fermions is introduced.

We close this section by addressing how the self-energy correction to fermions modify the damping term in the QNLσM given in Eq. (7.11). The damping remains to have the ω/q form. For the regime of our interest here, $\omega \sim q^3$, both the self-energy and vertex corrections to the damping term are negligble. For generic $|\omega| \ll q$, the self-energy and vertex corrections cancel with each other leaving a subleading contribution [68, 109].

7.5   Scaling With Fully Dressed Propagators

Now that we have the expression for the electron self energy we can finally incorporate it into the fixed point and redo the scaling analysis.

$$\mathcal{S}_m = \int d\omega d^{d-1}q_\perp dq_\parallel \, m^+ \left(q_\perp^2 + b\frac{\omega}{q_\perp}\right) m^- \tag{7.29}$$

$$\mathcal{S}_c = \int d\epsilon d^{d-1}k_\perp dk_\parallel \, \bar{\psi}_\sigma \left(|\epsilon|^{d/z_b} - v_F k_\parallel - a_\sigma k_\perp^2\right) \psi_\sigma \tag{7.30}$$

Note that the self energy correction to the fermion in $d = 3$ is actually $\epsilon \log \epsilon$, but for the purposes of scaling we can simultaneously treat the cases $d = 2$ and $d = 3$ by analyzing the form ϵ^{d/z_b}. To make every term in the quadratic action scale invariant we make the assignments:

$$
\begin{aligned}
\left[k_\perp\right] &= 1/d \\
\left[k_\parallel\right] &= 1 \\
\left[\epsilon\right] &= z_b/d = 3/d \\
\left[a_\sigma\right] &= 1 - 2/d \\
\left[\psi\right] &= -(3d + z_b - 1)/(2d) = -(3d + 2)/(2d) \\
\left[m\right] &= -(2d + z_b + 1)/(2d) = -(2d + 4)/(2d)
\end{aligned}
\tag{7.31}
$$

Inserting these dimensions into the Kondo coupling produces:

$$\left[J_K^\pm\right] = (3 - z_b)/(2d) = 0 \tag{7.32}$$

$$\left[J_K^z\right] = (3 - z_b - d)/d = -1 \tag{7.33}$$

In both $d = 2$ and $d = 3$, we find that the insertion of the self energies has led to the marginality of the transverse Kondo coupling, and the irrelevance of the longitudinal channel. This demonstrates that with the correct self energies built into the theory, which references the appropriate stable fixed point, there is never any unstable flow

of the Kondo coupling. The ferromagnetic phase with a small Fermi surface is stable to the Kondo coupling.

Parenthetically, note that the magnon scattering term scales like:

$$\mathcal{S}_m^{(4)} \sim g \int \left(d^{d-1}q_\perp dq_\parallel d\omega\right)^3 (q_\perp m)^4 \tag{7.34}$$

$$\implies [g] = -\frac{3(d-1+d+z_b) + 4 - 2(2d+z_b+1)}{d}$$

$$= \frac{1 - z_b - 2d}{d}$$

$$= -2\frac{d+1}{d} \tag{7.35}$$

which is always irrelevant.

7.6 The Effect of the Cutoff

Below the cutoff, $\omega < \omega_c \sim (I/W^2)\Delta^2$ and $q < q_c \sim (K_F/W)\Delta$, the transverse Kondo coupling becomes irrelevant in the RG sense due to phase space restrictions. The longitudinal Kondo coupling, having the scaling dimension $(1-d)/z_b$, is irrelevant as well. The non-Fermi liquid effect will therefore be cut off in this range.

To ascertain the strength of the non-Fermi liquid contribution, we can compare the continuum contribution to the self energy, Eq. (7.2), with the background Fermi liquid contribution at the cutoff frequency ω_c. Adding a Coulomb interaction u among the conduction electrons leads to a Fermi-liquid contribution to the self-energy of the order $\Sigma_{FL}(\epsilon) \sim u^2 \rho_0^3 \epsilon^2$. In $d = 2$ we have

$$\Sigma_{NFL}(\epsilon \sim \omega_c) \sim (\rho_0 J_K^4/I^2)^{1/3}\omega_c^{2/3} \sim J_K^{8/3}/W^{5/3} \tag{7.36}$$

$$\Sigma_{FL}(\epsilon \sim \omega_c) = u^2 \rho_0^3 \omega_c^2 \sim (u^2 I^2/W^7)J_K^4 \tag{7.37}$$

In the parameter range we consider, $J_K \ll |I| \ll W$, $\Sigma_{NFL}(\epsilon \sim \omega_c)$ is much larger than $\Sigma_{FL}(\epsilon \sim \omega_c)$. Note that in three dimensions, $\Sigma_{NFL}(\epsilon \sim \omega_c) \sim \rho_0 J_K^2 \omega_c/I \sim$

J_K^4/W^3, leading to a similar conclusion.

7.7 Absence of Loop Corrections

7.7.1 Vertex corrections

For problems involving forward scattering of conduction electrons, the inability of vertex corrections to qualitatively modify leading order results has been established in related problems by a numbers of authors [66, 68, 109, 49]. The essence of the argument is a sort of Migdal's theorem reminiscent of the suppression of vertex corrections in the electron-phonon problem [27]. Previous work utilized a large number of fermion flavors, but we will take a slightly different approach which is more in line with the spirit of the fermionic RG and, like the original work by Migdal, focuses more explicitly on kinematics and phase space. The conclusions are essentially the same. The small parameter in our problem is $\Lambda/K_F \equiv 1/N_\Lambda$ which we use to define the large-N_Λ expansion. (This $N_\Lambda \to \infty$ limit corresponds to asymptotically low energies, $i.e.$, with the fermions approaching the Fermi surface.) Denoting the number of loops by L, the structure of the beta function is given by:

$$
\begin{aligned}
\beta(J_K) &= b_0 J_K + \frac{d}{d\log s} \sum_{L=1}^{\infty} \frac{b_L(s)}{N_\Lambda^{e(L,d)}} J_K^{2L+1} \\
&\equiv b_0 J_K + \frac{d}{d\log s} \Delta J_K
\end{aligned}
\tag{7.38}
$$

where loop integrals are performed over shells of width $\Lambda - \Lambda/s \approx \Lambda \log s$ with scaling parameter $s \equiv e^\ell \gtrsim 1$. L is equal to the number of integrations needed to compute the diagram. If the exponents $e(L, d)$ are positive for all values of L and d (> 1), the beta function is given by the tree-level result $(b_0 J_K)$ in the large-N_Λ limit, which means vertex corrections can be neglected. Since we have already shown that $b_0 = 0$,

this would imply marginality to all orders. The goal of this section is to demonstrate that this is indeed the case.
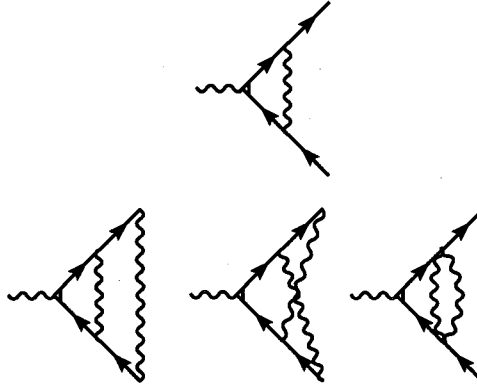

Figure 7.5 : $L = 1$ and $L = 2$ vertex corrections. All propagators are dressed.

In what follows, we give two general arguments that demonstrate that vertex corrections become increasingly suppressed in the loop expansion. Specifically, a diagram with L-loops will come with a factor of $1/N_\Lambda^{L(d+3)/3}$, *i.e.* $e(L,d) = L(d+3)/3$. We also illustrate the principle by calculating an example $L = 1$ diagram to demonstrate how this factor emerges. We work with cutoffs in units of K_F so that $N_\Lambda \equiv 1/\Lambda$.

The first argument is essentially just power-counting. Every loop integral will introduce a factor of Λ^{d+1} from the measure of integration. For L loops, there will be $2L$ fermion propagators (see Fig 7.5) each carrying a factor of $\Lambda^{-d/z}$ with $z = 3$. There will also be L boson propagators which, because of the ω/q form of the boson self energy, scale like $O(1)$. Thus, each diagram with L-loops contributes the following

amount of phase space.

$$\Delta J_K = \sum_{L=1}^{\infty} b_L(s) J_K^{2L+1} (\Lambda^{d+1})^L (\Lambda^{-d/z})^{2L} (\Lambda/\Lambda)^L$$

$$= \sum_{L=1}^{\infty} b_L(s) J_K^{2L+1} \Lambda^{[d(1-2/z)+1]L}$$

$$= \sum_{L=1}^{\infty} \frac{b_L(s)}{N_\Lambda^{(d+3)L/3}} J_K^{2L+1} \qquad (7.39)$$

Therefore $e(L,d) = (d+3)L/3 > 0$, vertex corrects are kinematically suppressed, and the tree level result (marginality) is the entire story.

The careful reader will have noticed that other classes of diagrams are possible. For example, Fig 7.6a shows a self-energy insertion into the boson propagator. Iterates of diagrams like this might at first appear to compensate for some powers of N_Λ due to the pure fermion loops. However, since we are using fully dressed propagators, this would be double counting. Such terms are already included by defining the fixed point action to have the ω/q self energy from the beginning.
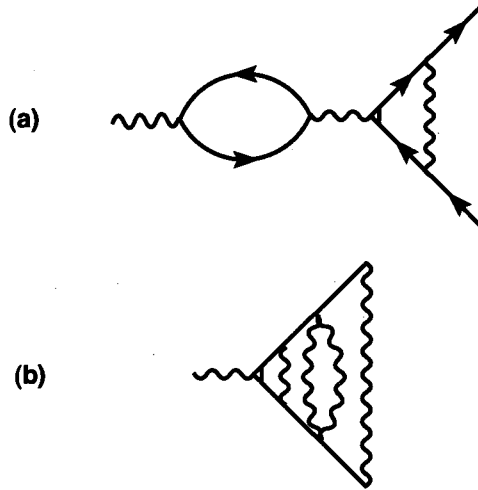

Figure 7.6 : (a) Diagram which is not included because self energy corrections are already built into the dressed propagators. (b) An example of $L = 4$ diagram with 6 fermion propagators and 4 boson propagators.

Another class of diagram is represented in Fig 7.6b, which is $L = 4$ and with

propagator powers of $G^6\chi^4 = G^{2L-2}\chi^L$. More generally, an exhaustive classification of diagrams at order L, with L even, will actually have $L/2+1$ subclasses which have factors

$$G^{2L}\chi^L, G^{2L-2}\chi^L, G^{2L-4}\chi^L, \cdots, G^L\chi^L$$

If L is odd, the series will terminate at $L+1$ rather than L, and there will be $(L+1)/2$ subclasses. However, since these subclasses only differ by *smaller* powers of G than the G^{2L} we considered above, it is easy to see that they will be subleading compared to the estimate given in equation 7.39.

The second way to obtain Migdal's theorem more closely mirrors the antiferromagnetic case [49] and the "leap to all loops" of the pure fermion problem [63]. Begin by writing the quadratic parts of the action and rescaling all momenta and energies by Λ so the limits of integration become dimensionless: $k \to \Lambda k$, $\epsilon \to \Lambda\epsilon$, etc.

$$\mathcal{S}_c = \Lambda^{d+1} \sum_{}^{N_\Lambda} \int d^d k d\epsilon \; \psi^\dagger (i\epsilon^{d/z}\Lambda^{d/z} - \Lambda k_\parallel - \Lambda^2 k_\perp^2)\psi \qquad (7.40)$$

$$\mathcal{S}_m = \Lambda^{d+1} \int d^d q d\omega \; m^+ (\Lambda^2 q^2 + \omega/q)m^- \qquad (7.41)$$

For simplicity, we have omitted some prefactors. To leading order in $1/N_\Lambda$ (small Λ), the dominant term in the fermionic part is $\epsilon^{d/z}$ ($\epsilon\log\epsilon$ in $d=3$), while the ω/q term is largest in the bosonic part. We therefore rescale fields according to these terms, obtaining:

$$\psi \to \Lambda^{-(4d/3+1)/2}\psi$$

$$m^\pm \to \Lambda^{-(d+1)/2}m^\pm \qquad (7.42)$$

This allows us to estimate the phase space contribution of the interaction term.

Rescaling according to this procedure, the Kondo coupling is given by:

$$J_K \int \Lambda^{2(d+1)} d^d k d\epsilon d^d q d\omega \Lambda^{-(4d/3+1)} \psi^\dagger \psi \Lambda^{-(d+1)/2} m^\pm \qquad (7.43)$$

$$\propto J_K \Lambda^{(d+3)/6} \qquad (7.44)$$

Associated with every power of J_K is a factor $1/N_\Lambda^{(d+3)/6}$, and within the loop expansion the Lth-order correction is given by $\Delta J_K / J_K \propto J_K^{2L} \propto 1/N_\Lambda^{(d+3)/3}$, or $e(L,d) = (d+3)/3 > 0$, which is the same result we found earlier. Therefore vertex correction can be neglected and the tree-level result is asymptotically exact to all orders.

Note that the analog of this field rescaling for the pure fermion problem results in a four-fermion coupling given by $\Lambda u \int \psi^4$. In this case, Shankar found that the four-fermion coupling is still marginal despite the additional factor of Λ induced by the field rescaling. We are simply to regard Λ as a small parameter (in units of K_F), not a running variable. Within the momentum shell approach, the beta function is determined by finding the dependence on the parameter $s = e^\ell$ and computing the derivative $d/d\ell$, not by finding any explicit dependence on Λ as is done in the field theory approach.

We have now proven that vertex corrections can be neglected in the large-N_Λ limit. To demonstrate how the peculiar exponent $e(L,d) = (d+3)/3$ arises in a concrete example, let us calculate the first, $L = 1$, vertex correction shown in figure 7.5.

$$\Delta J_K(\vec{p}, i\epsilon; \vec{Q}, i\Omega) = J_K^3 \int d^d q d\omega G(\vec{p}+\vec{q}, i\epsilon+i\omega) G(\vec{p}+\vec{q}+\vec{Q}, i\epsilon+i\omega+i\Omega)\chi(\vec{q}, i\omega)$$

$$(7.45)$$

We can set the fermionic variables $\vec{p} = 0$ (measured from the patch origin) and $\epsilon = 0$ since any deviation would be irrelevant in the RG sense. In contrast, the variables $\vec{Q}$ and Ω belong to the external boson which we keep nonzero, keeping in mind that our

problem has cutoffs ω_c and q_c.

$$\Delta J_K(0,0;\vec{Q},i\Omega) = J_K^3 \int d^d q d\omega \frac{1}{i\epsilon_0^{1/3}|\omega|^{2/3} - v_\uparrow q_\parallel - v_\uparrow q_\perp^2/(2K_{F\uparrow})} \frac{\sqrt{q_\perp^2 + q_\parallel^2}}{(q_\perp^2 + q_\parallel^2)^{3/2} + \gamma|\omega|}$$
$$\times \frac{1}{i\epsilon_0^{1/3}|\omega + \Omega|^{2/3} - v_\downarrow(q_\parallel + Q_\parallel) - v_\downarrow(q_\perp^2 + Q_\perp^2)/(2K_{F\downarrow})}$$

One way to demonstrate Migdal's theorem is to factorize integrands of momentum integrals according to a certain procedure, as detailed by several authors [68, 110, 111]. Physically, this relies of the fact that fermions are much faster than bosons. Formally, this can be accomplished by rescaling $v_F \to N v_F$ and similarly for the coupling; see Appendix A of of ref [111].

The validity of the factorization is not entirely obvious. Within a large-N treatment, a thorough analysis has been done where numerical comparisons show that the factorization approximation only begins to break down at relatively high temperatures [110], outside the regime we consider here. In the next section, we show that the factorization of momentum integrations applies in the large-N_Λ limit (without invoking large-N). For the rest of this section, we first proceed with such a factorization.

In such a case, the only parts of the integrand that depend on $q_\perp$ are the bosonic propagators. This allows us to define a momentum independent boson given by the fully momentum dependent propagator integrated along the Fermi surface:

$$\chi_1(i\omega; \Lambda_\perp, q_c) \equiv \int d^{d-1}q_\perp \chi(\vec{q}, i\omega)|_{q_\parallel = 0}$$
$$= \int d^{d-1}q_\perp \frac{\Theta(q_\perp - q_{c\perp})\Theta(\Lambda_\perp - q_\perp)}{q_\perp^2 + \gamma\frac{|\omega|}{|q_\perp|}} \qquad (7.46)$$

Note, once again, that we adopt the convention of ref. [68] in labeling parallel and perpendicular components. Also note that unlike other problems, we have a natural infrared regularization provided by the cutoff on bosonic modes. All integrals thus

have both UV regularizations Λ and IR regularizations q_c and ω_c. Moreover, loop integrals will be performed over momentum and energy shells, rather than extending the limits of integration to infinite intervals. This is the reason why we do *not* find a non-analytic $q^{3/2}$ correction to the static boson propagator, in contrast to theories for the itinerant ferromagnetic quantum critical point [112].

To leading order in large-N_Λ, the vertex correction can now be written in factorized form:

$$\Delta J_K(0,0;Q_\parallel,i\Omega) = J_K^3 \int d\omega \chi_1(i\omega;\Lambda_\perp,q_c)$$
$$\times \int dq_\parallel \frac{1}{i\epsilon_0^{1/3}|\omega|^{2/3} - v_\uparrow q_\parallel} \frac{1}{i\epsilon_0^{1/3}|\omega+\Omega|^{2/3} - v_\downarrow(q_\parallel+Q_\parallel)}$$

Note that the dimensional dependence is confined to $\chi_1(i\omega)$, while the $q_\parallel$ dependence is isolated in the fermionic propagators. The dependence on external $Q_\perp$ has dropped out, which is higher order in $1/N_\Lambda$. To proceed, we consider $d = 2$ for this illustrative example.

The range of integration requires some comment. Within the momentum-shell scheme, each loop integral consists of a number of "slabs" in phase space of width $\Lambda - \Lambda/s^\eta \approx \eta\Lambda \log s$, where η is the scaling dimension of the appropriate direction. Within each slab, the integrand can be approximated by its value at the cutoff. For example, at one-loop we can write

$$I \equiv \int d\omega dq_\parallel dq_\perp f(\omega, q_\parallel, q_\perp)$$
$$\approx [q_\perp]\Lambda_\perp \log s \int d\omega dq_\parallel [f(\omega, q_\parallel, \Lambda_\perp) + f(\omega, q_\parallel, -\Lambda_\perp)]$$
$$+ [q_\parallel]\Lambda_\parallel \log s \int d\omega dq_\perp [f(\omega, \Lambda_\parallel, q_\perp) + f(\omega, -\Lambda_\parallel, q_\perp)]$$
$$+ [\omega]\Lambda_\omega \log s \int dq_\parallel dq_\perp [f(\Lambda_\omega, q_\parallel, q_\perp) + f(-\Lambda_\omega, q_\parallel, q_\perp)]$$
$$\equiv (\Lambda_\perp I_\perp + \Lambda_\parallel I_\parallel + \Lambda_\omega I_\omega) \log s \tag{7.47}$$

We have divided the loop integral into a sum of $(d+1)$ terms which represent the slabs directed along each of the $(d+1)$ hyperplanes. This is simply the multidimensional generalization of the trivial result: $\int_{\Lambda/s^\eta}^{\Lambda} dx\, f(x) + \int_{-\Lambda}^{-\Lambda/s^\eta} dx\, f(x) \approx \eta\Lambda \log s[f(\Lambda) + f(-\Lambda)]$. Let us consider one of these slab integrals.

$$
\begin{aligned}
\Lambda_\omega I_\omega &= [\omega]\,\Lambda_\omega J_K^3 \int dq_\perp \frac{1}{q_\perp^2 + \gamma\frac{\Lambda_\omega}{|q_\perp|}} \int dq_\parallel \left[\frac{1}{i\epsilon_0^{1/3}\Lambda_\omega^{2/3} - v_\uparrow q_\parallel} \right. \\
&\quad \times \frac{1}{i\epsilon_0^{1/3}(\Lambda_\omega + \omega_c)^{2/3} - v_\downarrow(q_\parallel + q_c)} \\
&\quad \left. + \frac{1}{i\epsilon_0^{1/3}\Lambda_\omega^{2/3} + v_\uparrow q_\parallel}\, \frac{1}{i\epsilon_0^{1/3}(\Lambda_\omega - \omega_c)^{2/3} + v_\downarrow(q_\parallel + q_c)} \right]
\end{aligned}
\tag{7.48}
$$

where we have take the external frequency and moment down to the cutoffs q_c and ω_c, and assumed $0 < \omega_c < \Lambda_\omega$. This integral is factorized, with the first factor being given by

$$
\begin{aligned}
\chi_1(\omega = \Lambda_\omega) &= \chi_1(\omega = -\Lambda_\omega) \\
&= \int dq_\perp \frac{1}{q_\perp^2 + \gamma\frac{\Lambda_\omega}{|q_\perp|}} \\
&= (1/3)(\gamma\Lambda_\omega)^{-1/3}\left[2\sqrt{3}\arctan\left(\frac{1 - 2q_c(\gamma\Lambda_\omega)^{-1/3}}{\sqrt{3}}\right) \right. \\
&\quad - 2\sqrt{3}\arctan\left(\frac{1 - 2q_c(\gamma\Lambda_\omega)^{-1/3}}{\sqrt{3}}\right) \\
&\quad + 2\log(q_c + (\gamma\Lambda_\omega)^{1/3}) - 2\log(\Lambda_\perp + (\gamma\Lambda_\omega)^{1/3}) \\
&\quad - \log(q_c^2 - q_c(\gamma\Lambda_\omega)^{1/3} + (\gamma\Lambda_\omega)^{2/3}) \\
&\quad \left. + \log(\Lambda_\perp^2 - \Lambda_\perp(\gamma\Lambda_\omega)^{1/3} + (\gamma\Lambda_\omega)^{2/3}) \right]
\end{aligned}
\tag{7.49}
$$

For an estimate of this factor, we must first take the limit $q_c \to 0$, since this must be

smaller than the UV cutoffs:

$$\lim_{q_c \to 0} \chi_1(\omega = \Lambda_\omega) = (1/9)(\gamma\Lambda_\omega)^{-1/3}\left[\pi\sqrt{3} - 6\sqrt{3}\arctan\left(\frac{1 - 2\Lambda_\perp(\gamma\Lambda_\omega)^{-1/3}}{\sqrt{3}}\right)\right.$$

$$\left. -6\log(\Lambda_\perp + (\gamma\Lambda_\omega)^{1/3}) + 3\log(\Lambda_\perp^2 - \Lambda_\perp(\gamma\Lambda_\omega)^{1/3} + (\gamma\Lambda_\omega)^{2/3})\right] \tag{7.50}$$

next we set $\Lambda_\omega = \Lambda_\perp = \Lambda$, then take a small Λ expansion, finding:

$$\chi_1 \propto \Lambda/\gamma - \frac{2}{5\gamma^2}\Lambda^3 + O(\Lambda^5) \tag{7.51}$$

The second factor is a more complicated integral.

$$\int (GG|_{\Lambda_\omega} + GG|_{-\Lambda_\omega}) = \int dq_\parallel \Big[\frac{1}{i\epsilon_0^{1/3}\Lambda_\omega^{2/3} - v_\uparrow q_\parallel} \frac{1}{i\epsilon_0^{1/3}(\Lambda_\omega + \omega_c)^{2/3} - v_\downarrow(q_\parallel + q_c)}$$

$$+ \frac{1}{i\epsilon_0^{1/3}\Lambda_\omega^{2/3} + v_\uparrow q_\parallel} \frac{1}{i\epsilon_0^{1/3}(\Lambda_\omega - \omega_c)^{2/3} + v_\downarrow(q_\parallel + q_c)} \Big]$$

$$= \frac{1}{i\epsilon_0^{1/3}[(\Lambda_\omega + \omega_c)^{2/3} - \Lambda_\omega^{2/3}] - v_F q_c}$$

$$\times \Bigg\{ -\frac{2i}{v_\uparrow}\Big[\arctan\Big(\frac{v_\uparrow \Lambda_\parallel}{\epsilon_0^{1/3}|\Lambda_\omega|^{2/3}} \Big) - \arctan\Big(\frac{v_\uparrow q_c}{\epsilon_0^{1/3}|\Lambda_\omega|^{2/3}} \Big) \Big]$$

$$-\frac{1}{v_\downarrow}\Big(\frac{1}{2}\log\frac{\epsilon_0^{2/3}|\omega_c + \Lambda_\omega|^{4/3} + v_\downarrow^2(q_c - \Lambda_\parallel)^2}{\epsilon_0^{2/3}|\omega_c + \Lambda_\omega|^{4/3} + v_\downarrow^2(q_c + \Lambda_\parallel)^2}$$

$$-\frac{1}{2}\log\frac{\epsilon_0^{2/3}|\omega_c + \Lambda_\omega|^{4/3}}{\epsilon_0^{2/3}|\omega_c + \Lambda_\omega|^{4/3} + 4v_\downarrow^2 q_c^2}$$

$$+i\arg[i\epsilon_0^{1/3}|\omega_c + \Lambda_\omega|^{2/3} - v_\downarrow(q_c - \Lambda_\parallel)]$$

$$-i\arg[i\epsilon_0^{1/3}|\omega_c + \Lambda_\omega|^{2/3} - v_\downarrow(q_c + \Lambda_\parallel)]$$

$$+i\arg[i\epsilon_0^{1/3}|\omega_c + \Lambda_\omega|^{2/3}]$$

$$-i\arg[i\epsilon_0^{1/3}|\omega_c + \Lambda_\omega|^{2/3} - 2v_\downarrow q_c] \Big) \Bigg\}$$

$$+\frac{1}{i\epsilon_0^{1/3}[(\Lambda_\omega - \omega_c)^{2/3} - \Lambda_\omega^{2/3} - v_F q_c]}$$

$$\times \Bigg\{ -\frac{2i}{-v_\uparrow}\Big[\arctan\Big(\frac{-v_\uparrow \Lambda_\parallel}{\epsilon_0^{1/3}|\Lambda_\omega|^{2/3}} \Big) - \arctan\Big(\frac{-v_\uparrow q_c}{\epsilon_0^{1/3}|\Lambda_\omega|^{2/3}} \Big) \Big]$$

$$+\frac{1}{v_\downarrow}\Big(\frac{1}{2}\log\frac{\epsilon_0^{2/3}|-\omega_c + \Lambda_\omega|^{4/3} - v_\downarrow^2(q_c - \Lambda_\parallel)^2}{\epsilon_0^{2/3}|-\omega_c + \Lambda_\omega|^{4/3} - v_\downarrow^2(q_c + \Lambda_\parallel)^2}$$

$$-\frac{1}{2}\log\frac{\epsilon_0^{2/3}|-\omega_c + \Lambda_\omega|^{4/3}}{\epsilon_0^{2/3}|-\omega_c + \Lambda_\omega|^{4/3} - 4v_\downarrow^2 q_c^2}$$

$$+i\arg[i\epsilon_0^{1/3}|-\omega_c + \Lambda_\omega|^{2/3} + v_\downarrow(q_c - \Lambda_\parallel)]$$

$$-i\arg[i\epsilon_0^{1/3}|-\omega_c + \Lambda_\omega|^{2/3} + v_\downarrow(q_c + \Lambda_\parallel)]$$

$$+i\arg[i\epsilon_0^{1/3}|-\omega_c + \Lambda_\omega|^{2/3}]$$

$$-i\arg[i\epsilon_0^{1/3}|-\omega_c + \Lambda_\omega|^{2/3} + 2v_\downarrow q_c] \Big) \Bigg\} \tag{7.52}$$

where we have neglected terms of order $v_\uparrow - v_\downarrow \sim \Delta/\mu$, and used $\int dq_\parallel = \int dq_\parallel \Theta(q_\parallel - q_c)\Theta(\Lambda_\parallel - q_\parallel)$. Using the same procedure as for the previous factor, as well as the following simplifications, $q_c/\Lambda \ll 1$, $\omega_c/\Lambda \ll 1$, $\omega_c/q_c \ll 1$, and $\omega_c/\omega \ll 1$, we find the rather simple result:

$$\int (GG|_{\Lambda_\omega} + GG|_{-\Lambda_\omega}) \quad \propto \quad \Lambda^{1/3}\Lambda^{-2/3} = \Lambda^{-1/3} \tag{7.53}$$

Putting it all together, we find

$$\begin{aligned}
\Lambda_\omega I_\omega &\sim \quad [\omega]\, \Lambda(\log s)\Lambda\Lambda^{-1/3} \\
&= \quad \frac{3}{2}\Lambda^{5/3}(\log s) \tag{7.54}
\end{aligned}$$

By a similar analysis, the other slab contributions can be shown to have the same exponent: $\Lambda_\perp I_\perp \sim \Lambda^{5/3}$ and $\Lambda_\parallel I_\parallel \sim \Lambda^{5/3}$. Therefore, the one-loop correction to the beta function is given by:

$$\begin{aligned}
\delta J_K &\sim \quad \frac{d}{d\log s}\Lambda^{5/3}\log s \\
&= \quad \Lambda^{5/3} \\
&= \quad 1/N_\Lambda^{5/3} \tag{7.55}
\end{aligned}$$

which confirms our previous and more general derivations of Migdal's theorem: $e(L = 1, d = 2) = (2 + 3)/3 = 5/3$.

To summarize, we have demonstrated Migdal's theorem in three different ways, including an explicit calculation of the one-loop integral as a concrete example.

An interesting future direction would be to consider calculations of this sort with finite Λ/K_F, akin to $1/N_\Lambda$ corrections. In particular, it is easy to imagine that special bandstructures might possess Fermi surface features, such as nesting or van-Hove singularities, that might lead to significantly different conclusions. For such

cases, however, it would then be necessary to consider specific materials with realistic bandstructures, and we would lose our ability to make universal statements. For this reason we remain content with the $N_\Lambda = \infty$ limit which should be valid under generic circumstances, and leave to future work detailed investigations of material-specific bandstructures where $1/N_\Lambda$ corrections might play an important role. We also point out that identifying the $N_\Lambda = \infty$ theory is in itself a non-trivial result. After all, Landau Fermi liquid theory is the $N_\Lambda = \infty$ limit of the interacting fermion problem [63] which has been profoundly useful despite the fact that, by itself, $1/N_\Lambda$ corrections are not captured.

7.7.2 Factorization of momentum integrals

The property of $q_\parallel - q_\perp$ integrations has previously been discussed within a large-N limit, where N is the number of fermion flavors [110]. These theories typically perform loop integrations over all of phase space, in which case it becomes necessary to introduce the large factor N in order to properly weight the desired kinematic range. Working with cutoffs explicitly, as we do, the integrals are more difficult to compute without the technology of residue calculus, however, the physical kinematic regime is more naturally apparent. Here, we demonstrate the validity of the factorization approximation used in the previous section, but we do not require a large number of fermion flavors. Instead, our large parameter is the ratio $N_\Lambda \equiv K_F/\Lambda$.

Consider a low-energy fermion represented by a point infinitesimally near the Fermi surface. This point on the Fermi surface defines the origin of our coordinate system. Since this patch of surface is defined by its normal, we decompose the coordinate system into components parallel and perpendicular to this normal vector. A low energy, forward scattering excitation involving this state will be contained within

a box of size Λ near this point of the Fermi surface, and we demand $\Lambda \ll K_F$. The momentum transfer between these two fermion states we label with $\vec{q} = (q_\parallel, \vec{q}_\perp)$. The factorization approximation is valid in the limit where the dimension of the box along the Fermi surface is much smaller than the Fermi wavevector: $\Lambda_\perp \ll K_F$. There are three ways to choose a small cutoff, as depicted in Fig 7.7. Either set $\Lambda_\parallel \ll \Lambda_\perp \sim K_F$, or $\Lambda_\perp \ll \Lambda_\parallel \sim K_F$, or $\Lambda_\perp \sim \Lambda_\parallel \ll K_F$. The first choice might lead one to believe that the number of patches is not large, which is not the case. The second option appears to suggest that $q_\perp \ll q_\parallel$, which is opposite to the regime we wish to consider. Furthermore, it includes high-energy excitations far from the mass shell. The third choice seems most natural, and it turns out to be the most convenient in terms of calculations as well, as indicated in the previous section. It might lead one to believe that the scaling is isotropic, but we will show below that this is not the case. Finally, a fourth possibility, where $\Lambda_\perp \sim \Lambda_\parallel \sim K_F$ has been used in calculations by other authors. When calculating with the fourth option, where loop integrals essentially extend to infinity, it is necessary to rescale the Fermi velocity by a large factor such as an artificially large number of fermion flavors [111]. The hope is that the $N = \infty$ results will be connected to the $N = 2$ case we wish to understand, rather than the $N = 0$ limit which is qualitatively different [113, 68]. We choose, instead, to rely on the fact that $\Lambda \ll K_F$ which does not require us to resort to large-N, but only large-N_Λ which is simply the limit of the low-energy field theory.

To see the small error made by the factorization approximation when $\Lambda_\perp \sim \Lambda_\parallel \ll K_F$, consider the one-loop vertex correction we calculated in the previous section,

$$\Lambda_\parallel \ll \Lambda_\perp \approx \mathrm{KF} \qquad \Lambda_\perp \ll \Lambda_\parallel \approx \mathrm{KF} \qquad \Lambda_\perp \approx \Lambda_\parallel \ll \mathrm{KF} \qquad \Lambda_\perp \approx \Lambda_\parallel \approx \mathrm{KF}$$
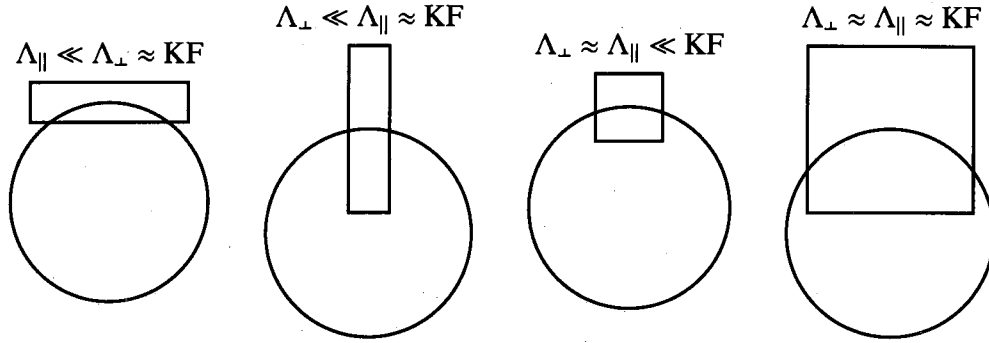
Figure 7.7 : This figure depicts the various choices we have in choosing the size of our integration cutoffs in relation to each other, and the scale set by the Fermi momentum K_F. To restrict to low-energy excitations we must have $\Lambda_\parallel \ll K_F$. To ensure that we have a large number of patches, we must insist that $\Lambda_\perp \ll K_F$. The most convenient and sensible choice is to take $\Lambda_\perp \sim \Lambda_\parallel \ll K_F$. Even though the cutoffs are of similar size, we still have $q_\perp \gg q_\parallel$, as indicated by the next figure.

with and without the factorization approximation:

$$\Delta J_K = J_K^3 \int d^d q\, d\omega \frac{1}{i\epsilon_0^{1/3}|\omega|^{2/3} - v_\uparrow q_\parallel - v_\uparrow q_\perp^2/(2K_{F\uparrow})} \frac{\sqrt{q_\perp^2 + q_\parallel^2}}{(q_\perp^2 + q_\parallel^2)^{3/2} + \gamma|\omega|}$$
$$\times \frac{1}{i\epsilon_0^{1/3}|\omega + \Omega|^{2/3} - v_\downarrow(q_\parallel + Q_\parallel) - v_\downarrow(q_\perp^2 + Q_\perp^2)/(2K_{F\downarrow})} \qquad (7.56)$$

$$\Delta J_K\Big|_{\text{factorized}} = J_K^3 \int d^d q\, d\omega \frac{1}{i\epsilon_0^{1/3}|\omega|^{2/3} - v_\uparrow q_\parallel} \frac{|q_\perp|}{q_\perp^3 + \gamma|\omega|}$$
$$\times \frac{1}{i\epsilon_0^{1/3}|\omega + \Omega|^{2/3} - v_\downarrow(q_\parallel + Q_\parallel)} \qquad (7.57)$$

The integrands are sharply peaked in phase space along surfaces defined by the zeros of the inverse propagators. For ΔJ_K this corresponds to the surface defined by:

$$G^{-1}(q_\perp, q_\parallel, i\omega)G^{-1}(q_\perp + Q_\perp, q_\parallel + Q_\parallel, i\omega + i\Omega)\chi^{-1}(q_\perp, q_\parallel, i\omega) = 0 \qquad (7.58)$$

while for $\Delta J_K\Big|_{\text{factorized}}$, the surface is defined by:

$$G^{-1}(0, q_\parallel, i\omega)G^{-1}(0, q_\parallel + Q_\parallel, i\omega + i\Omega)\chi^{-1}(q_\perp, 0, i\omega) = 0 \qquad (7.59)$$

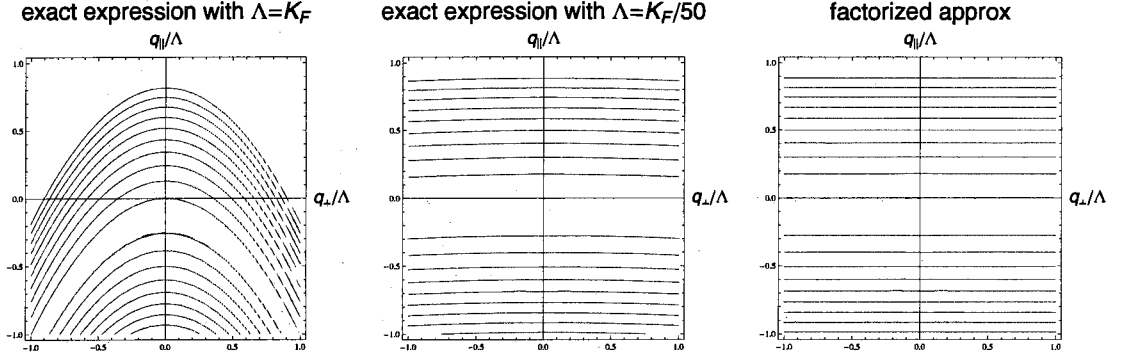| exact expression with Λ=K_F	exact expression with Λ=K_F/50	factorized approx

Figure 7.8 : The left panel shows constant energy contours defined by the equation $G^{-1}(q_\perp, q_\parallel, i\omega)G^{-1}(q_\perp + Q_\perp, q_\parallel + Q_\parallel, i\omega + i\Omega)\chi^{-1}(q_\perp, q_\parallel, i\omega) = 0$, corresponding to the peaked regions of the unfactorized ("exact") integrand of the one-loop vertex correction with the unphysical value $\Lambda = K_F$. The middle panel is the same exact expression, but with the more reasonable $\Lambda = K_F/50$. Finally, the right panel depicts the constant energy contours of the highly peaked regions of the integrand using the factorization approximation; these curves are defined by: $G^{-1}(0, q_\parallel, i\omega)G^{-1}(0, q_\parallel + Q_\parallel, i\omega + i\Omega)\chi^{-1}(q_\perp, 0, i\omega) = 0$. Clearly, the middle and right panels are very similar, justifying the use of the factorization approximation when K_F is the largest scale.

The difference between these two cases is depicted in Fig. 7.8, where contours of constant energy are plotted in the momentum plane for $d = 2$. Obviously, when $\Lambda \ll K_F$, the exact and factorized contours are almost indistinguishable. Only when $\Lambda \sim K_F$ does the curvature of the Fermi surface become apparent and the factorization approximation break down.

The figure also illustrates the fact that when $\Lambda \ll K_F$, the most highly peaked portions of the integrand occupy significant phase space where $q_\perp \gg q_\parallel$ for fixed energy (i.e. on each contour). This is so despite the fact that $\Lambda_\perp \sim \Lambda_\parallel$, and is the justification for the neglect of $q_\parallel$ terms in the bosonic propagators. At the same time, we neglect $q_\perp$ pieces of the fermionic propagators because K_F is large.

A less graphical way to see the above is as follows. Because $\Lambda \ll K_F$, the $q_\parallel$ integration is dominated by a horizontal strip of width Λ^2, corresponding to the curvature of the Fermi surface. Over this range, the fermionic propagator can be

approximated

$$G^{-1}(q_\perp, q_\parallel, i\omega) = \omega^{2/3} - v_F(q_\parallel + q_\perp^2/2K_F)$$

$$\approx \omega^{2/3} - v_F q_\parallel. \tag{7.60}$$

The fermionic propagator tells us that the most important regions of the integrand are for $q_\parallel \sim \omega^{2/3}$. At the same time, the bosonic propagator is most highly peaked around $q \sim \omega^{1/3}$. This means that $q^2 \sim \omega^{2/3}$. Since the pole of the fermion propagator will force $q_\parallel^2 \sim \omega^{4/3}$, this means that the boson propagator must have $q_\perp^2 \sim \omega^{2/3} \gg q_\parallel^2 \sim \omega^{4/3}$, and thus

$$\chi^{-1}(q_\perp, q_\parallel, i\omega) \approx q_\perp^2 + \gamma|\omega|/q_\perp \tag{7.61}$$

All these approximations become exact in the $N_\Lambda \to \infty$ limit. Eqs. (7.60,7.61) ensure the factorization of the $q_\parallel$ and $q_\perp$ integrations.

7.8 Non-Analytic Corrections

An intriguing question for future studies is the effect of non-analytic Fermi-liquid corrections. Such non-analytic corrections to susceptibility and other physical properties already exist in a standard Fermi liquid theory [114, 107]. In generic cases, such non-analytic corrections are relatively small. Just like it is important to establish the Fermi liquid fixed point before such non-analytic corrections are analyzed in detail, we have focused on the existence of a small-Fermi-surface ferromagnetic fixed point. In the case of *quantum critical point* of a weak ferromagnetic system, the existence of an extensive critical regime controlled by the fixed point without taking into account the non-analytic-Fermi-liquid corrections is supported by experimental observations [115].

Chapter 8

Conclusions

This thesis has focused on magnetically ordered phases of the Kondo lattice model, which is the theoretical paradigm for understanding heavy fermion systems. We developed effective nonlinear field theories that function well inside the antiferromagnetic and ferromagnetic phases, and studied them by renormalization group analyses. The main conclusion is that the Kondo coupling is exactly marginal to all order of perturbation theory within the limit $\Lambda/K_F \to 0$. The Fermi surface in these magnetic phases is therefore small: f-orbitals are localized and no static Kondo singlet exists. The RG analysis itself required the invention of new theoretical techniques, as discussed in detail in Chapter 4. Beyond the phases themselves, this work has implications for quantum critical points in heavy fermion metals where Kondo fluctuations may play an important role in addition to magnetism. Within the broader scope of strongly correlated systems, this work provides asymptotically exact statements in the limit where $N_\Lambda \to 0$. This is theoretically useful because although $1/N_\Lambda$ corrections might prove to be a fruitful topic for future studies, the construction of the $N_\Lambda = \infty$ theory we have given here represents an important anchoring point. After all, Landau Fermi Liquid Theory (LFLT) itself is the other example of an $N_\Lambda = \infty$ theory. Inclusion of $1/N_\Lambda$ corrections, superconductivity according to Kohn's theorem, approaching a QCP, and coupling to a gauge-field all appear to invalidate LFLT. Nonetheless, LFLT has served as an important conceptual paradigm for over half a century.

In addition to the theoretical implications of this thesis, this work is relevant to a number of real materials such as $YbRh_2Si_2$ (antiferromagnet) and $CeRu_2Ge_2$ (ferro-

magnet) as discussed earlier. For the ferromagnetic case, we made several predictions for non-Ferm liquid signatures that can be checked by experimental measurements of the resistivity and specific heat. For both ferromagnetic and antiferromagnetic heavy fermion materials, the existence of a small Fermi surface phase is testable by direct Fermi surface studies. Existing data on $YbRh_2Si_2$ [47] and $CeRu_2Ge_2$ [84] already confirm this idea, and we hope future experiments will further clarify the situation in these and other materials.

Bibliography

[1] N. W. Ashcroft and N. D. Mermin. *Solid State Physics*. Brooks Cole (1976).

[2] E. Stoner. "Collective electron ferromagnetism." *Proc. Roy. Soc. London Ser. A* **165** 0372–0414 (1938).

[3] J. R. Schrieffer. *Theory of Superconductivity*. Perseus Books (1999).

[4] A. Cho. "Atomic physics: Ultracold atoms spark a hot race." *Science* **301** 750 (2003).

[5] P. Coleman. "Heavy fermions: Electrons at the edge of magnetism." arXiv:cond-mat/0612006v3.

[6] H. von Loehneysen, A. Rosch, M. Vojta, and P. Woelfle. "Fermi-liquid instabilities at magnetic quantum phase transitions." *Rev. Mod. Phys.* **79** 1015–1075 (2007).

[7] K. Andres, J. Graebner, and H. Ott. "4f-virtual-bound-state formation in $CeAl_3$ at low-temperatures." *Phys. Rev. Lett.* **35** 1779–1782 (1975).

[8] F. Steglich, J. Aarts, C. Bredl, W. Lieke, D. Meschede, W. Franz, and H. Schafer. "Superconductivity in the presence of strong Pauli paramagnetism - $CeCu_2Si_2$." *Phys. Rev. Lett.* **43** 1892–1896 (1979).

[9] S. Sachdev. *Quantum Phase Transitions*. Cambridge University Press, Cambridge (1999).

[10] P. Gegenwart, T. Westerkamp, C. Krellner, Y. Tokiwa, S. Paschen, C. Geibel, F. Steglich, E. Abrahams, and Q. Si. "Multiple energy scales at a quantum

critical point." *Science* **315** 969–971 (2007).

[11] C. Lacroix and M. Cyrot. "Phase-diagram of the Kondo lattice." *Phys. Rev. B* **20** 1969–1976 (1979).

[12] P. Sinjukow and W. Nolting. "Exact mapping of periodic Anderson model to Kondo lattice model." *Phys. Rev. B* **65** (2002).

[13] M. Ruderman and C. Kittel. "Indirect exchange coupling of nuclear magnetic moments by conduction electrons." *Phys. Rev.* **96** 99–102 (1954).

[14] T. Kasuya. "A theory of metallic ferromagnetism and antiferromagnetism on Zeners model." *Progress of Theoretical Physics* **16** 45–57 (1956).

[15] K. Yosida. "Magnetic properties of Cu-Mn alloys." *Phys. Rev.* **106** 893–898 (1957).

[16] A. C. Hewson. *The Kondo Problem to Heavy Fermions.* Cambridge University Press, Cambridge (1997).

[17] Q. Si, S. Rabello, K. Ingersent, and J. Smith. "Locally critical quantum phase transitions in strongly correlated metals." *Nature* **413** 804–808 (2001).

[18] T. Senthil, M. Vojta, and S. Sachdev. "Weak magnetism and non-Fermi liquids near heavy-fermion critical points." *Phys. Rev. B* **69** 035111 (2004).

[19] C. Pepin. "Fractionalization and Fermi-surface volume in heavy-fermion compounds: The case of $YbRh_2Si_2$." *Phys. Rev. Lett.* **94** 066402 (2005).

[20] P. Coleman, J. Marston, and A. Schofield. "Transport anomalies in a simplified model for a heavy-electron quantum critical point." *Phys. Rev. B* **72** 245111 (2005).

[21] Q. Si, J. X. Zhu, and D. Grempel. "Magnetic quantum phase transitions in Kondo lattices." *J. Physics: Conden. Matter* **17** R1025–R1040 (2005).

[22] N. Read and D. Newns. "A new functional integral formalism for the degenerate Anderson model." *J. Phys. C* **16** 1055–1060 (1983).

[23] P. Coleman. "1/n expansion for the Kondo lattice." *Phys. Rev. B* **28** 5255–5262 (1983).

[24] A. Auerbach and K. Levin. "Kondo bosons and the Kondo lattice - microscopic basis for the heavy Fermi-liquid." *Phys. Rev. Lett.* **57** 877–880 (1986).

[25] R. M. Martin. "Fermi-surface sum-rule and its consequences for periodic Kondo and mixed-valence systems." *Phys. Rev. Lett.* **48** 362–365 (1982).

[26] M. Oshikawa. "Topological approach to Luttinger's theorem and the Fermi surface of a Kondo lattice." *Phys. Rev. Lett.* **84** 3370–3373 (2000).

[27] A. A. Abrikosov, L. P. Gorkov, and I. E. Dzyaloshinski. *Methods of Quantum Field Theory in Statistical Physics.* Dover Publications, New York (1975).

[28] Y. Onuki, R. Settai, K. Sugiyama, T. Takeuchi, T. Kobayashi, Y. Haga, and E. Yamamoto. "Recent advances in the magnetism and superconductivity of heavy fermion systems." *J. Phys. Soc. Jpn.* **73** 769–787 (2004).

[29] P. Rhodes and E. Wohlfarth. "Effective Curie-weiss constant of ferromagnetic metals and alloys." *Proc. Roy. Soc. London Ser. A* **273** 247 (1963).

[30] E. D. Bauer, A. D. Christianson, J. S. Gardner, V. A. Sidorov, J. D. Thompson, J. L. Sarrao, and M. F. Hundley. "Physical properties of the ferromagnetic heavy-fermion compound UIr_2Zn_{20}." *Phys. Rev. B* **74** 155118 (2006).

[31] J. D. Thompson. "Superconductivity in actinide materials." arXiv:cond-mat/0509078.

[32] D. Pines. *Elementary Excitations in Solids : Lectures On Phonons, Electrons, and Plasmons.* Westview Press (1999).

[33] S. Coleman. *Aspects of Symmetry: Selected Erice Lectures.* Cambridge University Press (1988).

[34] J. A. Hertz. "Quantum critical phenomena." *Phys. Rev. B* **14** 1165–1184 (1976).

[35] L. D. Landau and E. M. Lifshitz. *Statistical Physics.* Butterworth Heinemann (1980).

[36] A. Overhauser. "Giant spin density waves." *Phys. Rev. Lett.* **4** 462–465 (1960).

[37] A. J. Millis. "Effect of a nonzero temperature on quantum critical-points in itinerant fermion systems." *Phys. Rev. B* **48** 7183–7196 (1993).

[38] T. Moriya. *Spin Fluctuations in Itinerant Electron Magnetism.* Springer (1985).

[39] A. Schroder, G. Aeppli, E. Bucher, R. Ramazashvili, and P. Coleman. "Scaling of magnetic fluctuations near a quantum phase transition." *Phys. Rev. Lett.* **80** 5623–5626 (1998).

[40] A. Schroder, G. Aeppli, R. Coldea, M. Adams, O. Stockert, H. v. Loehneysen, E. Bucher, R. Ramazashvili, and P. Coleman. "Onset of antiferromagnetism in heavy-fermion metals." *Nature* **407** 351–355 (2000).

[41] Q. Si. "Is there more than one type of quantum critical points in heavy-fermion metals?" *J. Magn. Magn. Mater.* **226** 30–34 (2001).

[42] Q. Si, S. Rabello, K. Ingersent, and J. Smith. "Local fluctuations in quantum critical metals." *Phys. Rev. B* **68** 115103 (2003).

[43] A. Kosevich. "Topology and solid-state physics." *J. Low Temp. Phys.* **30** 97–117 (2004).

[44] L. Zhu, M. Garst, A. Rosch, and Q. Si. "Universally diverging Gruneisen parameter and the magnetocaloric effect close to quantum critical points." *Phys. Rev. Lett.* **91** 066404 (2003).

[45] R. Kuchler, N. Oeschler, P. Gegenwart, T. Cichorek, K. Neumaier, O. Tegus, C. Geibel, J. Mydosh, F. Steglich, L. Zhu, and Q. Si. "Divergence of the Gruneisen ratio at quantum critical points in heavy fermion metals." *Phys. Rev. Lett.* **91** 066405 (2003).

[46] P. Gegenwart, Q. Si, and F. Steglich. "Quantum criticality in heavy-fermion metals." *Nature Physics* **4** 186–197 (2008).

[47] S. Paschen, T. Luhmann, S. Wirth, P. Gegenwart, O. Trovarelli, C. Geibel, F. Steglich, P. Coleman, and Q. Si. "Hall-effect evolution across a heavy-fermion quantum critical point." *Nature* **432** 881–885 (2004).

[48] P. Coleman, C. Pepin, Q. Si, and R. Ramazashvili. "How do Fermi liquids get heavy and die?" *J. Phys.: Condens. Matter* **13** R723–R738 (2001).

[49] S. J. Yamamoto and Q. Si. "Fermi surface and antiferromagnetism in the Kondo lattice: An asymptotically exact solution in $d > 1$ dimensions." *Phys. Rev. Lett.* **99** 016401 (2007).

[50] S. J. Yamamoto and Q. Si. "Fermi surface and magnetism in the Kondo lattice: A continuum field theory approach." *Physica B* **403** 1414–1416 (2008).

[51] F. D. M. Haldane. "Nonlinear field theory of large-spin Heisenberg antiferromagnets: Semiclassically quantized solitons of the one-dimensional easy-axis Neel state." *Phys. Rev. Lett.* **50** 1153–1156 (1983).

[52] S. Chakravarty, B. Halperin, and D. Nelson. "Two-dimensional quantum Heisenberg antiferromagnet at low temperatures." *Phys. Rev. B* **39** 2344–2371 (1989).

[53] S. Sachdev, A. V. Chubukov, and A. Sokol. "Crossover and scaling in a nearly antiferromagnetic Fermi-liquid in 2 dimensions." *Phys. Rev. B* **51** 14874–14891 (1995).

[54] E. Fradkin. *Field Theories of Condensed Matter Systems.* Westview Press (1998).

[55] N. Nagaosa. *Quantum Field Theory in Condensed Matter Physics.* Springer (1999).

[56] T. Einarsson and H. Johannesson. "Effective-action approach to the frustrated Heisenberg-antiferromagnet in 2 dimensions." *Phys. Rev. B* **43** 5867–5882 (1991).

[57] L. Zhu and Q. Si. "Critical local-moment fluctuations in the Bose-Fermi Kondo model." *Phys. Rev. B* **66** 024426 (2002).

[58] M. E. Fisher, B. Nickel, and S. K. Ma. "Critical exponents for long-range interactions." *Phys. Rev. Lett.* **29** 917 (1972).

[59] K. G. Wilson and J. B. Kogut. "The renormalization group and ϵ-expansion." *Phys. Rep.* **2** 75–200 (1974).

[60] J. Feldman and E. Trubowitz. "Perturbation-theory for many fermion systems." *Helv. Phys. Acta.* **63** 156–260 (1990).

[61] G. Benfatto and G. Gallavotti. "Renormalization-group approach to the theory of the Fermi-surface." *Phys. Rev. B* **42** 9967–9972 (1990).

[62] R. Shankar. "Renormalization-group for interacting fermions in $d > 1$." *Physica A* **177** 530–536 (1991).

[63] R. Shankar. "Renormalization-group approach to interacting fermions." *Rev. Mod. Phys.* **66** 129–192 (1994).

[64] T. Vojta, D. Belitz, R. Narayanan, and T. Kirkpatrick. "Quantum critical behavior of clean itinerant ferromagnets." *Z. Phys. B: Condens. Matter* **103** 451–461 (1997).

[65] A. Abanov and A. V. Chubukov. "Anomalous scaling at the quantum critical point in itinerant antiferromagnets." *Phys. Rev. Lett.* **93** 255702 (2004).

[66] J. Polchinski. "Low-energy dynamics of the spinon gauge system." *Nucl. Phys. B* **422** 617–633 (1994).

[67] C. Nayak and F. Wilczek. "Renormalization-group approach to low-temperature properties of a non-Fermi liquid-metal." *Nucl. Phys. B* **430** 534–562 (1994).

[68] B. Altshuler, L. Ioffe, and A. J. Millis. "Low-energy properties of fermions with singular interactions." *Phys. Rev. B* **50** 14048–14064 (1994).

[69] M. Onoda, I. Ichinose, and T. Matsui. "Dissipative gauge-theory of fermions and its marginal-Fermi-liquid-like behavior." *Nucl. Phys. B* **446** 353–372 (1995).

[70] T. Holstein, R. Norton, and P. Pincus. "de-Haas-van-Alphen effect and specific-heat of an electron-gas." *Phys. Rev. B* **8** 2649–2656 (1973).

[71] C. M. Varma, Z. Nussinov, and W. v. Saarloos. "Singular or non-Fermi liquids." *Phys. Rep.* **361** 267–417 (2002).

[72] P. Lee, N. Nagaosa, and X. Wen. "Doping a Mott insulator: Physics of high-temperature superconductivity." *Rev. Mod. Phys.* **78** 17–85 (2006).

[73] F. Schutz, L. Bartosch, and P. Kopietz. "Collective fields in the functional renormalization group for fermions, Ward identities, and the exact solution of the Tomonaga-Luttinger model." *Phys. Rev. B* **72** 035107 (2005).

[74] S. Tsai, A. Castro Neto, R. Shankar, and D. Campbell. "Renormalization-group approach to strong-coupled superconductors." *Phys. Rev. B* **72** 054531 (2005).

[75] D. Nelson and R. Pelcovits. "Momentum-shell recursion relations, anisotropic spins, and liquid-crystals in $2 + \epsilon$ dimensions." *Phys. Rev. B* **16** 2191–2199 (1977).

[76] P. M. Chaikin and T. C. Lubensky. *Principles of Condensed Matter Physics.* Cambridge University Press, Cambridge, U.K. (1995).

[77] C. Pepin, J. Rech, and R. Ramazashvili. "Scaling approach to itinerant quantum critical points." *Phys. Rev. B* **69** 172401 (2004).

[78] A. J. Millis and P. A. Lee. "Large-orbital-degeneracy expansion for the lattice Anderson model." *Phys. Rev. B* **35** 3394–3414 (1987).

[79] I. Vekhter and A. V. Chubukov. "Non-Fermi-liquid behavior in itinerant anti-ferromagnets." *Phys. Rev. Lett.* **93** 016405 (2004).

[80] J. R. Schrieffer. "Wards identity and the suppression of spin fluctuation super-conductivity." *J. Low Temp. Phys.* **99** 397–402 (1995).

[81] S. J. Yamamoto and Q. Si. "Metallic ferromagnetism in the Kondo lattice." arXiv:0812.0819.

[82] D. Vollhardt. "Metallic ferromagnetism: Progress in our understanding of an old strong- coupling problem." *Adv. in Solid State Phys.* **38** 383–396 (1999).

[83] Y. Nagaoka. "Ferromagnetism in a narrow almost half-filled s-band." *Phys. Rev.* **147** 392 (1966).

[84] C. King and G. Lonzarich. "Quasi-particle properties in ferromagnetic $CeRu_2Ge_2$." *Physica B* **171** 161–165 (1991).

[85] H. Yamagami and A. Hasegawa. "Fermi-surface of $LaRu_2Ge_2$ and $CeRu_2Ge_2$ within local-density band theory." *J. Phys. Soc. Jpn.* **63** 2290–2302 (1994).

[86] H. Ikezawa, H. Aoki, M. Takashita, C. J. Haworth, S. Uji, T. Terashima, K. Maezawa, R. Settai, and Y. Onuki. "Fermi surface properties of ferromagnetic $CeRu_2Ge_2$." *Physica B* **237** 210–211 (1997).

[87] S. Sullow, M. Aronson, B. Rainford, and P. Haen. "Doniach phase diagram revisited: From ferromagnet to Fermi liquid in pressurized $CeRu_2Ge_2$." *Phys. Rev. Lett.* **82** 2963–2966 (1999).

[88] J. Larrea, M. Fontes, A. Alvarenga, E. Baggio-Saitovitch, T. Burghardt,

A. Eichler, and M. Continentino. "Quantum critical behavior in a CePt ferromagnetic Kondo lattice." *Phys. Rev. B* **72** 035129 (2005).

[89] S. Drotziger, C. Pfleiderer, M. Uhlarz, H. v. Loehneysen, D. Souptel, W. Loser, and G. Behr. "Suppression of ferromagnetism in $CeSi_{1.81}$ under temperature and pressure." *Phys. Rev. B* **73** 214413 (2006).

[90] V. Sidorov, E. Bauer, N. Frederick, J. Jeffries, S. Nakatsuji, N. Moreno, J. Thompson, M. B. Maple, and Z. Fisk. "Magnetic phase diagram of the ferromagnetic Kondo-lattice compound $CeAgSb_2$ up to 80 kbar." *Phys. Rev. B* **67** 224419 (2003).

[91] E. Bauer, V. Zapf, P. Ho, N. Butch, E. Freeman, C. Sirvent, and M. B. Maple. "Non-Fermi-liquid behavior within the ferromagnetic phase in $URu_{2-x}Re_xSi_2$." *Phys. Rev. Lett.* **94** 046401 (2005).

[92] C. Krellner, N. S. Kini, E. M. Bruening, K. Koch, H. Rosner, M. Nicklas, M. Baenitz, and C. Geibel. "CeRuPO: A rare example of a ferromagnetic Kondo lattice." *Phys. Rev. B* **76** 104418 (2007).

[93] S. S. Saxena. "Superconductivity on the border of itinerant-electron ferromagnetism in UGe_2." *Nature* **406** 587–592 (2000).

[94] F. Levy, I. Sheikin, and A. Huxley. "Acute enhancement of the upper critical field for superconductivity approaching a quantum critical point in URhGe." *Nature Physics* **3** 460–463 (2007).

[95] R. Settai, M. Nakashima, S. Araki, Y. Haga, T. Kobayashi, N. Tateiwa, H. Yamagami, and Y. Onuki. "A change of the Fermi surface in UGe_2 across the critical pressure." *J. Phys.: Condens. Matter* **14** L29–L36 (2002).

[96] N. B. Perkins, J. R. Iglesias, M. D. Nunez-Regueiro, and B. Coqblin. "Coexistence of ferromagnetism and Kondo effect in the underscreened Kondo lattice." *Euro. Phys. Lett.* **79** 57006 (2007).

[97] W. Nolting, W. Muller, and C. Santos. "Ferromagnetic Kondo-lattice model." *J. Phys. A* **36** 9275–9288 (2003).

[98] N. Read and S. Sachdev. "Continuum quantum ferromagnets at finite-temperature and the quantum Hall-effect." *Phys. Rev. Lett.* **75** 3509–3512 (1995).

[99] X. G. Wen and A. Zee. "Spin-waves and topological terms in the mean-field theory of two-dimensional ferromagnets and antiferromagnets." *Phys. Rev. Lett.* **61** 1025–1028 (1988).

[100] C. Gonzalez-Buxton and K. Ingersent. "Renormalization-group study of Anderson and Kondo impurities in gapless Fermi systems." *Phys. Rev. B* **57** 14254–14293 (1998).

[101] D. Withoff and E. Fradkin. "Phase-transitions in gapless Fermi systems with magnetic-impurities." *Phys. Rev. Lett.* **64** 1835–1838 (1990).

[102] B. Rainford, A. Neville, D. Adroja, S. Dakin, and A. Murani. "Low temperature excitations in $CeRu_2Si_{2-x}Ge_x$ alloys." *Physica B* **224** 163–165 (1996).

[103] T. Park, V. A. Sidorov, F. Ronning, J. X. Zhu, Y. Tokiwa, H. Lee, E. D. Bauer, R. Movshovich, J. L. Sarrao, and J. D. Thompson. "Isotropic quantum scattering and unconventional superconductivity." *Nature* **456** 366–368 (2008).

[104] A. Tsvelik. *Quantum Field Theory in Condensed Matter Physics.* Cambridge University Press, Cambridge (2003).

[105] P. A. Lee. "Gauge field, Aharonov-Bohm flux, and high-T_c superconductivity." *Phys. Rev. Lett.* **63** 680–683 (1989).

[106] J. Rech, C. Pepin, and A. Chubukov. "Quantum critical behavior in itinerant electron systems: Eliashberg theory and instability of a ferromagnetic quantum critical point." *Phys. Rev. B* **74** 195126 (2006).

[107] D. Efremov, J. Betouras, and A. Chubukov. "Nonanalytic behavior of two-dimensional itinerant ferromagnets." *Phys. Rev. B* **77** 220401(R) (2008).

[108] V. Oganesyan, S. Kivelson, and E. Fradkin. "Quantum theory of a nematic Fermi fluid." *Phys. Rev. B* **64** 195109 (2001).

[109] Y. Kim, A. Furusaki, X. G. Wen, and P. A. Lee. "Gauge-invariant response functions of fermions coupled to a gauge field." *Phys. Rev. B* **50** 17917–17932 (1994).

[110] A. Abanov, A. Chubukov, and J. Schmalian. "Quantum-critical theory of the spin fermion model and its application to cuprates: Normal state analysis." *Adv. Phys.* **52** 119–218 (2003).

[111] A. V. Chubukov and J. Schmalian. "Superconductivity due to massless boson exchange in the strong-coupling limit." *Phys. Rev. B* **72** 174520 (2005).

[112] A. V. Chubukov, C. Pepin, and J. Rech. "Instability of the quantum-critical point of itinerant ferromagnets." *Phys. Rev. Lett.* **92** 147003 (2004).

[113] T. R. Sedrakyan and A. V. Chubukov. "Fermionic propagators for 2d systems with singular interactions." arXiv:0901.1459.

[114] D. Belitz, T. Kirkpatrick, and T. Vojta. "How generic scale invariance influences quantum and classical phase transitions." *Rev. Mod. Phys.* **77** 579–632 (2005).

[115] R. P. Smith, M. Sutherland, G. G. Lonzarich, S. S. Saxena, N. Kimura, S. Takashima, M. Nohara, and H. Takagi. "Marginal breakdown of the Fermi-liquid state on the border of metallic ferromagnetism." *Nature* **455** 1220–1223 (2008).